Dissertation

submitted to the
Combined Faculties for the Natural Sciences and for Mathematics
of the Ruperto-Carola University of Heidelberg, Germany
for the degree of
Doctor of Natural Sciences

presented by

Diplom-Biologe Thomas Splettstößer
born in: Pasewalk
oral examination: 15.12.2010

ACTIN: Structure and Function

Towards an understanding of the conformational states
of actin monomer and filament

Referees: Prof. Dr. Jeremy C. Smith
            Prof. Dr. Robert Russell

Abstract

Actin is a major structural protein of the eukaryotic cytoskeleton and plays a crucial role in cell motility, adhesion, morphology and intracellular transport. Its biologically active form is the filament (F-actin), which is assembled from monomeric G-actin. In this thesis, the structural characteristics of both G- and F-actin are studied using molecular dynamics simulations. First, the crystallographically-determined 'open' and 'closed' conformational states of G-actin are characterized in aqueous solution, with either ATP or ADP bound in the nucleotide binding pocket. In both nucleotide states, the open state closes in the absence of the actin-binding protein profilin, suggesting that the open state is not a stable conformation of isolated G-actin. Further, the simulations reveal the existence of a structurally well-defined, compact, 'superclosed' state of ATP-G-actin, as yet unseen crystallographically and absent in the ADP-G-actin simulations. The superclosed state resembles structurally the actin monomer in filament models and we suggest it to be the polymerization competent conformation of G-actin. Furthermore, we introduce a new actin filament model, the Holmes-2010 model that incorporates the global structure of a recently published model but in addition conserves internal stereochemistry. The improved quality of the Holmes-2010 model is apparent in a comparison made with other recent F-actin models using molecular dynamics simulation, monitoring a number of structural determinants. In addition, simulations of the model are carried out in states with both ATP or ADP bound and local hydrogen-bonding differences characterized. The results point to the significance of a direct interaction of GLN137 with ATP for activation of ATPase activity after the G-to-F-actin transition. The findings presented here may thus be a step towards a better understanding of the nucleotide-dependent structural differences of actin that lead to its functional differences.
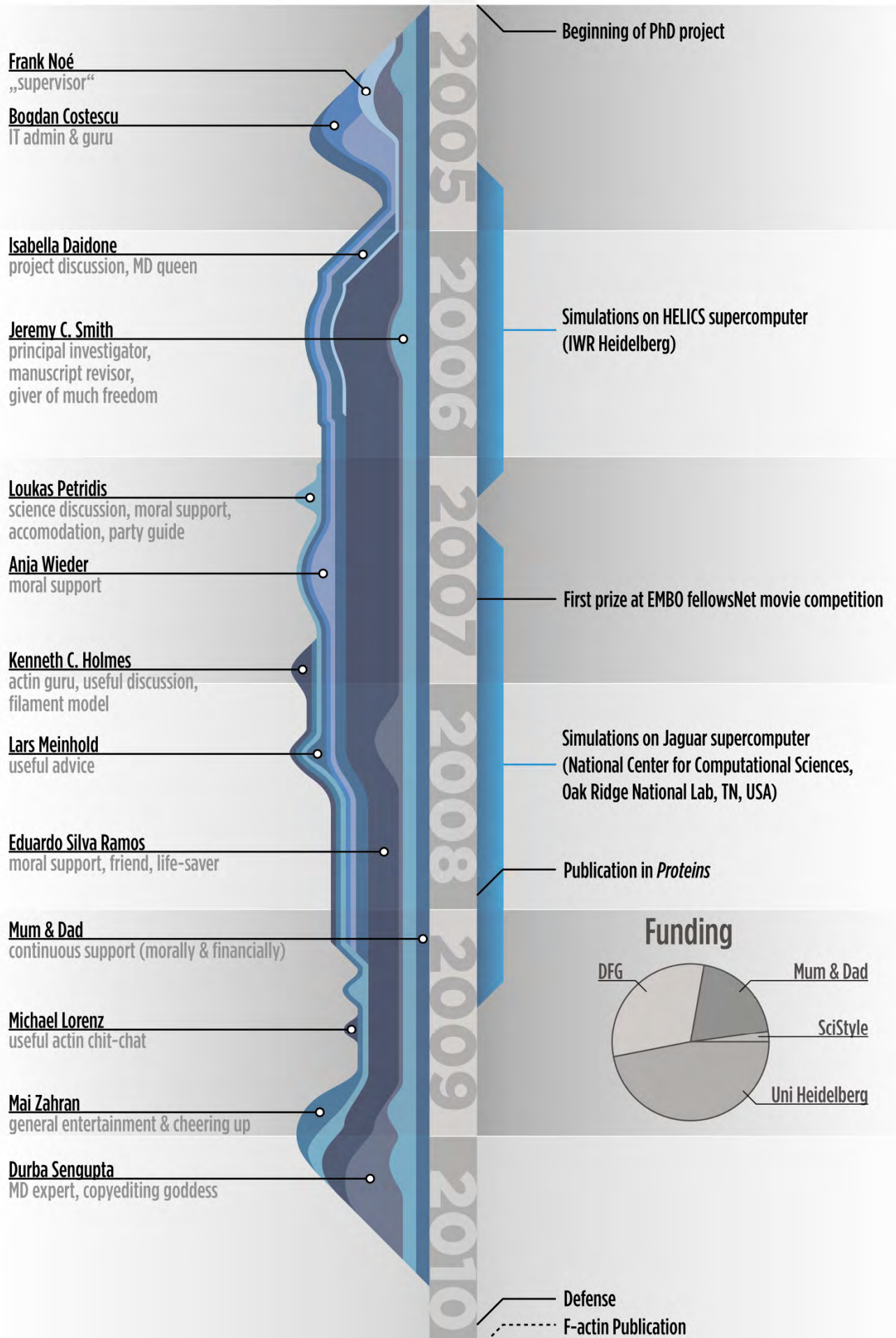
Zusammenfassung

Aktin ist ein wichtiges Strukturprotein des eukaryotischen Zytoskeletts und erfüllt zentrale Funktionen bei verschiedenen Formen von Zellbewegung, -adhäsion, -morphologie und beim intrazellulären Transport. Die biologisch aktive Form von Aktin ist das Mikrofilament (F-Aktin), welches aus globulären G-Aktin-Monomeren besteht. In dieser Studie werden verschiedene strukturelle Eigenschaften von G- und F-Aktin mittels Molekulardynamiksimulationen untersucht. Die durch Kristallstrukturanalyse bestimmten Konformationen von G-Aktin 'offen' und 'geschlossen' werden in wässriger Lösung in zwei Zuständen charakterisiert: zum einen mit ATP, zum anderen mit ADP in der Nukleotidbindestelle. Die offene Konformation von sowohl ATP- als auch ADP-gebundenem G-Aktin schließt sich in Abwesenheit von gebundenem Profilin was darauf hindeutet, dass die offene Konformation keinen stabilen Zustand des isolierten Aktinmonomers darstellt. Darüber hinaus offenbaren die Simulationen die Existenz einer strukturell klar abgegrenzten, kompakten 'superclosed' Konformation von ATP-gebundenem G-Aktin. Diese neue Zustandsform von G-Aktin wurde bisher nicht kristallographisch beobachtet und trat auch in den Simulationen von ADP-G-Aktin nicht auf. Die Struktur des 'superclosed'-Zustands ähnelt den Aktin-Monomeren in F-Aktin und entspricht möglicherweise der Konformation von ATP-G-Aktin, in der sich die Monomere an das Filament anlagern. Zudem wird ein neues Modell des Mikrofilaments vorgestellt, das Holmes-2010-Modell, deren Aktin-Monomere die globale Struktur eines zuvor publizierten Modells des Mikrofilaments berücksichtigen, jedoch zusätzlich die interne Stereochemie bewahren. Die verbesserten Eigenschaften des Holmes-2010-Modells im Vergleich zu anderen Modellen des Aktinfilaments werden durch Molekulardynamiksimulationen ersichtlich, bei welchen verschiedene strukturelle Bestimmgrößen überprüft wurden. Desweiteren wurden Computersimulationen des Modells im ADP- und ATP-Zustand ausgeführt und die Unterschiede in den Schemata der lokalen Wasserstoffbrückenbindungen untersucht. Die Ergebnisse deuten auf eine direkte Interaktion von GLN137 mit ATP für die Aktivierung der ATPase-Aktivität nach dem Übergang von G- zu F-Aktin hin. Die vorliegende Arbeit möchte dazu beitragen ein besseres Verständnis davon zu erlangen, wie die Nukleotid-abhängigen Strukturunterschiede von Aktin dessen Funktionsunterschiede bestimmen.

List of Publications

[1] Thomas Splettstoesser, Frank Noé, Toshiro Oda and Jeremy C. Smith. Nucleotide-dependence of G-actin conformation from multiple molecular dynamics simulations and observation of a putatively polymerization-competent superclosed state. *Proteins* **76**, 353-64 (2009).

[2] Thomas Splettstoesser, Kenneth C. Holmes, Frank Noé and Jeremy C. Smith. Structural modeling and molecular dynamics simulation of the actin filament. *submitted*

Acknowledgements

2005
2006
2007
2008
2009
2010

Beginning of PhD project

Simulations on HELICS supercomputer
(IWR Heidelberg)

First prize at EMBO fellowsNet movie competition

Simulations on Jaguar supercomputer
(National Center for Computational Sciences,
Oak Ridge National Lab, TN, USA)

Publication in *Proteins*

Funding

DFG
Mum & Dad
SciStyle
Uni Heidelberg

Defense
F-actin Publication

Contents

CHAPTER 0

ABOUT THIS THESIS

Actin is the most abundant intra-cellular protein in the majority of eukaryotic cells. It exists as a globular monomer called G-actin and as a filamentous helical polymer called F-actin, which is a linear chain of G-actin subunits. This thesis aims to understand the structural properties of G- and F-actin in relation to their functional cycle which is based on changes in the protein structure induced by the bound ATP or ADP nucleotide. The central questions this thesis will address are:

> What are the nucleotide-induced structural differences between the ATP- and ADP-bound forms of monomeric actin?

> What are the structural changes in the nucleotide binding site that allow ATP to hydrolyze in F-actin but not in G-actin?

> What is the structure of the actin filament and how can molecular dynamics (MD) simulations help to determine these structures?

To answer these questions, MD simulations were carried out on both G- and F- actin. The thesis is organized as follows:

Chapter 1 provides an introduction to the actin system in its monomeric and filamentous state. We first summarize the state of current research in this field as well as a historical perspective to place this work in context. Further, the ATP-driven cycle of polymerization/depolymerization of monomeric actin subunits to filaments is discussed, the understanding of which is one of the aims of this study. A number of structural features of actin monomer and filament that have been proposed to play a role in the functioning of this protein and are relevant to this thesis are also introduced.

Chapter 2 explains the methods used here, in particular molecular dynamics simulation. In addition to standard properties derived from MD simulations, several other parameters unique to the actin system are defined, such as the 'nucleotide cleft size'.

In chapter 3, MD simulation is used to explore the conformational states of the actin monomer bound to either ATP or ADP and in presence or absence of profilin, a nucleotide exchange factor of G-actin. The structural stability of the different crystallized protein states is shown to be related to the binding of profilin.

Chapter 4 discusses the 'superclosed' state of ATP-G-actin, a novel conformation of the actin monomer observed here in multiple independent simulations. We characterize the different structural and dynamic properties of this state and show that it is absent when ADP is bound. Comparison of the superclosed structure with protomers of the actin filament suggests its putative biological relevance in F-actin polymerization.

A new model of the actin filament structure, the Holmes 2010 model, is introduced in chapter 5. This new filament model along with two other recent efforts of modeling the actin fibril are subjected to MD simulation. The quality of the different models is assessed by examining their structural integrity upon MD simulation. In addition, simulations of the model are carried out in states with both ADP or ATP bound and local hydrogen-bonding differences characterized. The results point to the significance of a direct interaction of GLN137 with ATP for activation of ATPase activity after the G- to F-actin transition.

In conclusion, the thesis aims to provide a structural basis for actin function by probing the functionally relevant structural properties of actin. We show that molecular dynamics provides insight of the protein at an atomic resolution that is inherently not accessible with traditional experimental methods. The results presented here contribute to the understanding of the structure, dynamics and function of this ubiquitous protein.

CHAPTER 1

INTRODUCTION

The cell is the basic unit of all living organisms [1]. It is a complex but highly organized entity separated from the outside by a cell membrane. Two general cell types can be distinguished: prokaryotic and eukaryotic. Prokaryotes are single-celled organisms and comprise a single membrane-limited compartment. With few exceptions [2], a cell wall surrounds prokaryotic cells, providing structural support and protection. Eukaryotes comprise all members of the animal, plant and fungi kingdoms. Eukaryotic cells are more complex and typically much larger than that of prokaryotes. Unlike prokaryotes, eukaryotic cells also contain internal membranes and structures, called organelles and the cytoskeleton, that carry out specialized functions. The cytoskeleton is an array of fibrous proteins contained within the cytoplasm. It is composed of three classes of fibers: microtubules, built of polymers of the protein tubulin; intermediate filaments, built of one or more rod-shaped protein subunits; and microfilaments, which are also called actin filaments [1].

1.1 The actin based cytoskeleton and motility system

Actin filaments are fibers of 7-9 nm diameter that are built from small protein subunits (monomers) that are held together by non-covalent bonds. These filaments are an essential component of the intra-cellular cytoskeleton, and play important roles in cell motility and division. The actin cytoskeleton is highly organized into discrete structures: Bundles of actin filaments are often enforced by cross-linking proteins and are the most common form of organization. Axial filament bundles, called stress fibers, underlay the cell body and help withstanding strain and stress acting upon the cell, especially so in epithelia. Filament bundles are also found in cells such as the microvilli. Other forms of organization include networks in geodesic dome-like formation and

gel-like lattices. The different actin filament structures have a high degree of organizational flexibility, which is mostly based on great variability in filament length and the changing ratio of the different actin-binding and -regulating proteins involved. This enables the actin cytoskeleton to assemble or disassemble itself and continuously rearrange when necessary. Therefore, the cytoskeleton not only reinforces the cell but also has the ability to control the cell shape and vary it easily. This enables cell locomotion in mobile cells such as fibroblasts and white blood cells, which are able to crawl across surfaces with the help of dynamic structures formed by actin filaments, for example the lamellipodia and filopodia. Another example for a transient structure formed by actin is the contractile ring, which assembles during cytokinesis to divide the cell. Besides the rearrangements of the cytoskeleton, cells have evolved another basic mechanism for generating movement. Motor proteins such as myosin interact with actin (or microtubules) and walk or slide along them. This allows the transport of organelles and vesicles within the cell. Furthermore, in muscle cells a complex of actin and myosin filaments provides the machinery for muscle contraction.

All cell movements require energy. The large scale conformational changes of myosin are powered by hydrolyzation of adenosine-5'-triphosphate (ATP), the universal energy currency of cells. Energy from ATP is also used for the assembly and disassembly cycle of actin filaments, although by an entirely different mechanism explained in one of the next sections.

1.1.1 The actin system is evolutionarily very old

Actin is one of the most common and ubiquitous proteins and the actin-based cytoskeletal and motility system can be viewed as one of the hallmarks of eukaryotic organisms. While actin is unique to eukaryotes, structural work of the last 10 years has revealed a superfamily of proteins that includes bacterial [6, 7] and archaeal [8, 9] counterparts of actin.
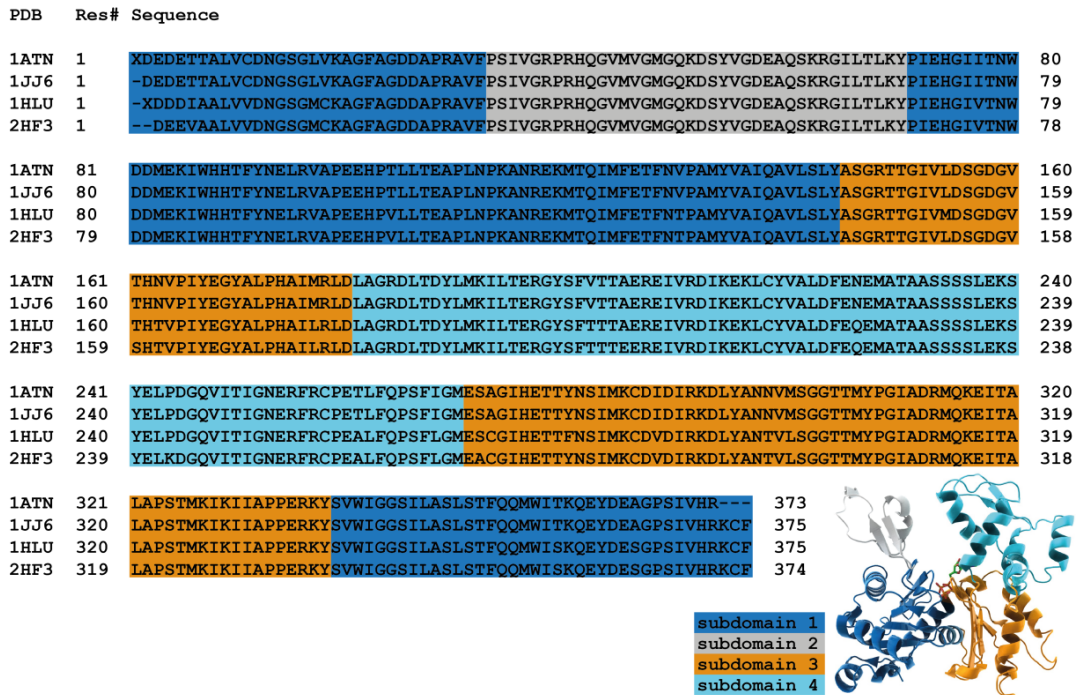
```
PDB     Res#  Sequence

1ATN    1     XDEDETTALVCDNGSGLVKAGFAGDDAPRAVFPSIVGRPRHQGVMVGMGQKDSYVGDEAQSKRGILTLKYPIEHGIITNW    80
1JJ6    1     -DEDETTALVCDNGSGLVKAGFAGDDAPRAVFPSIVGRPRHQGVMVGMGQKDSYVGDEAQSKRGILTLKYPIEHGIITNW    79
1HLU    1     -XDDDIAALVVDNGSGMCKAGFAGDDAPRAVFPSIVGRPRHQGVMVGMGQKDSYVGDEAQSKRGILTLKYPIEHGIVTNW    79
2HF3    1     --DEEVAALVVDNGSGMCKAGFAGDDAPRAVFPSIVGRPRHQGVMVGMGQKDSYVGDEAQSKRGILTLKYPIEHGIVTNW    78

1ATN    81    DDMEKIWHHTFYNELRVAPEEHPTLLTEAPLNPKANREKMTQIMFETFNVPAMYVAIQAVLSLYASGRTTGIVLDSGDGV    160
1JJ6    80    DDMEKIWHHTFYNELRVAPEEHPTLLTEAPLNPKANREKMTQIMFETFNVPAMYVAIQAVLSLYASGRTTGIVLDSGDGV    159
1HLU    80    DDMEKIWHHTFYNELRVAPEEHPVLLTEAPLNPKANREKMTQIMFETFNTPAMYVAIQAVLSLYASGRTTGIVMDSGDGV    159
2HF3    79    DDMEKIWHHTFYNELRVAPEEHPVLLTEAPLNPKANREKMTQIMFETFNTPAMYVAIQAVLSLYASGRTTGIVLDSGDGV    158

1ATN    161   THNVPIYEGYALPHAIMRLDLAGRDLTDYLMKILTERGYSFVTTAEREIVRDIKEKLCYVALDFENEMATAASSSSLEKS    240
1JJ6    160   THNVPIYEGYALPHAIMRLDLAGRDLTDYLMKILTERGYSFVTTAEREIVRDIKEKLCYVALDFENEMATAASSSSLEKS    239
1HLU    160   THTVPIYEGYALPHAILRLDLAGRDLTDYLMKILTERGYSFTTTAEREIVRDIKEKLCYVALDFEQEMATAASSSSLEKS    239
2HF3    159   SHTVPIYEGYALPHAILRLDLAGRDLTDYLMKILTERGYSFTTTEEREIVRDIKEKLCYVALDFEQEMATAASSSSLEKS    238

1ATN    241   YELPDGQVITIGNERFRCPETLFQPSFIGMESAGIHETTYNSIMKCDIDIRKDLYANNVMSGGTTMYPGIADRMQKEITA    320
1JJ6    240   YELPDGQVITIGNERFRCPETLFQPSFIGMESAGIHETTYNSIMKCDIDIRKDLYANNVMSGGTTMYPGIADRMQKEITA    319
1HLU    240   YELPDGQVITIGNERFRCPEALFQPSFLGMESCGIHETTFNSIMKCDVDIRKDLYANTVLSGGTTMYPGIADRMQKEITA    319
2HF3    239   YELKDGQVITIGNERFRCPEALFQPSFLGMEACGIHETTYNSIMKCDVDIRKDLYANTVLSGGTTMYPGIADRMQKEITA    318

1ATN    321   LAPSTMKIKIIAPPERKYSVWIGGSILASLSTFQQMWITKQEYDEAGPSIVHR---    373
1JJ6    320   LAPSTMKIKIIAPPERKYSVWIGGSILASLSTFQQMWITKQEYDEAGPSIVHRKCF    375
1HLU    320   LAPSTMKIKIIAPPERKYSVWIGGSILASLSTFQQMWISKQEYDESGPSIVHRKCF    375
2HF3    319   LAPSTMKIKIIAPPERKYSVWIGGSILASLSTFQQMWISKQEYDESGPSIVHRKCF    374
```

subdomain 1
subdomain 2
subdomain 3
subdomain 4

Fig. 1.1. **Alignment of amino acid sequences of the G-actin protein from different sources.** Shown here are four of the sequences of G-actin structures considered in this thesis: Protein Data Bank (PDB) entries 1ATN and 1J6Z: rabbit skeletal muscle; PDB entry 1HLU: bovine non-muscle cytoskeletal actin; PDB entry 2HF3: fruit fly cytoskeletal actin of non-muscle cells. The subdomains of the actin monomer are highlighted in color.

The structure and amino acid sequence of actin is evolutionary remarkably conserved (Fig. 1.1). There are no changes in amino acid sequence between chicken and human skeletal muscle actin isoforms and even the most dissimilar actins still share more than 85% of sequence identity [10].

The high degree of conservation of this evolutionary old system may be founded in the fact that the actin system is of fundamental importance for the functioning of the cell. However, defective assembly of actin filaments in skeletal muscle is directly implicated in a few diseases [11], mutants of nonmuscle cytoskeletal actin that affect polymerization have been found in cancerous cells [12] and mutations in cardiac actin that potentially affect polymerization cause heart disease.

1.1.2 Actin binding proteins

An unusual high number of actin binding proteins exist. More than 60 classes of proteins have been identified to associate with actin. As they are found across the phylogenetic tree, from protozoa via yeast to vertebrates, these actin binding proteins are assumed to be very ancient. Interestingly, the function of many of those actin-binding proteins appears to be highly redundant. Knock-out mutations of multiple actin-binding proteins strengthen this assumption [13]. The redundancy may be a mechanism to ensure the crucial actin system to be fail-safe. An alternative hypothesis suggests that the primary function of most of these proteins is not related to actin and their actin-binding ability is incidental. One example is DNase I of which the primary function is DNA cleavage. The protein also binds actin monomers with high and filaments with low affinity. The majority of actin-binding proteins exhibit a low affinity for actin. The weak binding may allow the cytoskeleton to remodel and change shape on fast time scales that are necessary for cell locomotion.

Some of the many classes of actin-binding proteins include: monomer-binding proteins such as profilin and DNase I, small actin-filament depolymerizing proteins like depactin, cofilin, capping and severing proteins of the filament end such as gelsolin, villin and Cap Z, lateral binding proteins like caldesmon, troponin and tropomyosin, crosslinking proteins like spectrin, dystrophin, fimbrin and alpha-actinin, membrane-associated actin binding proteins like axtolinkin and synapsins, microtubule-binding proteins and various myosins.
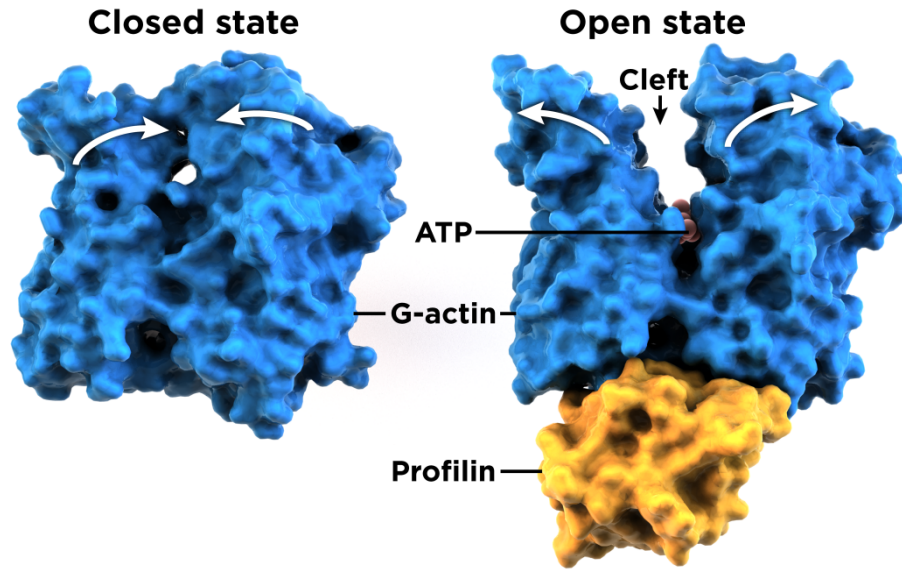
Fig. 1.2. The closed and open states of G-actin (blue). The actin monomer is divided by a deep cleft with a nucleotide binding site at its base. Profilin (orange) binds G-actin at the side opposite to the cleft (subdomains 1 and 3), thus facilitating the exchange of ADP by ATP.

The only known protein facilitating nucleotide exchange in actin is profilin. With 12-16 kDa, profilin is a relatively small actin-binding protein, present in all eukaryotic cells, though at a much lower concentration than G-actin. The protein fulfills two major functions: to promote assembly of actin monomers at the barbed end (*i.e.* growing end) of the filament, and greatly increasing the rate of nucleotide exchange in G-actin. For this study, only the latter function is relevant. Profilin binds ADP-G-actin monomers that disassemble from the filament end and promotes the exchange of ADP by ATP by a mechanism that is not well understood. A X-ray crystal structure of a profilin-G-Actin complex by Chik *et al.* lead to speculation about how the binding of profilin may influence the conformation of the actin monomer [14]. As shown in Fig. 1.2, the profilin-bound actin monomer of this X-ray structure adopts a conformation where the two actin domains diverge and is thus called the 'open state'. It has been suggested that the binding to profilin may be responsible for the increased size of the inter-domain cleft in the actin molecule and that this may facilitate nucleotide exchange. However, all other X-ray structures of the profilin-actin complex do not exhibit a similar increase in the size of the inter-domain cleft and some have argued that the profilin-induced open state of actin may be an artifact altogether [15, 16].

Similarly to free ATP-G-actin, complexes of profilin-bound G-actin are able to assemble at the barbed filament end (following dissociation of profilin) but

not the pointed end. This, too, raises doubt whether the binding of profilin induces such a large-scale conformational change in actin. Chapter 3 investigates the influence of binding of profilin on the structure of monomeric actin.

1.1.3 Filament dynamics: ATP hydrolysis, polarity and treadmilling

The actin cytoskeleton of cells is dynamic, with filaments able to grow and shrink rapidly. The cycle of assembly and disassembly is powered by ATP. Each actin monomer contains a bound ATP molecule, which is hydrolyzed after polymer formation. F-actin is a remarkable slow ATPase. The half time of hydrolysis following the assembly of an ATP-bound actin subunit to the filament is two seconds. Further, the half time for release of inorganic phosphate from the actin fibril is about six minutes. These slow rates are relevant for the transient rearrangements of the actin cytoskeleton since many actin binding proteins involved exhibit binding affinities that depend on the nucleotide state in the filament. After hydrolysis of ATP in the fibril, the critical concentration for binding of the ADP-bound protomers increases significantly. The weaker binding results in instability of the filaments and increases disassembly.
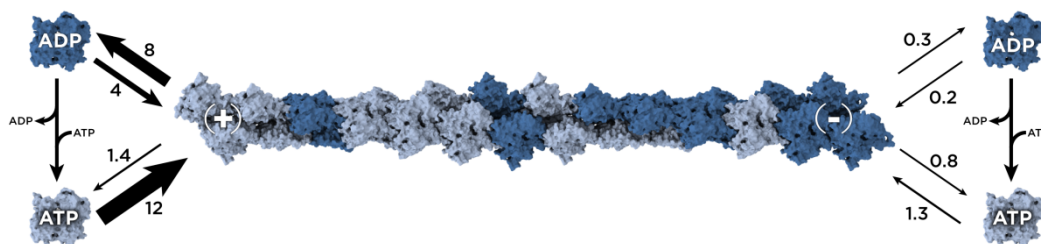

Fig. 1.3. Rates of association and dissociation of actin monomers at the pointed (-) and barbed (+) end of the filament.

Actin filaments exhibit structural and functional polarity based on the head-to-tail orientation of the subunits. The two ends are dramatically different in the components that bind to them (Fig. 1.3). This includes actin subunits that polymerize much faster onto one end (the (+) or barbed end) than they do on the other (the (-) or pointed end). Generally, subunits that polymerize on the (+)

end are more likely to contain ATP than on the (-) end. Therefore, the (-) end is most likely to have an ADP-bound subunit and depolymerize. The dissociating ADP-G-actin molecules are recharged, often mediated by profilin, which also delivers the ATP-bound actin subunits to the (+) end, thus closing the nucleotide-facilitated polymerization cycle of actin (Fig. 1.4).

When the ATP-G-actin concentration is between the critical concentration for the (+) and (-) ends, the filament grows at the (+) end while actin subunits disassemble from the other end. The overall length of the filament remains constant and subunits that polymerize on the barbed end travel through the filament to the pointed end as if on a treadmill. At the leading edge of migrating cells, treadmilling is believed to be the responsible mechanism for turnover of actin filaments, with actin monomers added to filaments near the leading edge of the cell and lost from the other end toward the rear. This is just one example of how the directed assembly and disassembly of individual filaments driven by ATP produce the complex rearrangements of the actin cytoskeleton that are required for actin-based motility.
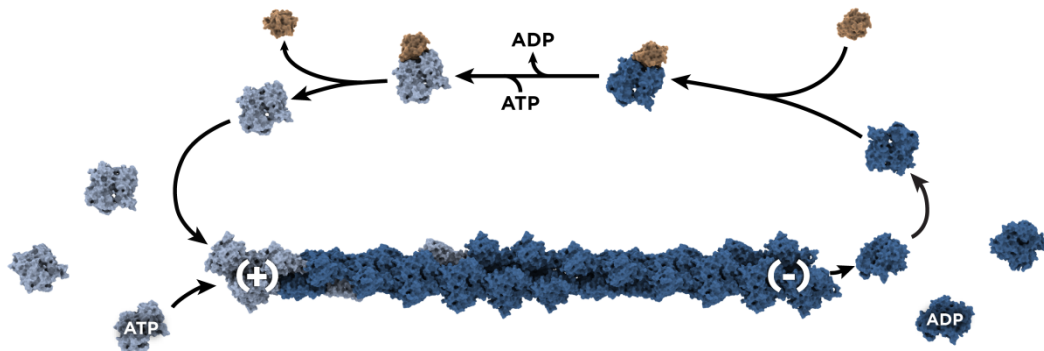

Fig. 1.4. Regulation of actin filament polymerization and treadmilling. The different critical concentrations of actin monomers on the filament ends cause newly added subunits at the (+) end to travel through the filament as if on a treadmill until they reach the (-) end. The dissociating ADP-bound monomers (dark blue) form a complex with profilin (orange) and ADP is replaced by ATP. Profilin then delivers the ATP-bound actin monomers (light blue) to the (+) end.

Actin exists in two forms: the monomer and the filament.

1.2 The actin monomer – building block of the actin filaments

The major building block of the actin based cytoskeleton and the thin filament in the muscle apparatus is the actin molecule or actin monomer. The actin molecule is also referred to as *G-actin* (globulous actin), when unbound from other actin monomers or *protomer* when part of an actin filament.

1.2.1 Structural details of G-actin

G-actin consists of a single polypeptide chain of 375 residues arranged into two domains and has a molecular weight of 42,000. Monomeric actin is a platelike molecule measuring about $55 \times 55 \times 35$ Å. The protein is divided by a central cleft into two major approximately equally sized domains. These two lobes can be further divided into four subdomains, two in each domain, surrounding a deep cleft containing ATP or ADP and a tightly bound Mg^{2+} ion. Due to purification procedures, this Mg^{2+} ion is replaced by Ca^{2+} in the majority of experimental studies (including X-ray crystallography.)

The nucleotide binds at the bottom of the cleft and contacts both lobes, thus stabilizing the protein. Without a bound nucleotide, G-actin denatures rapidly. The nature of the actin-bound nucleotide, ATP or ADP, is a key determinant for the conformation of the actin molecule. However, what the discrete conformational differences between the ATP- and ADP state of G-actin are, is subject of continuous debate and one of the issues addressed in this thesis.

The four subdomains are designated 1-4: subdomain 1 (residues 1-32, 70-144, and 338-375), subdomain 2 (residues 33–69), subdomain 3 (residues 145-180 and 270-337), and subdomain 4 (residues 181-269), with the cleft being located between subdomains 2 and 4 (see Fig. 1.5). The floor of the cleft acts as a hinge that allows the lobes to flex relative to each other. Subdomain 2 is the smallest and most flexible subdomain. It contains a very versatile domain that binds to DNase I and thus is called DNase I binding loop (HIS40-GLY48). The conformation of this loop has been suggested to be linked to the nucleotide state of G-actin and will be discussed in detail, subsequently.

The N and C-termini lie in subdomain 1. The N-terminal residue is acetylated and HIS73 is methylated in almost all actins. This methylation is an important structural determinant for actin and has been proposed to regulate the release

of inorganic phosphate from the interior of actin following polymerization-dependent hydrolysis of bound ATP. Because of this, the methylation of HIS73 was included in the molecular dynamics simulations of this study.
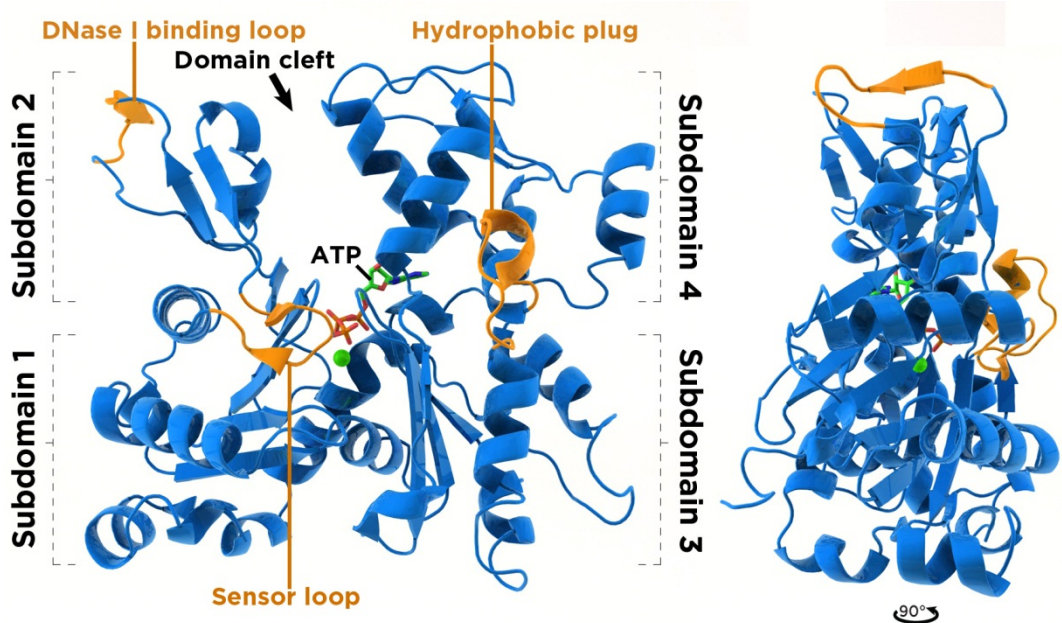

Fig. 1.5. G-actin. The two lobes of the actin monomer, divided by a deep cleft, can be further divided into four subdomains. The DNase I binding loop (HIS40-GLY48), the hydrophobic plug (PHE262-ILE274) and the sensor loop, carrying a methylated histidine (PRO70-ASP78) are relevant structural features in this study.

Polymerization of G-actin into F-actin can be induced by addition of Mg^{2+}, K^+ or Na^+ ions to a solution of monomeric actin. This process can also be reversed by lowering the ionic strength of the solution. Thus, low affinity cation binding sites must exist besides the high affinity binding site in the nucleotide binding pocket, which is usually occupied by an Mg^{2+} ion. Crystallographic evidence about the location of the low-affinity binding sites is inconclusive but several binding sites that may induce the polymerization of G-actin molecules have been proposed [17, 18].

1.2.2 Actin exists in different isoforms

Multiple forms of actin exist. These isoforms are products of different genes of a large gene family and exhibit only minor sequence differences but generally

performing different cellular functions. While most yeasts express only one actin isoform, humans encode six isoforms and some plants have as many as 60. In vertebrates the six isoforms include, α-cardiac, α-skeletal, α-vascular, non-muscle β- and γ-actin as well as a smooth muscle γ-isoform. The expression patterns of the various actin isoforms are temporally and spatially regulated depending on cell type. Indeed, differential localization of different isoforms also occurs within the cell. The different actin isoforms usually differ only in a few positions throughout the sequence, but concentrated in the N-terminus. Despite the small number of amino acid substitutions, critical concentrations of assembly of muscle and non-muscle actins into filament structures are equal under near physiological conditions.) Under certain conditions different actin isoforms have been shown to be able to co-polymerize within an actin filament *in vitro*.

Much of the work in this thesis is based on α-skeletal muscle actin of rabbit. But some of the monomer simulations involve bovine β-actin and cytosolic γ-actin from *Drosophila melanogaster*. We generally interpret the results of the simulations of different isoforms as interchangeable and assume that our findings are generally applicable because the main focus of the present work lies on general principles of the functioning of actin that are shared by all isoforms. Due to the remarkably high conservation of actin throughout evolution, different classes of actin polymerize similarly *in vitro* and form copolymers with each other despite subtle differences in the filament structure [3]. Large differences were found in the affinity of different isoforms to actin binding proteins such as profilin [4]. However, that aspect is not relevant for this study.

1.2.3 What we know – previous research of G-actin

Understanding of the functioning of G-actin made a leap forward, when the first X-ray structure of G-actin was solved by Kabsch *et al.* in 1990 [19]. Obtaining a protein crystal of G-actin is challenging due to the propensity of actin monomers to polymerize to F-actin, especially so at high concentrations of G-actin. To obtain crystals of G-actin the protein needs to be maintained in a monomeric state. In case of the Kabsch structure, this has been achieved by co-crystallization with the actin-binding protein DNase I. Subsequent attempts to render G-actin non-polymerizable for crystallization include co-crystallization with other actin-binding proteins [20], chemical modification by

adding a fluorescent dye (tetramethyl-rhodamine maleimide) to the C-terminus [21], introducing point mutations [22] or cleaving the DNase I binding loop in subdomain 2 [23]. However, it is possible that the structures of actin complexes or modified actin monomers do not faithfully reflect the true structure of an uncomplexed form. To date, more than 50 crystallographic structures of G-actin have been solved, both in the ATP and ADP state.

1.2.4 What we don't know

Despite the large number of both experimental studies and solved crystallographic structures of G-actin, questions regarding the relation of structure and function remain. The structural and dynamic properties of actin depend, at least in part, on the state of the bound nucleotide [21, 24, 25, 26]. In fact, the state of the nucleotide bound to actin, ATP or ADP, is the driving force of the actin cycle of polymerization and depolymerization. The nucleotide state of G-actin determines the binding affinities of ATP- and ADP-bound G-actin molecules to the filament (Fig. 1.3). Also, certain G-actin-binding proteins distinguish actin monomers depending on the bound nucleotide. Actin-depolymerizing factor cofilin, for instance, binds preferentially to the ADP-actin monomers that accumulate toward the pointed end of the filament, accelerating their dissociation. Other proteins such as profilin and thymosin-$\beta 4$ bind ATP-actin with higher affinity than ADP-actin, maintaining a pool of ATP-actin monomers ready for assembly to the (+)-end of the filament. However, how the bound nucleotide, ATP or ADP, affects the conformation of the molecule remains an active area of research for almost 20 years. Although a number of G-actin crystal structures have been solved in the ATP and ADP state, the conformational transition induced by a change of the nucleotide state is still not understood, though several hypotheses have been postulated. Crystal structures and electron microscopy (EM) have revealed different conformations of the DNase I binding loop and changes in the width of the inter-domain cleft. However, the conformations of ATP– and ADP–actin are remarkably similar in most G-actin crystal structures. So we lack a consistent basis for the observed differences in biochemical assays.

1.2.4.1 Open *vs* closed state

The U-shape of the actin monomer allows movements between pairs of subdomains, and it has been shown that the largest degree of hinge motion appears to be between subdomains 1 and 3 at the base of the nucleotide binding cleft [27]. Thus, it has been proposed that the largest conformational change of the actin monomer is associated with a transition between an open-cleft structure, 'open state', and one where the cleft between the two domains is closed ('closed state'). Other proteins with a fold similar to that of actin show such a conformation change: hexokinase, as part of its catalytic mechanism [28] and Hsp70-related proteins adopt an open state that is regulated by binding of nucleotide exchange factors [29]. Further, numerous other approaches such as kinetics of nucleotide exchange [30, 31], actin sensitivity to limited proteolysis [32, 33] and synchrotron X-ray radiolysis [34] made observations consistent with an equilibrium between open and closed cleft conformations with of G-actin. In contrast to the biochemical studies that imply a high level of structural plasticity, actin crystal structures available to date paint a different picture. All but one of them found actin in a conformation with the nucleotide binding cleft closed. However, in a particular crystal form of profilin-bound G-actin, the cleft between the two domains is significantly larger. This open nucleotide site conformation (Protein Data Bank (PDB) [35] entry 1HLU [14]) has been the most compelling, and frequently quoted, structural evidence for an open conformation of the actin nucleotide. Varying interpretations of this structure exist. Some have argued that this is the conformation of ADP-bound G-actin [36, 37], while the closed state corresponds to the ATP-bound state of G-actin. The other view is that any nucleotide-bound form of actin exists in the closed conformation and the open conformation represents the nucleotide-free form and that the opening of the actin structure might have been induced by the binding of profilin which serves as a nucleotide exchange factor [15, 25]. The hypothesis of the open state crystal structure corresponding to the ADP-bound conformation of G-actin raises several issues. In the open state crystal structure PDB entry 1HLU, the bound nucleotide is actually ATP, not ADP. Furthermore, in another crystal structure of profilin bound actin that was reported (PDB entry 2BTF) actin adopted the closed conformation. Finally, for the formation of the open state crystals, a salt molarity of 1.8 M KPO_4 appears to be crucial. When the molarity was changed from 1.8 M to 3.6 M, the dimensions of the unit cell decreased to that of a closed state crystal, raising

doubt about the stability of the open state structure outside the crystal lattice. For these and other reasons the relevance of this structure to the putative open conformation in solution has been questioned [15, 16].

1.2.4.2 Relation between nucleotide state and DNase I binding loop

The first crystallographic structure solved in absence of any actin-binding proteins is PDB entry 1J6Z by Otterbein *et al*. [21] Actin was rendered non-polymerizable with a large hydrophobic probe, tetramethyl-rhodamine, which was covalently bound to the C-terminus. A significant conformational change detected in the ADP-bound actin crystal structure 1J6Z is the α-helical conformation of the DNase I binding loop in subdomain 2. In contrast, the loop is either unresolved [22, 25] or disordered [14, 20] in the majority of other G-actin crystal structures (see Fig. 1.6 for various conformations of the loop). Such conformational variability might be expected to be associated with large sequence variability, but subdomain 2 is actually the most conserved part of the actin molecule. Because PDB entry 1J6Z was the first crystal structure of uncomplexed ADP-bound actin, it has been hypothesized that based on the nucleotide state of actin, the sensor loop (PRO70-ASP78) in the nucleotide binding site may induce a conformational transition in subdomain 2 from disordered loop (ATP-state) to α-helix (ADP-state) [21]. Although a crystal structure with an α-helical DNase I binding loop was never reproduced, some computational studies are consistent with a nucleotide-induced loop-to-helix transition. An MD study of monomeric actin found the α-helix to be more stable in ADP-bound G-actin than the ATP-bound form [38]. However, while the study observes helix to loop transition (*i.e.* unfolding) when ADP is exchanged for ATP in the nucleotide binding pocket, the reverse transition – formation of an α-helix – was not demonstrated.

Another computational study investigated the influence of the state of the bound nucleotide on the conformational free-energy landscape of actin [39]. A similar relative free-energy of the folded and unfolded states of the DNase I binding loop was found in the ADP-bound monomer. However, the study suggests the folded DNase I binding loop to be stable and in a free-energy minimum in the ADP-bound actin trimer (and thus the filament). Others have contested that a helix in subdomain 2 represents a structural determinant for discrimination between ATP and ADP states of actin. Sablin *et al*. suggested
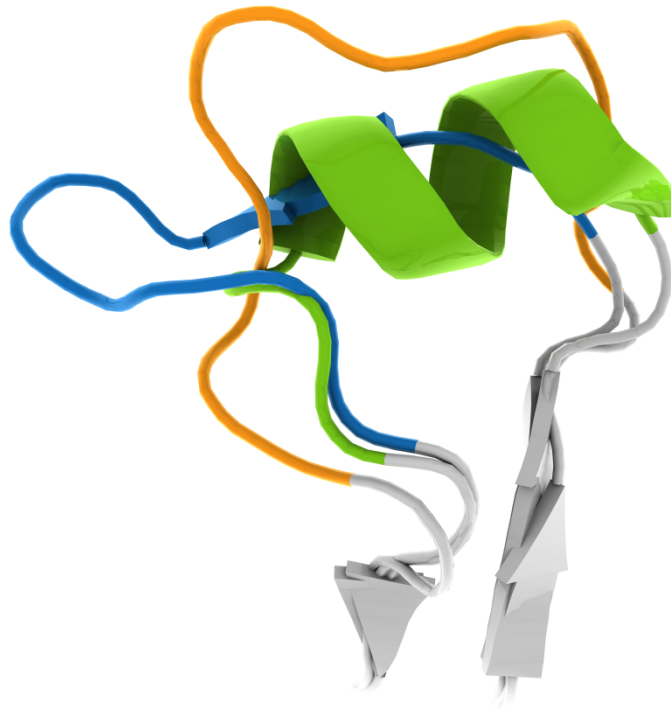
Fig. 1.6. Different conformations of the DNase I binding loop. In most crystal structures the loop is not resolved. In the structure of PDB entry 1ATN the loop forms a β-strand (blue), in PDB entry 1J6Z the loop forms an α-helix (green) and a unstructured open loop in the protomers of the Oda 2009 model (orange).

that the poorly structured features of subdomain 2 may be designed to accommodate varied binding interactions with other proteins. In the absence of specific binding partners, loops of subdomain 2 could adopt stochastic conformations so that even crystal contacts could alter them. The α-helical DNase I binding loop of subdomain 2 in actin crystals of PDB entry 1J6Z is packed against three helices (amino acid residues 80-93, 223-230, and 252-262, respectively) from two neighboring actin symmetry molecules [21] that might trigger helix formation in this loop [36]. However, in the actin filament these helices are not located near the DNase I binding loop [40]. Another reason for the observation of an α-helical fold in subdomain 2 may be the modification of the C-terminus by covalent addition of tetramethyl-rhodamine [41]. Such modifications of the C-terminus have been shown to be coupled to conformational changes in subdomain 2 and *vice versa*. These interactions exist in both G-actin [42, 43] and F-actin [44]. However, in the crystal structure of

tetramethyl-rhodamine-bound G-actin in the ATP state the DNase I binding loop was disordered [25].

An MD study investigating the nucleotide-mediated conformational changes of monomeric actin found the DNase I binding loop to be highly flexible regardless of the nucleotide state [45]. More recently, additional X-ray structures of G-actin in absence of actin-binding proteins or covalently attached molecules have been solved. Actin was rendered non-polymerizable by introduction of point mutations. The DNase I binding loop was disordered in both the ATP- and ADP state [22].

1.3 The actin filament – the biologically active form

1.3.1 Relation of structure and function in filamentous actin

F-actin is a helical filamentous polymer of globular G-actin subunits oriented in the same direction. The structural and dynamical properties of actin depend on the state of the bound nucleotide [21, 24, 25, 26]. ATP-bound G-actin has a higher binding affinity to the filament than ADP-bound monomers. After assembly to the filament, ATP hydrolysis takes place with a half-time of two seconds, making actin a particularly slow ATPase. However, F-actin hydrolyzes its bound ATP about 40,000 times faster [46] than monomeric actin [22], but the mechanism is a major unsolved challenge [47]. Changes in the nucleotide-binding site, induced by the G- to F-actin transition are assumed to increase the ATPase activity of polymerized actin. Several studies have investigated possible mechanisms of hydrolysis of ATP in actin [48, 49, 50] and showed that in G-actin the conformation of the nucleotide-binding site depends on the bound nucleotide [39, 45]. An experimental study of actin mutants revealed the significance of GLN137 for filament polymerization and cleavage of the γ-phosphate group: replacing this glutamine with an alanine caused a 4-fold slowdown of ATP-hydrolysis [50]. Further, in Ref. [50] it was suggested that the flattening twist of the ATP-bound actin monomer upon integration into the filament leads to relocation of GLN137 bringing it in close proximity to ATP [51]. Furthermore, crystal structures of G-actin show that GLN137 coordinates a water molecule that might attack the bound ATP [21, 25].

Following ATP-hydrolysis, inorganic phosphate is released from the filament with a half-time of six minutes, inducing a conformational transition within the

actin fibril and destabilizing the actin-actin bonds within the filament [52]. This structural change is evident from discrimination between different nucleotide states by various actin binding proteins and from significant differences of the flexural rigidity of ATP- and ADP-bound actin filaments [24]. The underlying structural basis for this conformational transition is not understood. One electron microscopy study suggested that the conformational change that accompanies release of inorganic phosphate from the fibril is an opening of the inter-domain cleft of the protomers [36]. However, others have contested the findings [25, 39] and recent high-resolution fiber diffraction data of F-actin in the ADP-state does not support an open protomer conformation [51].

1.3.2 A brief history of F-actin research

As one of the most abundant proteins in eukaryotes, actin has been a major target of structural studies for decades [53, 54, 55]. X-ray fiber diffraction experiments of the actin filament were carried out as early as 1947 and suggested a helical conformation [56, 57] and this was confirmed in 1963 by electron microscopy [58]. Subsequent cryo-electron microscopic studies of actin in the 1980s reached resolutions of 20-30 Å [59]. All attempts obtain a high-resolution X-ray structure were unsuccessful to date due to the difficulties involved in crystallizing the filament. One of the problems preventing crystallization of F-actin is the tendency of monomeric actin to form polymers of varying lengths. However, a turning point in structural biological research of the actin structure occurred in 1990 when the first X-ray structure of G-actin (in complex with DNase I) was solved [19]. The atomistic structure of G-actin in conjunction with the experimentally obtained radius of gyration of the actin filament and X-ray fiber diffraction patterns of well oriented F-actin sols allowed the construction of the first structure of the actin filament by Holmes *et al*. [40]. The F-actin model structure was obtained by searching for an orientation and position of the actin monomers in the filament that would account for the X-ray fiber diffraction patterns. Only one unique orientation and position was found with a sufficiently small residual error between the model and the experimental pattern. It was also suggested that there is only a small difference between the structure of the actin monomer resolved by X-ray crystallography and the actin monomers in the filament. This assumption formed the basis for following studies to refine the atomic model of F-actin

using different approaches such as a directed mutation algorithm [60], normal mode analysis [61] or electron cryo-microscopy data to complement the X-ray fiber diffraction data [62].

Until recently, the global conformational change of the actin monomer during transition from G- to F-actin, though crucial for understanding actin polymerization, was not well understood. To address this issue, Oda *et al.* combined several technical advances such as controlled filament length and improved parallel orientation of F-actin sols by the use of an superconducting magnet (actin filaments are diamagnetic). The final resolution of the fiber diffraction patterns that was obtained was 3.3Å in the radial direction and 5.6 Å along the equator. A model of the F-actin structure was constructed by altering the crystal structure of G-actin (PDB entry 1J6Z) [21] by use of the normal modes of actin and a molecular dynamics simulation. The high resolution model of the filament revealed the major conformational change that occurs during the incorporation of G-actin monomers into the filament: the protomers within the filament have a flatter global conformation that is achieved by a 20° domain rotation. This rotation is reflected in a twist of the two domains that has been termed 'propeller rotation' and is discussed below. The conformational transition proposed by Oda *et al.* is convincing in its simplicity [63] but the model itself needs further testing. As an attempt to further improve the Oda 2009 model a new F-actin structure – called the Holmes 2010 model – was proposed and is discussed as part of this thesis (Chapter 5). This model is based on the global conformation of the Oda model but differs in the structural details at the interface.

Propeller Rotation

It has been shown that the U-shape of the actin monomer allows movement between the two large domains [27]. In addition to the opening/closing motion of the structure, discussed in Chapter 1.2.4.1, a propeller-like rotation of the two domains has been observed [64].

A similar movement of domains has also been observed in hexokinase [65, 66], Hsc70 [67], and ARP2/3 [68], all structural homologs of actin [69], suggesting that such an inter-domain hinge motion is common to proteins in this superfamily [70]. The hinge around which this motion occurs is located around the residue GLN137 and the α-helix formed by residues 331–337 [71]. The biological significance of the propeller rotation stems from the hypothesis that GLN137 is involved in the activation of ATPase activity of the actin molecule

following G- to F-actin transition. Because GLN137 is located at the hinge between the two domains, the propeller angle of the actin molecule might determine the position of the residue and thus induce the hydrolysis of the bound ATP. Indeed, in G-actin the two domains are related by a propeller-like twist but it has been shown that upon integration of actin monomers into the filament the propeller angle changes by about 20°, which reduces the twist and flattens the molecule (Fig. 1.7) [63]. This newly found flat conformation of the actin molecule is featured in the Oda 2009 filament model but not earlier models of F-actin [51].

G-actin   **G-actin**   **F-actin**

Fig. 1.7. Propeller rotation of the actin monomer. In G-actin (shown in cartoon and schematic view) the two domains are twisted in a propeller-like fashion by ~20°. During the transition from G- to F-actin the propeller angle is reduced, which results in a flat conformation of the actin molecule.

Hyrophobic plug

When the first actin filament model was proposed in 1990, K. C. Holmes and colleagues suggested the importance of a loop with a hydrophobic tip (GLN263-SER271) located between subdomains 3 and 4, the so-called 'hydrophobic plug', for the structural stability of F-actin [40]. In their model the loop was rebuilt into a β-hairpin that protrudes from the actin surface and extends to a hydrophobic pocket on the surface of the opposite strand, thus stabilizing the filament structure (Fig. 1.8). Several biochemical experiments support this observation [72, 73, 74]. It was shown that mutations in the hydrophobic plug produce effects consistent with a weakening of this proposed plug-pocket interaction and lead to disassembly of filaments at 4 °C [72]. However, some experimental studies [74, 75] demonstrated that rather than being in the

extended position, the hydrophobic plug resides predominantly in a 'parked' position within the filament but is able to dynamically populate other conformational states.
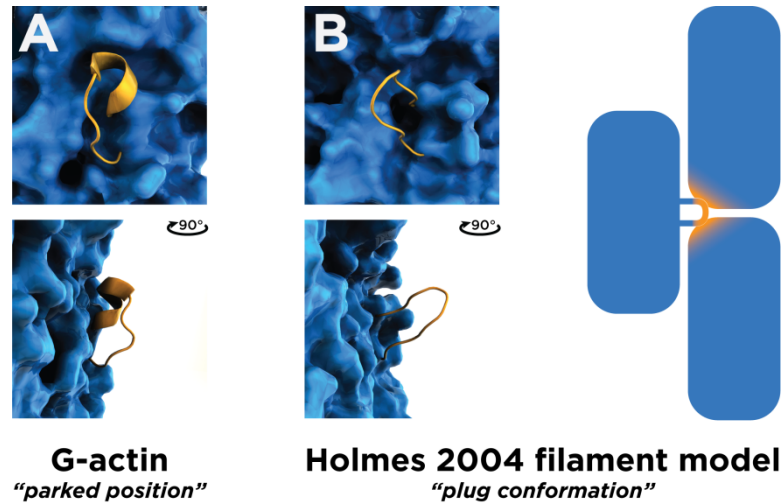

G-actin
"parked position"

Holmes 2004 filament model
"plug conformation"

Fig. 1.8. The hydrophobic loop (GLN263-SER271) in G-actin and F-actin models.
A - In G-actin crystal structures, the Oda 2009 and Holmes 2010 models, the loop (orange) is in a 'parked' position, close to the surface of the protein.
B - In the Holmes 1990 and 2004 filament models the hydrophobic loop (orange) was modeled to extend from the surface of the protomer and reach into a hydrophobic pocket of the opposite strand of the filament, thus called 'hydrophobic plug'.

The early filament models were built to fit the published radius of gyration of 25 Å, but later the three-dimensional map independently reconstructed from cryo-electron micrographs at the resolution of 13.8 Å suggested a smaller diameter of 23.7 Å. The smaller diameter is generally accepted by the time of writing. Because of the narrower inter-strand gap, it seems unlikely that the hydrophobic plug largely alters its conformation upon G- to F-actin transition [51]. However, older filament models such as the Holmes 2004 model still contain the extended hydrophobic plug and have a larger radius of gyration (24.8 Å) while newer filament models have the smaller radius of gyration (23.7 Å) and a hydrophobic loop in the 'parked' position, either identical with the loop conformation in G-actin (Holmes 2010 model) or slightly modified (Oda 2009 model).

1.4 Approach of this study

The present work is aimed at shedding light on the nucleotide-induced conformational changes in G-actin that promote filament polymerization in ATP-bound G-actin but not the ADP-bound form. This study focuses in particular on the question whether the open state structure of G-actin is thermodynamically stable. MD simulations have been carried out to model the thermodynamic properties of the open state actin X-ray structure, outside the crystal lattice, in an aqueous environment with profilin removed. To investigate the effects of the nucleotide on the actin structure unbiased by profilin, additional simulations were performed using other X-ray structures of higher resolution. Furthermore, all simulation models were carried out both, with ATP and ADP in the nucleotide-binding site. Structural properties of the resulting actin trajectories were calculated.

The atomistic structure of the actin filament is unknown. Here, a comparison is made of the Holmes 2010, Oda 2009 and the Holmes 2004 filament models using molecular dynamics simulation. A number of structural determinants were analyzed such as the protomer propeller angle, the number of hydrogen bonds and the structural variation among the protomers and validate the quality of the structural models.

In addition, simulations of the Holmes 2010 model are carried out in states with ATP or ADP bound and local hydrogen-bonding differences are analyzed in order to characterize the differences between ATP and ADP filament and address the activation mechanism of ATPase activity in F-actin which currently is not well understood.

CHAPTER 2

METHODS

This chapter presents the theoretical foundations of the present work. First, an introduction to the different G- and F-actin structures used in this study is presented. Next, a molecular modeling introduction is given, including energy minimization methods and a description of the molecular dynamics simulation technique and the potential energy function (force field) used. Finally, the different observables used to analyze the simulated actin structures are introduced.

2.1 Simulation models

A summary of the simulation models and the system sizes is given in Table 2.1.

Monomer Simulation

PDB entry	Actin state	Bound Profilin	Nucleotide	System size [atoms]	Simulation time
1HLU	Open	No	ATP	77,321	10 x 4 ns
1HLU	Open	Yes	ATP	122,034	10 x 4 ns
2BTF	Closed	No	ATP	77,321	20 x 4 ns
1HLU	Open	No	ADP	77,328	10 x 4ns
1HLU	Open	Yes	ADP	122,025	10 x 4 ns
2BTF	Closed	No	ADP	77,343	20 x 4 ns
MD structure	Superclosed	No	ATP	77,321	20 x 1 ns
MD structure	Superclosed	No	ADP	77,343	20 x 1 ns
2HF4	Closed	No	ATP	77,300	10 x 4 ns
2HF3	Closed	No	ADP	77,357	10 x 4 ns
1J6Z	Closed	No	ADP	77,324	13 x 30 ns

Filament Simulation

Model	# of Actin molecules	Nucleotide	System size [atoms]	Simulation time
Holmes 2004	13	ADP	597,540	30 ns
Oda 2009	13	ADP	601,443	30 ns
Holmes 2010	13	ADP	601,413	30 ns
Holmes 2010	13	ATP	601,476	30 ns

Table 2.1. Overview of the models studied by MD simulation.

2.1.1 G-actin

The first set of simulations investigates the stability of the open state as a function of nucleotide and profilin binding. The only existing X-ray structure of G-actin with an open cleft, PDB entry 1HLU [14], was used to model the open state. The co-crystallized profilin was included in one set of simulations and removed in a further set.

Closed state simulations were conducted based on two PDB structures:

> 1) PDB entry 2BTF [20], chosen because the amino acid sequence is identical with that of the 1HLU structure, used in the open-state simulations. The profilin coordinates were removed.

> 2) To examine whether the results of closed state simulations based on PDB 2BTF also hold for other PDB structures, simulations were also performed on PDB entry 2HF3 for the ADP-state and 2HF4 for the ATP-state [22]. Unlike 1HLU and 2BTF, 2HF3 and 2HF4 are from *Drosophila melanogaster* and are unbiased by co-crystallized proteins or attached molecules. Instead, actin was rendered unpolymerizable by introducing two point mutations. Here, these mutations were reverted so as to simulate actin in its native form.

Another set of simulations was performed, using two models aimed at determining the stability of a newly-found 'superclosed' state, described below, as a function of the bound nucleotide. Since the superclosed state has a cleft size of around 13.7 Å, the starting structure for these simulations was chosen as the lowest-potential energy structure from all closed-ATP-simulation structures with cleft sizes in the range 13.6 to 13.8 Å. For the simulations of the superclosed state with ADP in the nucleotide binding pocket, the γ-phosphate group of ATP was removed and the number of counter ions adjusted to neutralize the system.

2.1.2 F-actin

Actin filaments consist of identical actin molecules (protomers). Each of these protomers contains 375 residues (without ATP or ADP). F-actin models in this study consist of 13 protomers, corresponding to a 180° turn of the helical actin filament. The filament model by Holmes *et al.* [40] was employed to determine the initial organization among protomers in the filament: the actin molecule rotates 166.2° clockwise and translates 27.5 Å along the longitudinal axis to generate the filament. After 13 rotations, the monomer roughly repeats itself in the longitudinal axis. Protomers of the Holmes 2004, Oda and Holmes 2010 models are based on the modified structure of ADP-G-actin, PDB entry 1J6Z.

2.1.3 Preparation of protein structures

In all simulations of G-actin and F-actin the crystallographic or modeled structures were prepared as follows. The N-terminal residue was acetylated and the protonation states of the histidine residues were derived by calculating pK values using the H++ webserver [76]. *In vivo* HIS73 is methylated and has been shown to be a structural determinant of actin that may be involved in phosphate release [77]. Experiments suggest this methylation to be a major determinant of stability and conformational flexibility of the actin monomer [77]. Hence, a patch was applied to HIS73 to remove the relevant hydrogen atom and replace it with the methyl group, using standard CHARMM parameters. The proteins were solvated with 12 Å of water. Overlapping water molecules within 1.4 Å of the protein were deleted. The resulting cubic boxes have an edge length of 91 Å for the simulations of G-actin without profilin and 104 Å for the simulations of profilin-bound G-actin. The rectangular boxes used in the simulations of F-actin models have an edge length of 125 Å in the square cross-section (Fig. 2.1). The length of the box is 358 Å, allowing the filament ends to interact seamlessly with the corresponding filament ends of the images generated by periodic boundary conditions. This setup generates a virtual infinite filament without solvent-exposed ends. Thus each protomer is exposed to the same environment.
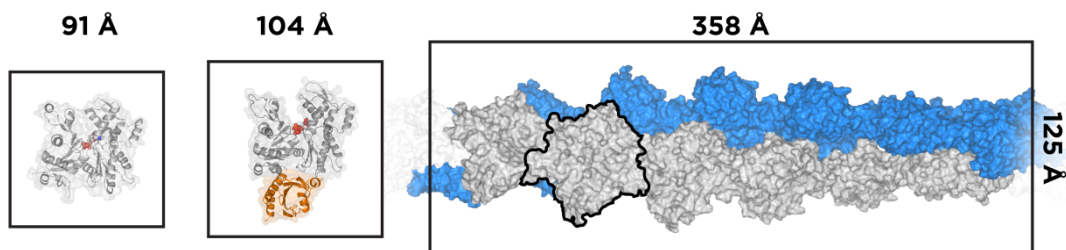
Fig. 2.1. System setup. MD simulations of G-actin were carried out in a cubic simulation box containing TIP3P water of 91 Å length. The primary simulation cell of profilin-bound actin had a length of 104 Å. The 13-subunit repeat of an F-actin model is shown in its rectangular simulation box with of 358 Å length with one protomer highlighted. Periodic boundary conditions produce longitudinal periodicity of the helical filament.

Physiological concentrations of 139 mM K$^+$, 12 mM Na$^+$ and 16 mM Cl$^-$ were used, mimicking cytosolic conditions, and the number of Cl$^-$ ions was adjusted to produce overall charge neutrality. In the crystallographic structures of G-actin calcium or strontium ions are present in the nucleotide binding pocket. These were replaced by a magnesium ion, again to reflect *in vivo* conditions [17]. Apart from the tightly bound magnesium ion in the nucleotide binding site, several low-affinity binding sites for divalent cations have been observed in crystal structures of G-actin. However, some of these binding sites may be artifacts of protein crystallization. Occupation of these low-affinity cation binding sites induces polymerization of the actin filament, suggesting their importance for the integrity of the F-actin polymer [17]. Therefore, it was decided to include these cations in the molecular dynamics simulations of the filament models. We scanned the PDB for X-ray structures of G-actin that included any low affinity binding sites and chose to use those sites that have been reported in at least two structures, derived independently from each other. As a result it was decided to place magnesium ions in the following three locations on the surface of each actin protomer: ASP286/ASP288, GLU270/SER271 and ASP222/GLU224.

Most of the simulations were carried out both of the ATP- and ADP-bound state of actin monomer or filament. These simulations are mostly based on the same crystallographic or modeled structures where one nucleotide was exchanged for the other.

PDB entries 1HLU and 2BTF represent ATP-bound G-actin. For simulations of these structures in the ADP-state, the γ-phosphate group was removed from the nucleotide and replaced by two water molecules.

To generate the ATP-bound form of the Holmes 2010 filament model, the ADP coordinates were replaced with the ATP coordinates of the ATP-G-actin structure of PDB entry 1ATN [19] before the structure was solvated.

2.2 Computer simulations of proteins

Molecular dynamics (MD) simulation provides the methodology for detailed modeling on the atomic scale. This technique is a scheme for the study of the natural time evolution of the system that allows prediction of the static and dynamic properties of biomolecules directly from the underlying interactions between the atoms. Dynamical simulations monitor time-dependent processes in molecular systems in order to study their structural, dynamic, and thermodynamic properties by numerically solving Newton's equation of motion. Thus, MD provides information about the time dependence and magnitude of fluctuations in both positions and velocities.

The structure of a protein is determined by its potential energy landscape whose global minimum corresponds to the native state. The energy landscape of a protein is described by its potential energy, which in the case of biological systems is a complicated, multidimensional function of the *3N* Cartesian coordinates of the system. The energy landscape of a biomolecule possesses an enormous number of minima, or conformational substates. Because proteins are complex biological systems containing several hundreds to thousands of atoms, accuracy has to be sacrificed to a reasonable extend for computational efficiency when simulating these large systems.

This is the aim of empirical potential energy functions *i.e.* molecular mechanics force fields, which are used as an alternative to quantum chemical calculations, the computational cost of which renders their use unfeasible for multi-atomic systems of the size of proteins. The empirical force fields were developed to describe molecular structures and properties in an accurate manner while being computationally efficient. However, the approximations introduced in this method lead to limitations compared to quantum chemical calculations. For instance no bond breaking or making events can be modeled via molecular mechanics since electrons are not considered explicitly. One of the basic assumptions underlying all molecular mechanics force fields is the validity of the Born-Oppenheimer approximation of the Schrödinger equation, *i.e.* the decoupling of electronic and nuclear degrees of freedom. The energy of

the system is written as a function of the nuclear positions only. Thus, nuclear motions, vibrations and rotations can be studied independently from electronic fluctuations since the electrons are assumed to adjust instantly to any movement of the nuclei.

In molecular mechanics, the nuclei and electrons are treated together as spherical atom-like particles possessing a net point charge [78]. The radii and the net charges are measured experimentally or obtained from high-level quantum calculations. The interactions between atoms are based on harmonic approximations or classical potentials and determine the spatial distribution of atoms and their corresponding energies. The potential energy function used to calculate the energy and geometry of a molecule is called the force field. Further, atom types have to be defined to describe the atoms in a molecule. Parameters for bond lengths, bond angles, *etc.* are also required.

Current generation force fields provide a reasonably good compromise between accuracy and computational efficiency. Their ability to reproduce experimentally-measured physical properties has been extensively tested. These properties include structural data obtained from X-ray crystallography and nuclear magnetic resonance spectroscopy (NMR), dynamic data obtained from spectroscopy and inelastic neutron scattering as well as thermodynamic data. Among the most commonly used potential energy functions are the AMBER [79], CHARMM [80], OPLS [81] and GROMOS [82] force fields.
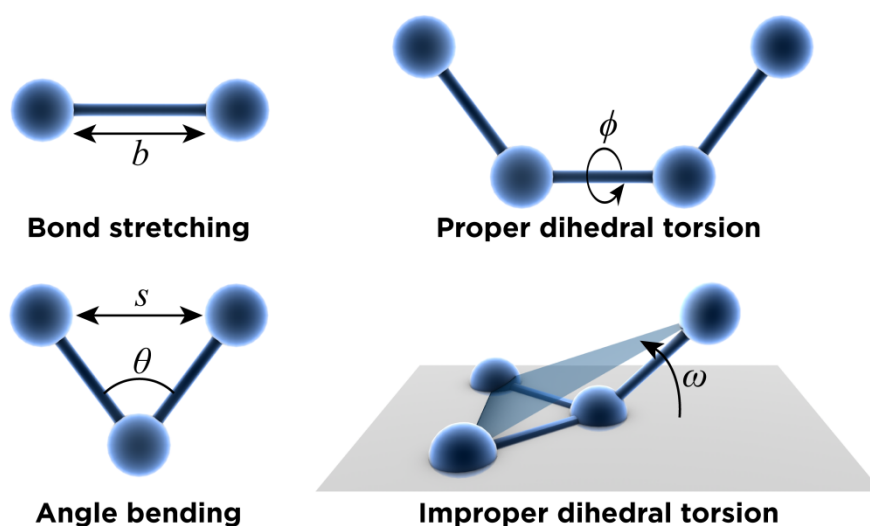

Fig. 2.2. Schematic representation of the bonded interaction terms contributing to the CHARMM force field: bond stretching, angle bending, proper and improper dihedral torsions.

The energies of the biomolecules studies in this thesis were calculated using the CHARMM 22/27 force field. In the CHARMM force field, the potential energy is calculated as a sum of bonded and non-bonded energy terms. The bonded terms, E_{bonded} describe the energy of the protein in terms of bond stretching, angle bending and dihedral rotation as explained in Fig. 2.2. The non-bonded terms, $E_{nonbonded}$ account for interactions between non-bonded atoms *i.e.*, atoms separated by 3 or more covalent bonds. The total energy, E_{total} is given by:

$$E_{total} = E_{bonded} + E_{nonbonded}$$

$$= \underbrace{E_{bonds} + E_{angles} + E_{impr} + E_{UB} + E_{dihedrals}}_{E_{bonded}} + \underbrace{E_{vdW} + E_{elec}}_{E_{nonbonded}}$$

where, E_{bonds} is the bond stretching energy term, E_{angles} is the angle bending energy term, $E_{dihedrals}$ accounts for rotation along a bond, E_{impr} is the distortion energy term, E_{UB} is the Urey-Bradley term, E_{vdW} the van der Waals energy and E_{elec} the electrostatic energy. E_{bonds} is given by a harmonic potential representing the interaction between atom pairs separated by one covalent bond (*i.e.* 1,2-pairs). The term accounts for the energy of a bond length, b as a function of displacement from the ideal bond length, b_o. The force constant, K_b determines the strength of the bond. Both, the ideal bond length, b_o and the force constant, K_b depend on the chemical type of the atom-constituents and are specific for each pair of bound atoms.

$$E_{bonds} = \sum_{bonds} K_b (b - b_0)^2$$

E_{angles} accounts for deviations of the bond angles, θ from the equilibrium values θ_0 with a harmonic potential.

$$E_{angles} = \sum_{angles} K_\theta (\theta - \theta_0)^2$$

The Urey-Bradley (E_{UB}) term is an interaction term based on the distance between atoms separated by two bonds *i.e.* atoms bound to a common atom (1,3-configuaration):

$$E_{UB} = \sum K_{UB}(s - s_{eq})^2$$

where K_{UB} is the Urey-Bradley force constant and s the distance between the two atoms in consideration.

The torsional terms are weaker than the bond stretching and angle bending terms. They describe the rotational barriers existing between four bonded atoms. There are two types of torsional terms: proper and improper dihedrals. Proper torsional potentials represent the torsion angle potential function which models the presence of torsional barriers between atoms separated by 3 covalent bonds (*i.e.* 1,4-pairs). The term describes the rotation by a dihedral angle, ϕ around a given bond with force constant, K_ϕ, phase, γ and multiplicity, n.

$$E_{dihedrals} = \sum_{1,4-pairs} K_\phi \left(1 + \cos(n\phi - \gamma)\right)$$

The improper dihedral term is designed both to maintain chirality about a tetrahedral heavy atom and to maintain planarity about certain atoms. It is described by a harmonic function:

$$E_{impr} = \sum K_\omega \left(\omega - \omega_{eq}\right)^2$$

where ω is the angle between the plane formed by the central atom and two peripheral atoms and the plane formed by the peripheral atoms.

The contribution of non-bonded interactions has two components in the energy function: the van der Waals interaction energy and the electrostatic interaction energy. The calculation of these interactions is the most time-consuming part, because they contain long-range interactions of the atoms in the system. In the CHARMM force field, the hydrogen bond interactions are accounted for by the electrostatic and van der Waals interactions.

The van der Waals force acts on atoms in close proximity (short-range interactions). At short range it is strongly repulsive and at medium range it is weakly attractive. The van der Waals term, E_{vdW} is commonly modeled by a Lennard-Jones 12-6 potential. The Lennard-Jones potential arises from a balance of two terms, a short range repulsive and a slower decaying attractive force. The attractive $^1/_{r^6}$ -term arises from spontaneous dipoles including opposing dipoles in nearby atoms. The repulsive force is predominant at short distances where the electron-electron repulsion is strong. The Lennard-Jones potential is determined by two parameters: the collision parameter, σ and the depth of the potential, A. The collision parameter is the distance between two atoms at which the van der Waals energy is zero.

$$E_{vdW} = \sum_{i,k} A \left(\frac{\sigma_{ik}}{r_{ik}^{12}} - \frac{\sigma_{ik}}{r_{ik}^{6}} \right)$$

In order to reduce the number of interaction terms and thus the calculation time, the Lennard-Jones potential is often truncated. This is done by defining an appropriate cutoff distance and calculating the pair-wise interactions only for the atoms lying within this distance. All van der Waals interactions of atoms beyond this cutoff are set to zero. Several methods have been developed for the truncation of the Lennard-Jones term. One way is to abruptly set the potential to zero at the cutoff distance. However, this causes discontinuities in the force at the cutoff distance. An alternative method is to shift the whole potential to higher values so as to achieve a zero value exactly at the cutoff distance. This method leads to an artificially-induced overestimation of the Lennard-Jones potential. Another method is to use a switching function to taper the interaction potential over a predefined range of distances. The potential takes its usual value up to the first cutoff and is then switched to zero smoothly between the first and the second cutoff. This model suffers from strong interaction forces in the switching region.

E_{elec}, the electrostatic interaction between a pair of atoms is represented by the Coulomb potential. The Coulomb potential is inversely proportional to ϵ, the effective dielectric function for the medium and r_{ik}, the distance between two atoms with charges q_i and q_k.

$$E_{elec} = \sum_{i,k} \frac{q_i q_k}{\epsilon r_{ik}}$$

In MD simulations, the force field described above is used to study the temporal behavior of molecules. In most computational studies of complex systems such as biomolecules, it is the classical mechanics Newtonian equation of motion that is being solved rather than the quantum mechanical equation. In its most simplistic form, Newton's equation of motion states that

$$F_i = m_i a_i$$

where F_i is the force acting on particle i, m_i is the mass of particle i, a_i is its acceleration. The force F_i is determined by the gradient of the potential energy function, which is a function of all the atomic coordinates r.

The first MD simulation dates back to the year 1957. Alder and Wainwright investigated phase transition behavior in a system of hard-spheres. But it took another twenty years for the first simulation of a protein to become feasible. In 1977 McCammon *et al.* simulated the bovine pancreatic trypsin inhibitor, BPTI in vacuum for a timespan of ~9ps [83]. Today molecular dynamics simulations are a common tool for theoretical studies on biological macromolecules such as proteins. Of particular interest is the broad range of characteristic motions that are displayed by proteins. These range from the fast and localized motions characteristic of atomic fluctuations to the slow large-scale motions involved in the folding transition. Many of these motions, on each and every time scale, have an important role in the biological function of proteins.

2.2.1 Molecular dynamics simulation setup

All MD calculations were performed using the NAMD simulation package [84]. The CHARM22/27 [80] force field, in conjunction with the particle mesh

Ewald sum method [85], was used in calculating electrostatic interactions. All intra-molecular hydrogen bonds were constrained using the SHAKE [86] algorithm, allowing for an integration time step of 2 fs.

The TIP3P water model [87] was used for the simulation of explicit solvent. A smooth switching function at 8 Å and a cutoff of 10 Å was applied for short-range electrostatics and van der Waals interactions. Long-range electrostatic interactions were computed with the particle mesh Ewald procedure [85] and were updated every 4 fs. The systems including G-actin were minimized using the conjugate gradient algorithm for 5000 steps with the protein and nucleotide atoms harmonically constrained. The simulation systems with F-actin were energy minimized using the conjugate gradient algorithm for 30000 steps with the protein and nucleotide atoms harmonically constrained during the first 20000 steps.

The MD simulations were performed using the leap-frog integrator in the isothermal-isobaric ensemble (NPT) at 1 atm pressure, with periodic boundary conditions applied. The Nosé-Hoover Langevin piston [88] was employed, using a decay period of 500 fs for the simulations of G-actin and 50 fs for the filament simulations. The systems were gradually heated to 300 K with the harmonic constraints still in place. In the simulations of G-actin the constraints were gradually lifted ($0.5 \rightarrow 0.25 \rightarrow 0.05$ kcal/mol/Å^2) during the three subsequent equilibration steps of 25 ps length each. After the heating and equilibration period 4 ns of production run were carried out for each simulation. For each G-actin system, 10 or 20 individual molecular dynamics simulations were carried out by assigning different initial distributions of starting velocities to the minimized protein structure. In contrast, only one simulation was carried out for each F-actin system. Following two equilibration steps of 100 ps length each, constraints on C-atoms were gradually lifted ($1 \rightarrow 0.1 \rightarrow 0$ kcal/mol/Å^2) and 30 ns of production run were carried out for each F-actin system.

The majority of the computations of the G-actin systems were performed on the HeLiCs supercomputer (http://helics.unihd.de) at the Interdisziplinäres Zentrum für Wissenschaftliches Rechnen (IWR) in Heidelberg. Simulations of the F-actin systems were carried out on the Jaguar Cray XT supercomputer at the National Center for Computational Sciences at Oak Ridge National Lab (Fig.2.3).

Fig. 2.3. The computationally most expensive calculations of this work were carried out on the Cray XT5 supercomputer 'Jaguar' at the National Center for Computational Sciences, Oak Ridge National Laboratory, which is the world's fastest supercomputer at the time of writing. (Image courtesy of the National Center for Computational Sciences)

2.3 Analysis

There are many different possible ways of analyzing MD trajectories. The quantities relevant for this study can be calculated directly from the trajectories of the atoms in the system. Some of the observables can then be compared to the values obtained experimentally. It is also possible to calculate quantities inaccessible to experiments which enable new ways of understanding the system under scrutiny.

To assess the quality of the structures of the three filament models by MD simulation, properties determining structural defects and the stability of models were calculated. For some of these properties a meaningful comparison among the three models is possible only on the level of the protomer. For example, when calculating the RMSD of the entire MD filament structure, a slight bending of the 13-subunit repeat that does not affect the filament's structural integrity, would result in a large increase in RMSD, overshadowing localized structural defects such as unfolding of secondary structure elements that lead to smaller increases in RMSD. Moreover, only those properties calculated on the protomer level may be compared with the simulations of G-

actin. Therefore, most properties were assessed on the level of the protomer structure of actin and then averaged over the 13 protomers in the filament.

Nucleotide Depth

The nucleotide phosphate groups may be buried to various extents in the nucleotide binding cleft. In this regard the open and closed X-ray structures differ greatly: in the closed state, the nucleotide is positioned deep in the binding pocket, while in the open structure it is almost outside the pocket (Fig. 2.4).
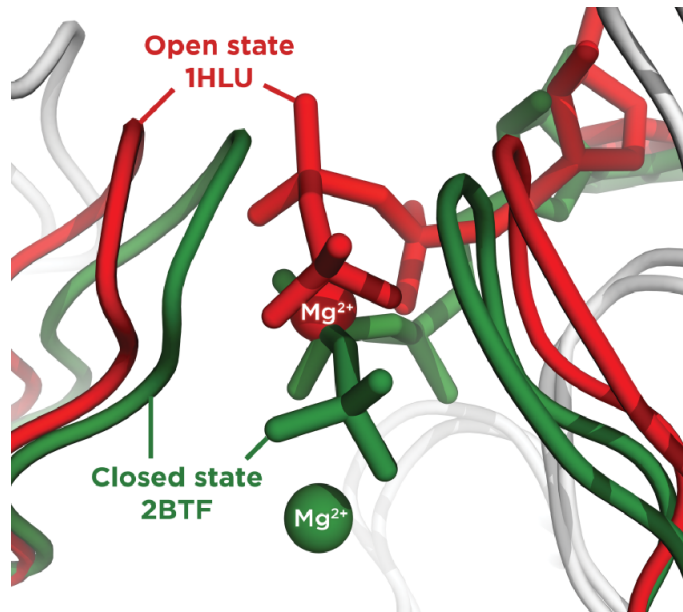

Fig. 2.4. The nucleotide binding site of actin crystal structures PDB entry 1HLU (red, open state) and 2BTF (green, closed state). For clarity, the phosphate sensor loop is not shown. In the closed state ATP is buried in the nucleotide binding pocket with the two binding loops closed above. In contrast the ATP of the open state is located 2.8 Å away from the binding pocket, wedged between the two binding loops.

Determination of the relative nucleotide position in the MD trajectories is non-trivial because of the flexible topology of the binding pocket. The following procedure was adopted. The crystallographic open and closed structures were superimposed using least-squares alignment and a 'depth vector' defined, connecting the positions of the two β-phosphate atoms. The structure of every MD frame was then least-squares aligned with the open-state

structure. For a given trajectory frame the nucleotide depth is defined as the distance between the projection of the β-phosphate onto the depth vector and the position of the open state β-phosphate (Fig. 2.5). A nucleotide depth value of zero corresponds to the open state nucleotide depth and a value of 3.3 Å to that of the closed state.
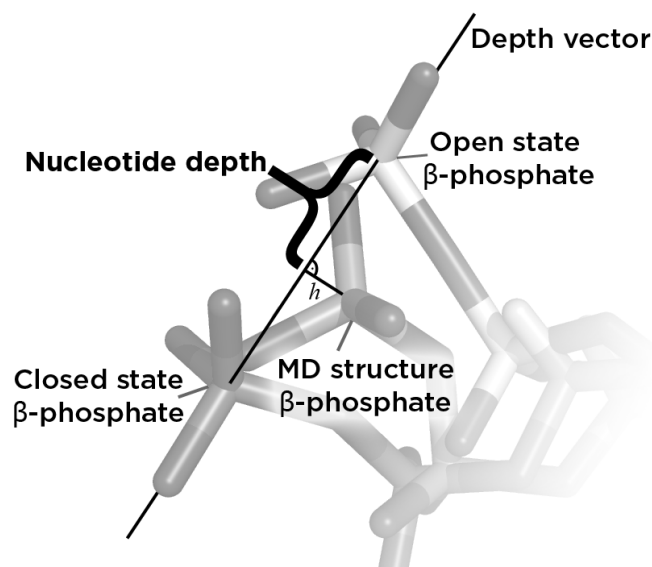

Fig. 2.5. The nucleotide depth. The projection of the - phosphate onto the depth vector allows the effective nucleotide depth to be calculated relative to the two states. The distance between this projection and the open state - phosphate position is defined as nucleotide depth.

Subdomain rotation

The program DynDom Domain Select [89] determines axes and degrees of rotation of domains between two structures. For this calculation, subdomains 1 and 3 of the two structures were aligned with an RMSD fit and the rigid-body movements of subdomains 2 and 4 were then determined using DynDom.

Monomer propeller angle

An actin monomer consists of four subdomains which form a U-shaped structure (Fig. 2.6). The dihedral angle between the centers of mass of the four subdomains (excluding the very flexible DNase I binding loop, ARG39-LYS50, and the hydrophobic plug, GLN263-SER271) is referred to here as the 'propeller angle'. A lower angle corresponds to a flatter structure of the actin molecule.
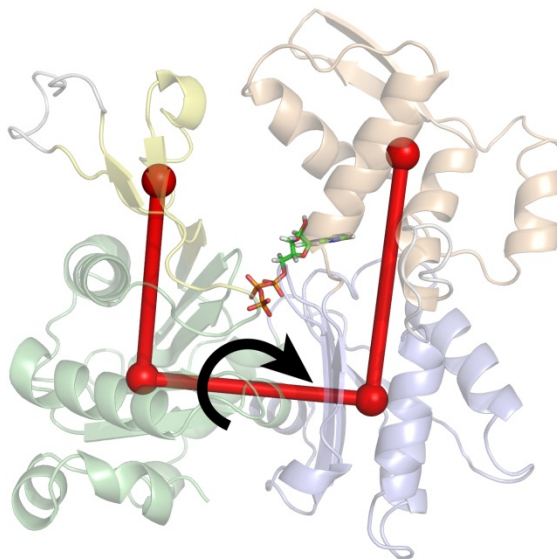
Fig. 2.6. The propeller angle is the dihedral angle, formed by the centers of mass of the four subdomains. It is significantly lower in F-actin than G-actin.

RMS deviation over protomers

To examine structural variation among the individual protomers in the 13-subunit repeat, an appropriate RMS backbone atom deviation was calculated: For any given time step the average protomer structure was calculated from the 13 actin molecules and the RMS deviation of this average protomer structure from each of the 13 actin molecules was calculated and averaged.

Hydrogen-bonding patterns and calculation of average protomer

Default CHARMM settings with a distance cutoff of 2.4 Å and no limit of the angle of linearity were used to determine the hydrogen bonds. Patterns of hydrogen bonds between the nucleotides and protein are summarized in Tables 5.1-5.3. The occupancy of each hydrogen bond over the last 5 ns of the simulation was calculated for each protomer, and averaged over the 13 protomers. In some protomers a change in position of the nucleotide within the binding pocket changed lead to an atypical hydrogen binding pattern. To calculate meaningful average interactions, hydrogen bonds formed during more than 30% of the simulation time of the last 5 ns were chosen to represent typical non-bonded interactions. Only those protomers with a high occupancy of these >30%-interactions were considered for further analysis and used to calculate the average protomer structure.

CHAPTER 3

THE STABILITY OF THE OPEN AND CLOSED STATES OF G-ACTIN

The G-actin monomer is the building block of the biologically active form of the protein, the actin filament (F-actin). The monomer binds either ATP or ADP in a nucleotide binding site located between its two symmetric domains. However, the two states differ in their polymerization propensity. More than 40 X-ray crystallographic structures of G-actin have been solved, both in the ATP- [20, 25] and ADP-bound [21] states, but the nature of the conformational difference between the two states that could explain their different biochemical properties remains unclear and is the subject of ongoing debate [22, 90]. The understanding of the differences between the two states is complicated by the fact that monomeric actin is difficult to crystallize. To date no unmodified G-actin has been crystallized due to its propensity to assemble into actin fibers. A myriad of sequestering agents have been used to crystallize G-actin and include proteins such as DNase I [19], profilin [14, 20], gelsolin [91, 92, 93], vitamin-D-binding protein (DBP) [94], and a hybrid between gelsolin domain 1 and thymosin-β4 [95]; small molecules such as macrolides [96]; actin crosslinked to itself [97] or rhodamine [21]; and in combination with many binding partners such as ciboulot/latrunculin [98] and the Bni1 formin homology domain 2 (FH2)/rhodamine [99]. Actin structures may be classified as 'open', as observed in a profilin:actin structure [14], or 'closed', as is seen for all others, including a form of profilin:actin [20]. The closed state refers to crystal structures where the cleft between the two lobes of actin, subdomains 2 and 4, is closed. Minor differences can be seen between closed-form structures, which are most apparent in the conformation of a loop of subdomain 2 (DNase I binding loop) and variations in the angle between the two domains of actin. In the open state, subdomain 2 rotates away from subdomain 4 to open the

nucleotide-binding cleft and leave a clear path for nucleotide exchange. Although the large number of known structures that have the closed conformation clearly suggest it to be the structure of the monomer, it has been suggested that many of the agents used to stabilize the crystallized structures may also affect nucleotide exchange. In contrast to the other agents, profilin serves as a nucleotide exchange factor and might facilitate the opening of the cleft. Therefore, the ATP- and ADP-bound structures of the actin monomer in isolation are not known with absolute certainty.
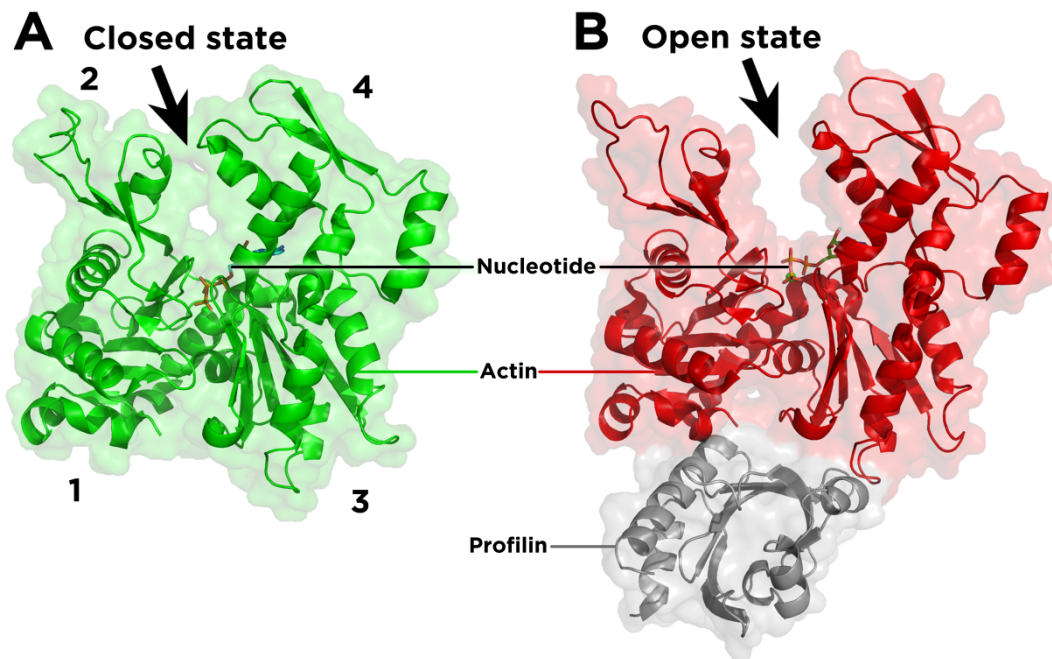

Fig. 3.1. The closed and open states of G-actin. The nucleotide (ATP or ADP) is located in the centre of the protein. The main difference between the two structures is the size of the cleft between subdomain 2 and 4 indicated by an arrow.
A - The closed state of G-actin based on PDB entry 2BTF. The bound profilin is not shown. Subdomains 1-4 are labeled. The cleft between subdomain 2 and 4 is closed.
B - G-actin in the open state (PDB entry 1HLU) with bound profilin. The inter-domain distance is considerably longer than in the closed state

It has also been hypothesized that the 'open state' of actin (PDB code 1HLU) [14] represents the ADP-state of monomeric actin [36, 37], while the 'closed state' may correspond to the ATP form (Fig. 3.1). Furthermore, electron microscopic studies of yeast actin filaments showed that the cleft between subdomain 2 and 4 is open in ADP-filaments but closes when those filaments

are incubated with the γ-phosphate analogue BeF_3^-, thus supporting the 'open' *vs* 'closed' state hypothesis [26]. However, this hypothesis has been challenged [21, 25] and a competing model suggests a nucleotide-dependent conformational change in the DNase I binding loop of subdomain 2 (residues 40-51) to be responsible for the functional difference [21]. According to this model the DNase I binding loop is disordered in the ATP state but folds into an α-helix in the ADP state. Unlike most other crystal structures reported, the recent structures of ATP- and ADP-G-actin by Rould *et al.* were free of co-crystallized proteins or attached chemical compounds [22]. Apart from the γ-phosphate sensor loop the two structures are strikingly similar and appear to support neither of the above hypotheses.

Several previous studies have addressed the nucleotide dependence of the G-actin structure by molecular dynamics simulation. In a study of the open *vs* closed model, it was found that in the open state of actin, the nucleotide-binding pocket of ATP-G-actin closes in absence of the co-crystallized profilin but remains open if profilin is present [16]. No significant structural changes were observed in the simulations of the closed state. However, only one simulation of one ns was conducted for each of the ATP and ADP states, precluding a statistically significant assessment of the relationship between nucleotide state and monomer structure. In a more recent study by Dalheimer *et al.*, MD simulations were conducted of G-actin in the closed state [45]. It was concluded that the nucleotide binding cleft is closed regardless of the nucleotide binding state. In addition, no correlation of the conformation of the DNase I binding loop with either ATP or ADP binding was found. In contrast to the study by Dalhaimer *et al.*, the conformation of the DNase I binding loop was observed to be nucleotide dependent in the molecular dynamics study of Zheng *et al.* [38]. In Zheng's study, again single simulations were performed on closed-state structures based on PDB entries 1J6Z and 1NWK, and the helical DNase I binding loop was seen to unfold in the ATP state but remains stable in the ADP state over a time span of 50 ns. In summary, the nucleotide-mediated changes in G-actin conformation remain the subject of debate.

The aim of the present work is to use MD simulation to shed light on the nucleotide-induced conformational changes in G-actin that allow the ATP-bound form to polymerize but prevent ADP-bound actin from doing so. The approach of the work is similar to that of Refs. [16, 38, 45] above. However, here a large number of multiple nanosecond-timescale MD simulations of open- and closed-state actin are performed, with a total simulation time of 440 ns. As a result, some observations are found to be statistically significant. Both

the open state [14] and the closed state [20] structures used were co-crystallized with profilin and the bound nucleotide, ATP. For the formation of the open-state crystals, a salt molarity of 1.8 M KPO_4 appears to be crucial. When the molarity was changed from 1.8 M to 3.6 M, the dimensions of the unit cell decreased to that of a closed state crystal, raising doubt about the stability of the open state structure outside the crystal lattice [25]. Therefore, to examine whether the open state is also stable in absence of profilin, MD simulations were carried out with and without profilin. For comparison, structures of the closed state of actin were also simulated. To further investigate the effects of the nucleotide on the actin structure unbiased by profilin, additional simulations were performed using other X-ray structures of higher resolution [22]. All simulations were carried out both with ATP and ADP in the nucleotide-binding pocket.

3.1 The open state structure is instable in absence of profilin

Open-state G-actin molecular dynamics simulations were performed to investigate the stability of the open domain cleft and the effects on it of the binding of ATP, ADP and profilin. Furthermore, ATP and ADP-actin were studied in the closed state. For each state studied at least 10 simulations of 4 ns were performed, from different distributions of starting velocities, in order to determine the statistical significance of the phenomena observed.

3.1.1 Size of the nucleotide binding cleft

The cleft size is a measure of how 'open' or 'closed' a G-actin structure is, and is defined [100] as the distance between the centers of mass of the protein backbone of residues 57-69, and 30-33 in subdomain 2 and residues 203-216 in subdomain 4. In Fig. 3.2 are shown time series of this domain cleft size. Each line in the figure is an average over 10 MD simulations for the open state results and over 20 simulations for the ATP and ADP closed states.

In the open state crystal structure (1HLU) the cleft size is 21.1 Å whereas it is 16.7 Å in the closed state crystal structure (2BTF). All average MD domain cleft distances stabilize after 100-1000 ps. The profilin-bound open-state simulations (with either ATP or ADP bound) remain the most widely open,

with an average cleft size of ~20.5 Å, close to that of the starting structure (21.1 Å). The profilin-bound actin cleft is ~4 Å wider than the closed state MD systems and 1-2 Å wider than the corresponding open state simulations without profilin.
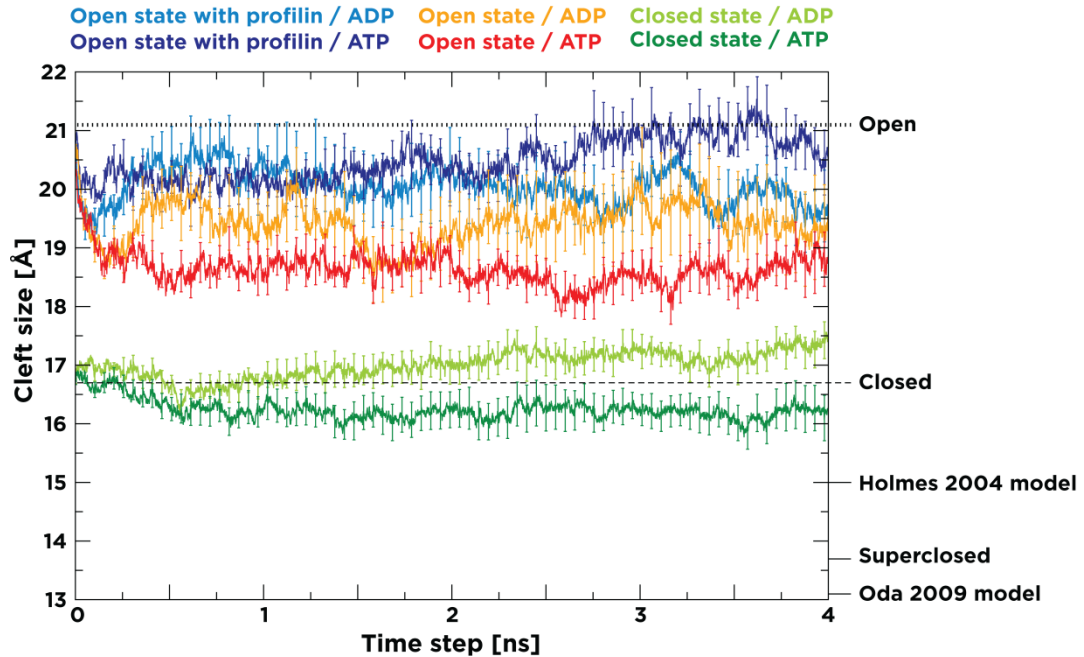

Fig 3.2. Time series of the average size of the cleft size during MD simulations of different states, bound nucleotide and with or without profilin. All graphs of the open state show the average over 10 MD simulation runs. The closed state graphs represent the average over 20 MD simulations each. The data are shown only for the production runs of 4 ns. The error bars correspond to one standard deviation of the mean. The black dotted line represents the domain distance of the open state and the dashed line that of the closed state starting structures.
On the right axis are marked the cleft sizes of the open and closed starting structures together with the Holmes 2004 and Oda 2009 filament models and the average superclosed state

   The removal of profilin is accompanied by a significant partial closing of the cleft, visible in Fig. 3.2 as a sharp decrease in the inter-domain distance over the first ~300 ps of the simulation sets concerned. The two simulation sets of the closed state, again with ATP and ADP, exhibit stable domain distances close to their starting value of 16.7 Å and approximately 3 Å narrower than the corresponding simulations of the open state. Finally, Fig. 3.2 also shows that, for the simulations in the absence of profilin, the ADP-bound structures are slightly, but significantly, wider open than those with ATP.

In Fig. 4.1 the same data as in Fig. 3.2 are shown as time-averaged probability densities of the cleft size. In the two open-state simulation sets with bound profilin the density has slightly shifted from the open-state starting point towards the closed state. However, this shift is much more prominent in the two open-state simulations without profilin, and the main peak of both open-state non-profilin simulations is closer to that of the crystal structure of the closed than the open state. In the two closed-state simulation sets the cleft size probability maximum remains close to the starting value.

3.1.2 Cleft size and its relation to the nucleotide position

Visual inspection of the MD trajectories and comparison with the open and closed starting structures (Fig. 3.3) showed significant variations in the nucleotide position. In the closed-state X-ray structure the nucleotide is located in its binding pocket, stabilized by multiple hydrogen bonds. In contrast, in the open state the nucleotide is less deeply buried, wedged between its two binding loops, with many of the stabilizing interactions present in the closed state disrupted. In the majority of open-state trajectories in which the nucleotide relocated into the binding pocket, an accompanying closure of the domain cleft was observed. However, in some open-state simulations the nucleotide remained in its position or moved out of the binding site even further, and in these simulations the cleft tended to remain open, with larger cleft-size fluctuations. This tendency is more prominent in the simulations of the open state with ADP, explaining the larger average cleft size in the ADP rather than ATP state.

The depth of the nucleotide in the binding pocket was calculated (see Chapter 2.3) for each simulation frame (Fig 3.3) and its correlation with the corresponding inter-domain cleft size computed. For simulations without profilin, the average correlation coefficient between nucleotide depth and cleft size is 0.64. Thus, the cleft size is clearly related to the position of the nucleotide in the binding pocket.
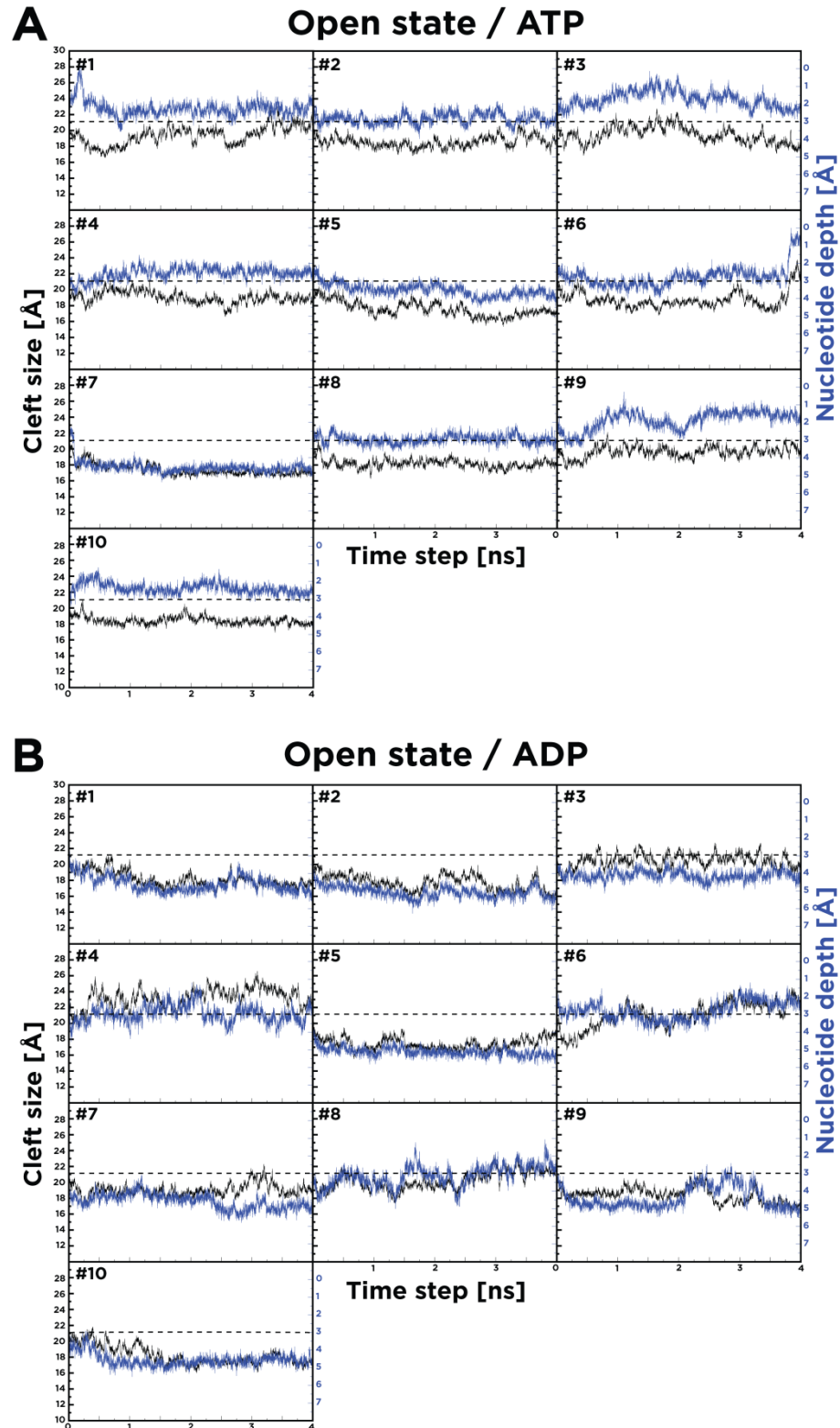
Fig. 3.3. Cleft size (black) and nucleotide depth (blue) over simulation time of
A - 10 open state ATP-G-actin simulations and
B - 10 open state ADP-G-actin simulations.

3.1.3 Hydrogen bonding pattern of the nucleotide in the binding site

The hydrogen bonding pattern between the protein and the nucleotide is dependent on the cleft size (Fig. 3.4). In the ATP-bound closed and open state simulations (without profilin), structures with a closed domain cleft possess an average number of nucleotide:protein hydrogen bonds of 10 to 12. In contrast, the average number of hydrogen bonds decreases with an increasing cleft size, becoming <7 for the most open structures. The averages of the ADP simulations are generally lower, owing to the missing phosphate group. However, due to the poor stabilization of the ADP in the initial open state structure, the corresponding simulations show less variation with cleft size of the H-bond occupancy and over a larger range of cleft sizes than the other simulations.
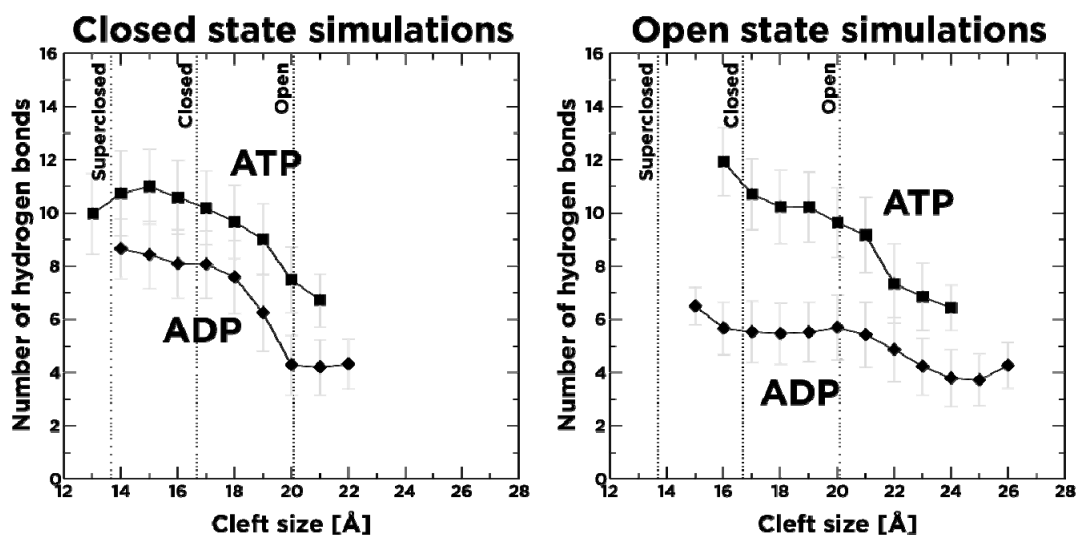
Fig. 3.4. Average number of hydrogen bonds between nucleotide and protein plotted versus the cleft size. The left panel shows the number of hydrogen bonds averaged over the 40 simulations of the closed state and the right panel over the 20 open state simulations in absence of profilin. The bars of the data points give the standard error. In general, MD structures of actin with a smaller cleft size are accompanied by a high number of hydrogen bonds while there are fewer in open conformations. The overall low hydrogen occupancy in simulations of open state actin with ADP is attributed to the poorly hydrogen-bonded ADP in the starting structure of this simulation model, leading to a destabilization of the tertiary structure which in turn explains the large fluctuations in cleft size.

In Fig. 3.4, even at cleft sizes around the range of the closed state, the open state simulations with ADP show a much lower number of hydrogen bonds than their closed-state counterparts. This difference suggests that the cleft size parameter alone may not be a good indicator of whether a MD structure has adopted the overall conformation of the closed state as found in crystal structures: open-state ADP simulations that exhibit small cleft sizes may not have necessarily reached the closed state.

3.2 The structure of the DNase I binding loop

To examine the possibility of a nucleotide-mediated conformational change in the DNase I binding loop, an analysis was performed of the secondary structure of the binding loop in the present simulations using the DSSP tool [101]. In both of the present starting conformations the loop is disordered. During all simulations the α-helical fold occurred very rarely in the DNase I binding loop and was short lived - in the 80 ns of closed-state ATP simulation the DNase I binding loop adopted an α-helical conformation only 0.011% of the simulation time, this percentage being 0.114% in the corresponding closed-state ADP simulations. In the open state simulations, the α-helical fold was similarly rare. Therefore, there is no evidence from the present simulations for a coupling between the nucleotide-binding state and the conformation of the DNase I binding loop.
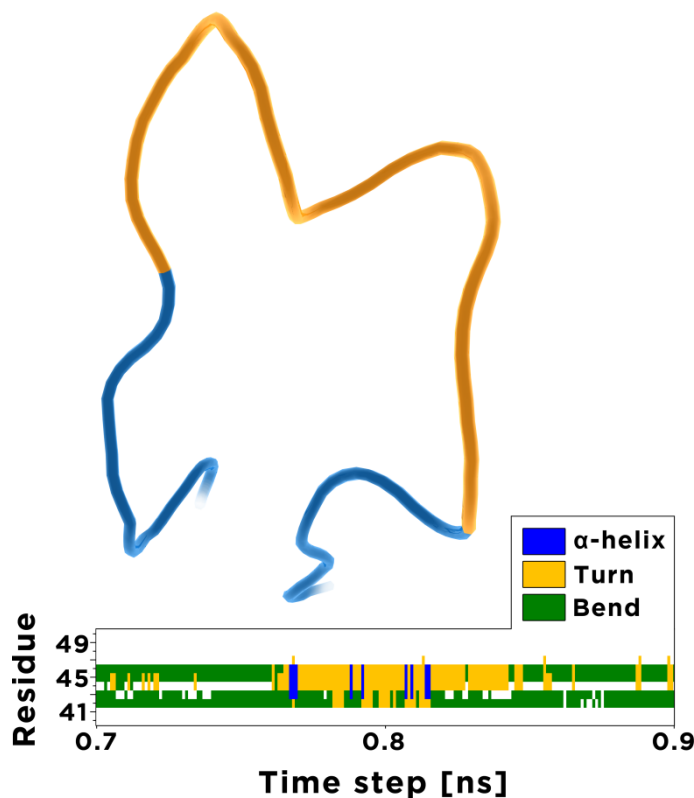
Fig. 3.5. Snapshot of the DNase I binding loop (yellow) in a short-lived α-helical conformation in the MD simulation of the ATP-bound closed state of PDB entry 1J6Z.

3.3 Discussion

The present simulations indicate that the open state of G-actin is unstable in absence of profilin, in agreement with a previous single-trajectory MD study [16]. The correlation of the nucleotide depth with the cleft size suggests that the instability is based on the initial position of the open-state nucleotide which is located partially out of the binding pocket and poorly stabilised *i.e.* with few hydrogen bonds. In contrast, the open conformation of actin remains relatively stable when bound to profilin. Occasional, short-lived opening of the cleft to the extent of the open state structure was observed in only 4 out of the 40 simulations of the closed state. Thus, the profilin-bound, open-state crystal structure (1HLU) may represent a stable actin-profilin-complex in which actin is opened to facilitate nucleotide exchange, but is unlikely to represent a stable conformation of the isolated actin monomer. Further, the instability of the

open state suggests that this state is not responsible for the different polymerization rates of ATP and ADP-G-actin.

A clear correlation is found between the cleft size and the position of the nucleotide. In crystal structure of the open state PDB 1HLU the ATP is wedged between two lateral nucleotide binding loops, which are located at the base of subdomains 2 and 4, respectively. Keeping the loops apart prevents actin from adopting a closed state. The nucleotide position variations do not converge in the simulations. Consequently, in simulations where the nucleotide phosphate groups remained partly outside the pocket or the nucleotide slipped further out, the protein was left in a more highly fluctuating open conformation. In simulations in which the nucleotide fully entered the binding pocket and where its position is stabilized, full closure of the cleft was observed. The absence of convergence in nucleotide position/cleft size resulted in a stable closure of the cleft being observed only in half of the open state simulations without profilin, and this explains why the average cleft sizes of simulations with ATP bound starting from the crystal structures of the open and closed states did not converge.

Of all the simulations performed, those of the open-state ADP-bound actin without profilin exhibited the largest range of cleft sizes (15 to 26 Å), the lowest average number of nucleotide:protein hydrogen bonds (Fig. 3.4) and the largest propeller angle. This may be due to the starting structure being far from native, as it was taken from a crystal structure in which both the profilin and the γ-phosphate group were removed, leaving the ADP in a solvent exposed, poorly hydrogen-bonded position. The resulting lack of nucleotide stabilization leads to highly fluctuating behavior.

In general the average number of hydrogen bonds to the nucleotide is high at smaller cleft sizes and low at larger cleft sizes. This correlation does not depend on the nucleotide or whether the simulation was started with an open or a closed actin conformation. This may be an indication that the closed state, as found in most X-ray studies, is favorable because the nucleotide holds together the two domains of actin - nucleotide-free G-actin has been shown to denature rapidly in absence of stabilizing agents [102]. With an increased number of nucleotide:protein hydrogen bonds the protein adopts a more compact state.

The conformation of the DNase I binding loop was observed to be nucleotide dependent in the single 50 ns molecular dynamics study of -actin by Zheng *et al.* [38]. In the present study on β-actin (sequence identity with -actin of >90%), using 140 simulations for a total simulation time of 440 ns, no indication was found of a nucleotide dependence of the DNase I binding loop conformation.

This is also in agreement with a previous single 5 ns simulation study by Dalheimer *et al.* [45]. In the present work very few, short-lived (<500 ps) instances occurred of the DNase I binding loop adopting an α-helix fold in either ATP- or ADP-bound state. The results therefore provide no evidence for a nucleotide-induced change to the α-helix conformation.

3.4 Summary

  The assembly of monomeric G-actin into filamentous F-actin is nucleotide dependent. Structural differences between ATP- and ADP-G-actin are examined here using multiple molecular dynamics simulations. The 'open' and 'closed' conformational states of G-actin in aqueous solution are characterized, with either ATP or ADP in the nucleotide binding pocket. With both ATP and ADP bound the open state closes in the absence of actin-bound profilin. Thus, the open state is not a stable form of monomeric actin in solution. Furthermore, the position of the nucleotide in the protein is found to be correlated with the degree of opening of the active site cleft. We speculate that the observed open state is a short-lived intermediate in the pathway of nucleotide exchange.

  We also analyzed conformational changes within the DNase I binding loop which have been hypothesized to depend on the nucleotide state. Only very few, short-lived instances occurred of the DNase I binding loop adopting an α-helix fold, remaining mainly in a random coil conformation. Therefore our simulations do not provide evidence for a nucleotide-dependent conformational change to the α-helix conformation.

CHAPTER 4

THE SUPERCLOSED STATE –

A NOVEL CONFORMATION OF G-ACTIN

The structural and dynamic properties of actin depend, at least in part, on the state of the bound nucleotide [21, 24, 25, 26]. In fact, the state of the nucleotide bound to actin, ATP or ADP, is the driving force of the actin cycle of polymerization and depolymerization. One of the effects of the nucleotide state of G-actin is the determination of the binding affinities of ATP- and ADP-bound G-actin molecules to the filament. Thus, the nucleotide-dependent conformational states of G-actin have been extensively discussed but no consensus has been reached about the switch between the ATP- and ADP-bound forms of the actin monomer. A large number of crystallographic structures of G-actin are available but due to the static nature of the technique only states that can be crystallized have been identified. An analysis of the dynamics of the protein therefore may reveal further (*e.g.* short-lived) states.

In this chapter we reanalyze the simulations presented in Chapter 3 to investigate the population of the different states of G-actin. Two structural features, the nucleotide binding cleft and propeller angle, are used to classify the different states. We identified a novel state which we call the superclosed state. This state is characterized by a tight nucleotide binding cleft and a low propeller angle, giving it a flat conformation that resembles the structure of the protomers in F-actin.

4.1 A newly identified state of G-actin

Examination of the cleft size probability density in Fig. 4.1 shows a close similarity between the ATP and ADP closed state simulation sets. In both cases the main peak is at ~16 Å, close to the initial value of those simulations, 16.7 Å. However, in the closed ATP simulations there is a second, smaller peak in the distribution at ~13.7 Å.
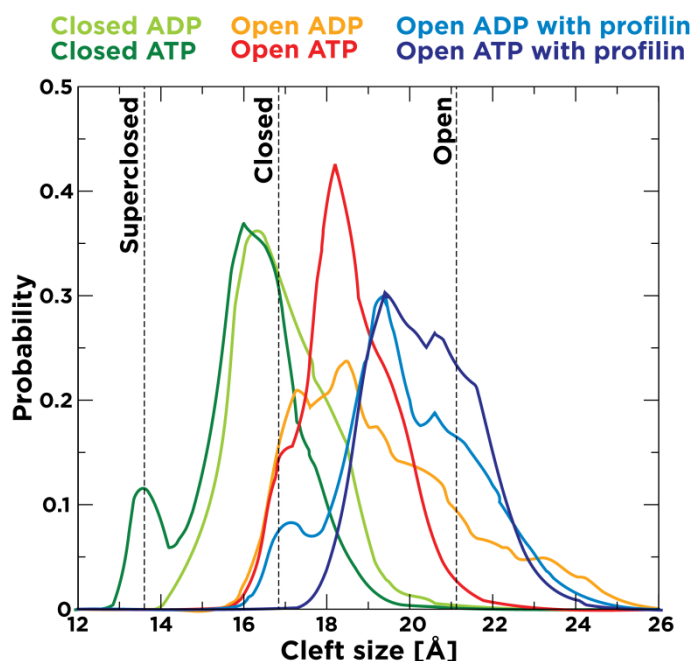
Fig. 4.1. Probability density of the cleft size between subdomain 2 and 4 over the entire simulation time. Each open state graph represents the data of 10 simulations (20 for closed state). The vertical dashed lines indicate the cleft sizes of the crystallographic open and closed states and the average superclosed state proposed here. The cleft size distribution of profilin-bound actin (blue) appears to be broader with the main peak slightly shifted from the open state towards the closed state. The shift of the open state simulations without profilin (red) is much stronger, with the main peak being closer to the closed state than to the open state. The two closed state simulations (green) show little spread in comparison and remain in close proximity to the starting value. In the ATP-bound closed-state simulations an additional smaller peak appears at 13.7 Å corresponding to the superclosed state that does not appear in the corresponding ADP-closed state simulations.

This additional state of ATP-G-actin possesses a cleft size ~3 Å smaller than that of the closed state and we therefore label it the 'superclosed state'. This

state was strongly populated in four out of the 20 closed ATP simulations but never populated in the corresponding ADP simulations.

Fig. 4.2 shows time series of the cleft size for the four superclosed-state simulations. In each of these simulations the superclosed state is seen to persist for several nanoseconds. Apart from the similar cleft sizes, the structures of the four superclosed-state trajectories also show other very similar structural features.
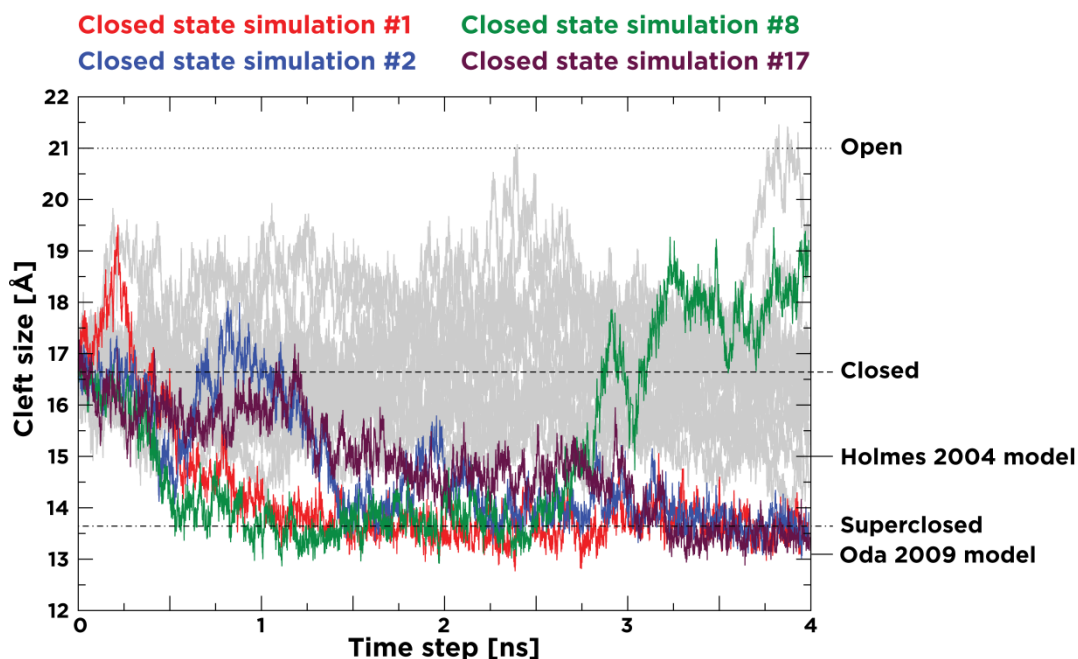
Fig. 4.2. Time series of the cleft size of 20 MD simulations of ATP-bound actin in the closed state. The 4 simulations in which the protein structure adopts the superclosed conformation are shown in color, the remaining simulations in grey. On the right axis the cleft sizes of the open and closed crystal structures (21.1 Å and 16.7 Å), the Holmes 2004 and Oda 2009 filament models (15 Å and 13.1 Å) and the average superclosed state (13.7 Å) are marked for comparison.

To further characterize the superclosed state, a representative superclosed-state structure was taken as a starting structure to perform additional MD simulations (see Chapter 2). Twenty short (1 ns) simulations were performed with this superclosed ATP-actin as the starting structure and another 20 simulations in which the nucleotide γ-phosphate group was removed so as to replace ATP by ADP. In 6 of the 20 simulations of superclosed ADP-actin the protein structure left the superclosed state within the relatively short 1 ns of simulation time. In contrast, only 2 of the 20 ATP-bound actin simulations left the superclosed state, confirming that ATP stabilizes the superclosed state.
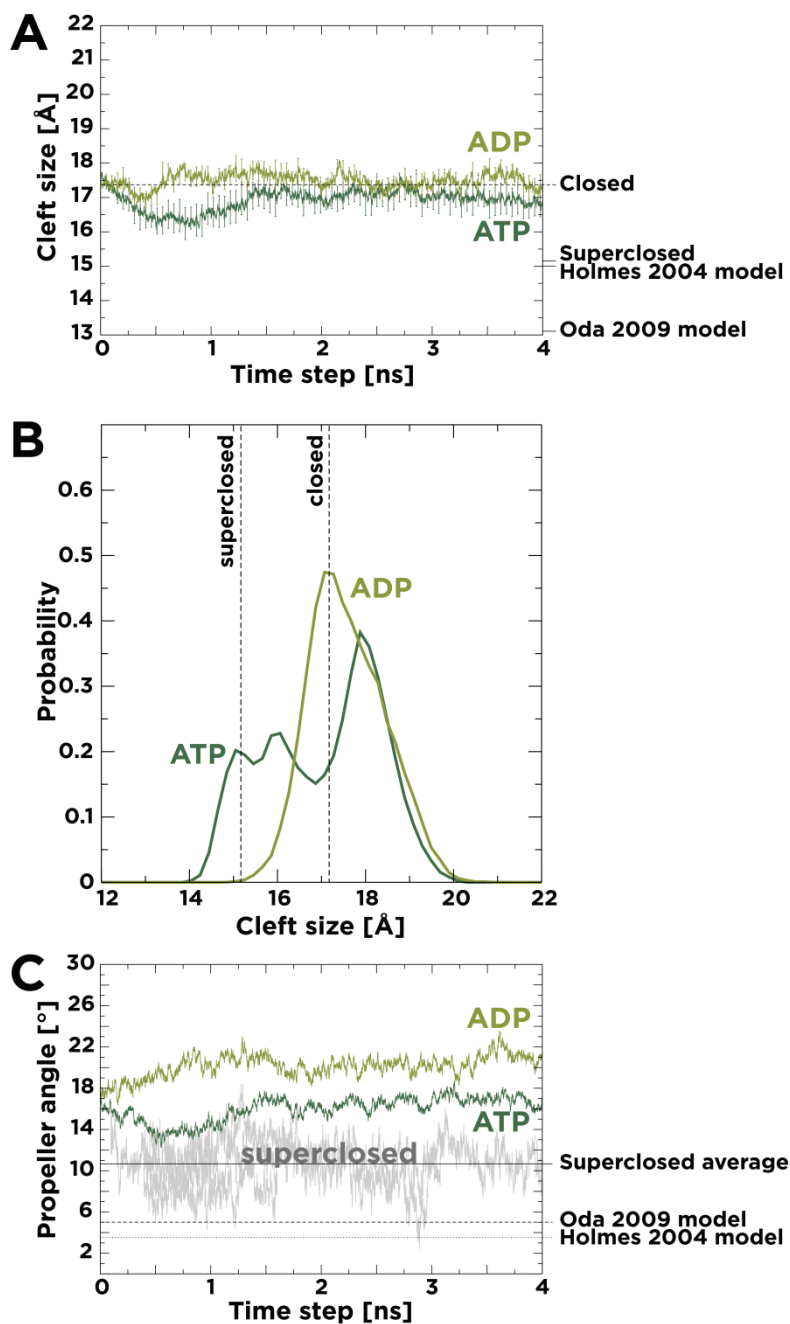
Fig. 4.3. Results of 10 MD simulations of PDB entries 2HF4 (ATP closed state) and 2HF3 (ADP closed state).

A – Time series of the average cleft size between subdomains 2 and 4 during MD simulations of ATP-and ADP-G-actin.

B – Probability density of the cleft size between subdomain 2 and 4 over the entire simulation time.

C – Change of propeller angle over simulation time. Averages over 10 simulations each. Superclosed sections of the ATP closed simulations are shown in grey.

Two sets of simulations (with ATP and with ADP) were also performed starting from closed-state structures crystallized in the absence of profilin (1.8 Å resolution structures of free ATP- and ADP-bound actin by Rould *et al.*) [22]. 10 simulations of 4 ns were carried out each. In agreement with the previous simulations, ATP-G-actin occupies both the closed and superclosed states while the ADP-bound form adopts the closed state only (Fig. 4.3).

4.2 Structural features of the superclosed state

The increased cleft closure in the superclosed state is achieved by rotations of subdomains 2 and 4 (Fig. 4.4). Relative to the closed state starting structure, in the average superclosed state structure, subdomains 2 and 4 are rotated by about 8° and 13°, respectively. These rotations remove the steric hindrance between the subdomains that would prevent the closed state from further closing its cleft.

A comparison of the superclosed structure with that of recent filament models by Holmes and Oda revealed similar orientations of subdomains 2 and 4. For example, in Fig. 4.4 C are shown the superclosed state and a monomer taken from the Oda 2009 filament model, both aligned to the structure of the closed state. The arrows in the figure indicate the similar subdomain orientations of superclosed state and the Oda 2009 model, which are clearly different from the structure of the closed state. Furthermore, the cleft distances of 15 Å in the Holmes 2004 model and 13.1 Å in Oda's model are similar to that of the average superclosed state (13.7 Å).
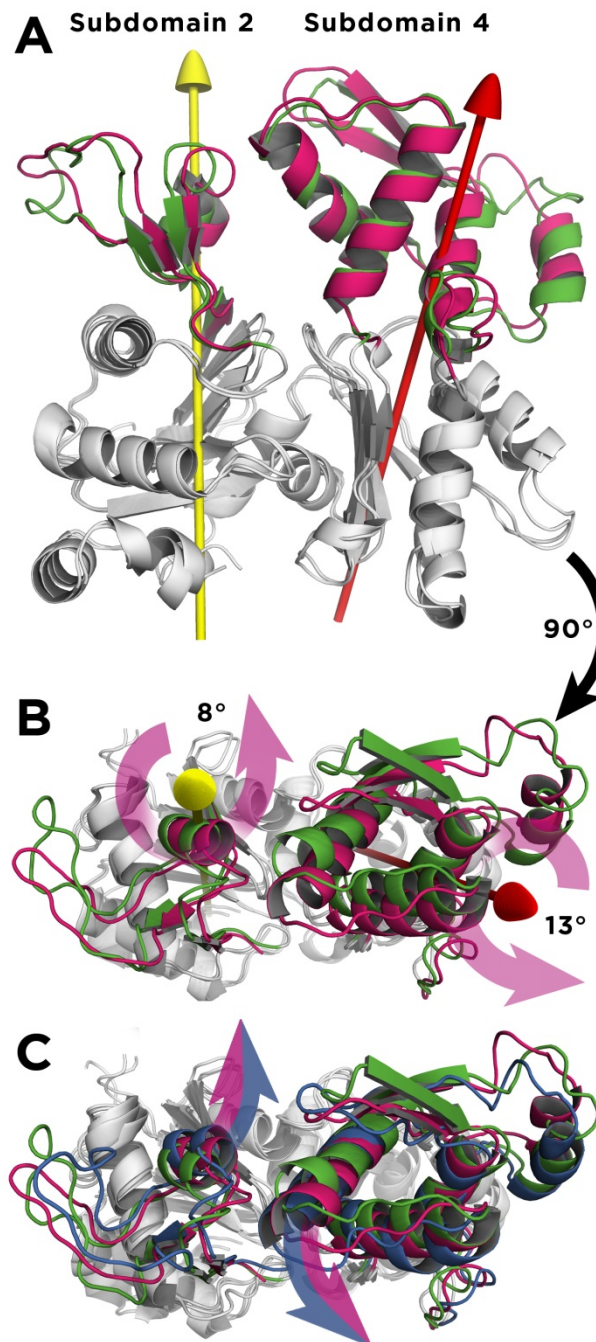
Fig. 4.4. Comparison of the structures of the closed state (2BTF, green), the average superclosed structure (violet) and the Oda 2009 filament model (blue).

A, B - Subdomain 1 and 3 (white) of closed and superclosed state aligned and the axes of rotation of subdomain 2 (yellow) and 4 (red) determined. The rotation angle of superclosed subdomain 2 is 8.3° and 13° for subdomain 4.

C - Superclosed state and Oda 2009 filament model aligned to the structure of the closed state, taking into account the backbone of the entire actin molecule. The purple-blue arrows indicate the rotations of subdomains 2 and 4 in the superclosed and filament model structures.

Also of interest is the propeller angle, defined by the dihedral angle of the centers of masses of the four subdomains. The average propeller angle of G-actin (Fig. 4.5) converged to about 16.3° in all but the open ADP simulations for which the mean is 19.8°±0.75. However, the average of the four superclosed trajectory segments is 10.7±1.77°, much smaller than the average closed-ATP-simulation propeller angle. Similar results were observed in the simulations performed starting from structures crystallized in the absence of profilin (PDB entries 2HF3 and 2HF4) - the average propeller angles of these ATP- and ADP-states were found to be 20.6±0.79° and 16.5±0.79°, whereas the average superclosed-state propeller angle is 10.5±2.13°. In comparison, the propeller angles of the Holmes 2004 and Oda 2009 filament models are 3.6° and 5°, respectively. Thus, also with respect to the propeller angle, the superclosed state is the G-actin conformation that is most similar to the filament models.

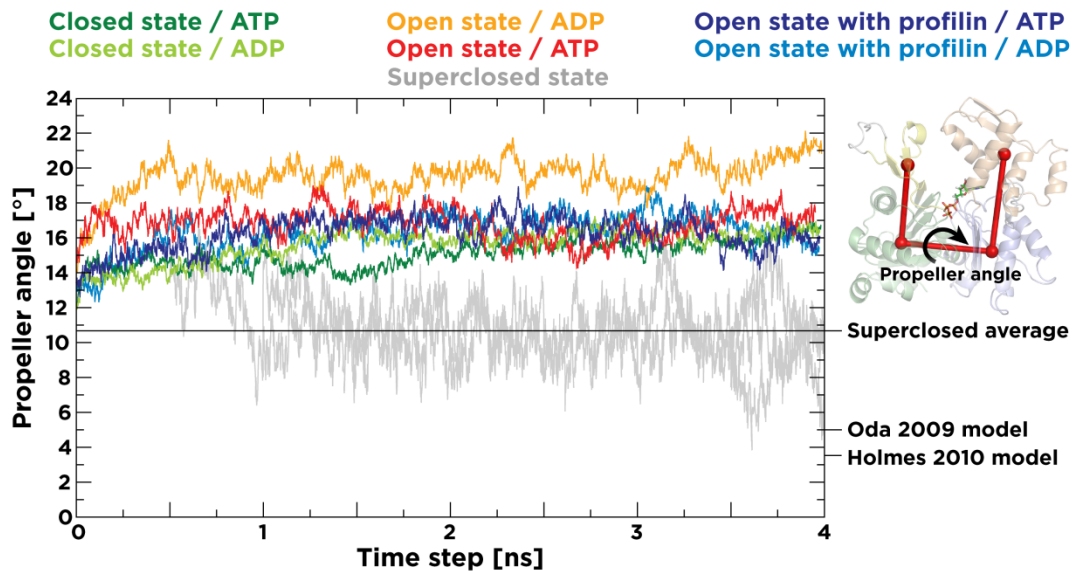**Fig. 4.5. Time series of propeller angles.** Each graph of the open and closed state simulations represents the average over 10 and 20 simulations, respectively. The four superclosed parts of the closed state ATP-actin trajectories are shown in grey. Their average angle is 10.7° (solid line). In comparison, the angle of an actin monomer in the Oda 2009 filament model is 5° and in the Holmes 2004 filament model 3.6°.

4.3 Discussion

The present MD simulations of G-actin reveal a new distinct state, found exclusively in closed ATP-bound actin, that is more compact than the regular closed state and is thus referred to as 'superclosed'. In comparison to a typical closed state structure (*e.g.* 2BTF), in the superclosed state subdomains 2 and 4 have a different relative orientation, thus allowing the cleft to be completely closed. The possibility exists that the newly-observed superclosed state of ATP-G-actin may be the polymerization-competent conformation that is required for filament assembly. The superclosed structure displays striking similarities with proposed low-resolution filament models derived from experiment. The same orientation of the two subdomains, complete cleft closure and similar propeller angles are also present in actin filament models. This well-defined superclosed state was observed in several independent ATP-actin simulations, indicating its statistical relevance. Furthermore, formation of the superclosed state was observed in ATP-actin simulations of different PDB starting structures (2BTF and 2HF4).

The increased compactness of the superclosed state may be a requirement for polymerization. Furthermore this state occurs only in ATP-G-actin simulations of the closed state but in none of the ADP-simulations. This is consistent with the behavior of actin *in vivo*, where only ATP-G-actin assembles to F-actin but not the ADP-bound form. Our findings are in agreement with experimental proteolysis [103] and spectroscopy studies [104] where ATP-G-actin was found to undergo conformational changes leading to a 'F-actin-monomer' (or 'G*-actin') form which favors polymerization. This proposed form of ATP-G-actin showed characteristics of both G- and F-actin and may correspond to the superclosed state of actin described in this study.

Why hasn't a superclosed structure been observed crystallographically? The crystallization of actin has always been a challenge, as at high concentrations G-actin tends to polymerize to F-actin rather than to crystallize. Because of this problem, G-actin has been co-crystallized with an actin-binding protein [14, 20], chemically modified [21], mutated [22] or otherwise rendered non-polymerizable [23]. These alterations, possibly together with the non-physiological conditions of the crystalline state, might prevent formation of the superclosed state.

Although the present superclosed state is a putative candidate for the *polymerization-competent* form of G-actin, the closed state may still be the

predominant state of ATP-G-actin in equilibrium and therefore much more likely to be observed experimentally. Fig 4.6 shows the possible mechanism for actin polymerization. In this speculated sequence of events the closed state structures of ATP- and ADP-bound G-actin have similar low propensities for assembly to the filament end. However, ATP-G-actin may switch into the less populated superclosed state, which resembles the structure of F-actin protomers and therefore has a high binding affinity to F-actin.
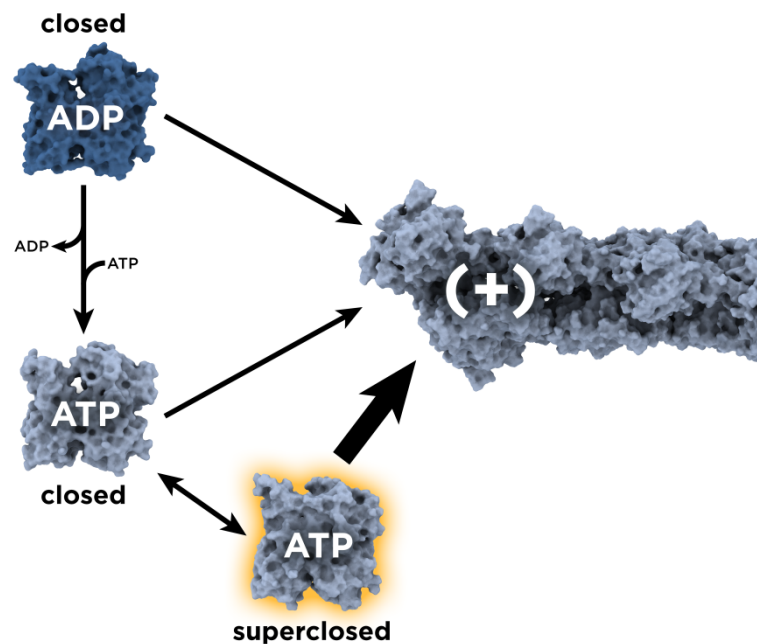
Fig. 4.6. Proposed mechanism of assembly of actin monomers at the barbed end of the filament. The structurally similar closed state conformations of ATP- and ADP-bound G-actin have similar low propensities for assembly to the filament end. Unlike ADP-G-actin, ATP-G-actin may switch into the superclosed state, which resembles the structure of F-actin protomers and has a high binding affinity to F-actin.

Further experimental studies on actin are required to confirm or otherwise whether the superclosed state is that involved in G-actin polymerization. Electron paramagnetic resonance experiments of the actin protein with spin-labeled subdomains 2 and 4 may shed further light into the nucleotide dependence of the domain cleft size. Because of the similarities with actin monomers of present medium-resolution filament models, the superclosed structure might prove useful for interpreting to fiber diffraction data or electron micrographs of F-actin so as to derive improved models in the future.

4.4 Summary

The simulations reveal the existence of a structurally well defined, compact, 'superclosed' state of ATP-G-actin, as yet unseen crystallographically and absent in the ADP-G-actin simulations. The superclosed state is characterized by a nucleotide binding cleft that is several Ångstrom smaller than in the closed state as well as a low propeller angle. The state resembles structurally the actin monomer in filament models derived from fiber diffraction. Subdomains 2 and 4 in the superclosed state reorient, and are positioned similar to that of the protomers in F-actin. Due to the structural similarities we suggest the superclosed state to be the polymerization competent conformation of ATP-G-actin.

CHAPTER 5

COMPARISON OF ATOMISTIC F-ACTIN MODELS

F-actin has been a major target of structural studies for decades [53, 54, 55]. However, owing to the difficulties involved in crystallizing the filament the atomic-detail structure of F-actin is still unknown.

In 1990 the first atomic-detail structure of monomeric G-actin was determined by X-ray crystallography [19]. This achievement allowed the first high-resolution filament model to be proposed [40]. In this and subsequent work [51, 105], a helix of G-actin monomers was fitted to the X-ray fiber diffraction pattern of oriented actin gels. However, the resolution of the fiber diffraction patterns was only about 6-8 Å and thus the refinement underdetermined [105]. In subsequent years new filament models were proposed using different approaches of optimizing the refinement [60, 61] and, very recently, Oda *et al.* were able to obtain resolutions of 3.3-5.6 Å, currently the highest reported [51]. Global properties of the helical actin filament, such as diameter of the fibril, helix parameters and orientation of the actin protomers in the filament have now been reliably determined [106] and are incorporated in the recent model of Oda *et al.*, which we label 'Oda 2009'.

The nature of the actin-bound nucleotide, *i.e.* ATP or ADP, is a key determinant of the conformation of the filament. Experimental studies indicate that release of γ-phosphate, following ATP hydrolysis in the filament, alters properties of F-actin, such as the persistence length and the binding affinity of certain proteins associating with the filament [24, 107]. However, the conformational transition associated with ATP hydrolysis is not well understood, due in part to the lack of a high-resolution X-ray structure of the actin filament and also because available F-actin models have been derived mostly based on structures of only ADP-F-actin, which is the predominant state of the actin filament.

Also, conformational events accompanying to the G- to F-actin transition have been the subject of debate. For example the 'hydrophobic plug' (GLN263-

SER271), a loop with a hydrophobic tip, has been suggested to functionally alter its position upon integration of the G-actin monomer into the filament [40]. Furthermore, the conformation of the DNase I binding loop (ARG39-LYS50), the most flexible part of the G-actin structure, has been hypothesized to be coupled to the nucleotide-binding state [21].

To clarify questions such as the above further improvements of the F-actin structure are required. In the present work we propose a new model of the actin filament, which we label 'Holmes 2010'. This model was built using a straightforward approach in which priority was given to keeping the stereochemistry within the actin protomer intact while altering the position of the two actin domains to account for the global conformational change during the G- to F-actin transition. The low-resolution, global tertiary structure of the new model (defined by the orientation and position of the four subdomains relative to each other) is derived from, and thus similar to, the Oda 2009 model [51], but in terms of secondary structure and specific interactions, such as in the nucleotide binding site, the new model mostly resembles the G-actin structure [21] upon which it is based. The fiber diffraction pattern calculated from the new model matches the experimental pattern very well.

Furthermore, a comparison is made of the structures and dynamics of Holmes 2010 with other recent models by subjecting them to MD simulation. The models chosen for comparison are Oda 2009 and another model by Holmes *et al.* [105], based on a previously obtained diffraction pattern (6–8 Å), which we name 'Holmes 2004'. The MD comparison is found to reflect the evolution in quality of the actin models over the last six years.

Finally, simulations are performed on how the nucleotide (ATP or ADP) affects the conformation of the Holmes 2010 actin filament, with a particular focus on the phenomenon of G- to F-actin ATPase activation. In agreement with previous studies, we predict the importance of GLN137 for ATP hydrolysis, which in the model, and even more so in the MD simulation, comes into close proximity to the ATP.

5.1 The Holmes 2010 actin filament model

The F-actin model proposed here, 'Holmes 2010', was constructed starting from the tetramethylrhodamine-labeled G-actin X-ray structure (PDB entry 1J6Z) of Ref. [21]. The global conformational transition accompanying the G- to F-actin transition is a flattening of the actin molecule by a twist of the two domains relative to each other, as shown in Fig. 5.1.
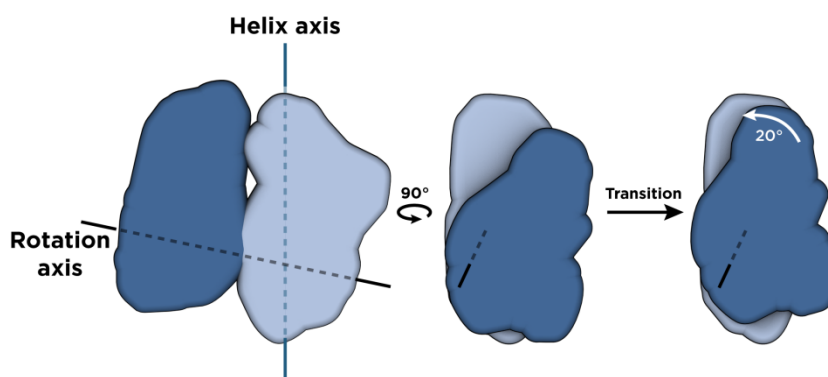
Fig. 5.1. Schematic depiction of the major conformational change during the transition from G- to F-actin. The two domains of the actin molecule, shown in yellow and blue, are connected by residues 139-140 and 341-342. During the G- to F-actin transition a domain rotation by 20° brings the two domains closer to each other and results in a substantially flatter structure of the monomer.

Therefore, in the modeling the two domains of the G-actin monomer were fitted separately (junctions at residues 139-140, 341-342) to the two domains of the Oda 2009 model. The α-helical conformation of the DNase I binding loop in PDB 1J6Z has been suggested to be an artifact [36] and thus was discarded and replaced by the random coil coordinates of the Oda 2009 model (residues 35-69). Phalloidin was added in and the coordinates refined against the fiber diffraction data and EM data [62], weighted in favor of the fiber data. The final radius of gyration is 23.7 Å. Figure 5.2 A shows that the diffraction pattern calculated from our Holmes 2010 F-actin model is consistent with the observed pattern. Coordinates of Holmes 2010 are deposited at:

http://cmb.ornl.gov/Members/spe/5_actin.pdb/view
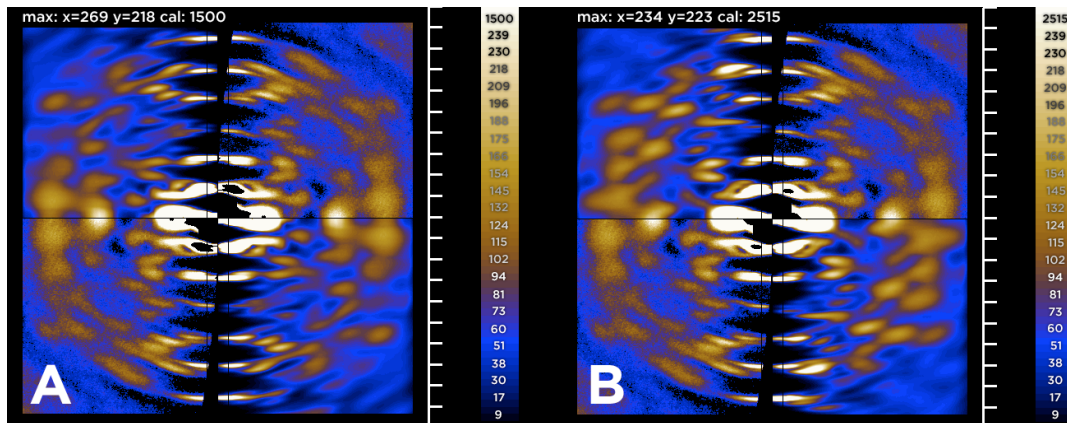
Fig. 5.2. Comparison between observed and calculated diffraction patterns. The edges of diffraction are 0.12 Å⁻¹ (8.3 Å resolution)
A - Top right and bottom left: experimental pattern (Holmes *et al.* 1990). Top left and bottom right: calculated from Holmes 2010 model.
B - Top right and bottom left: experimental pattern (Holmes *et al.* 1990). Top left and bottom right: calculated from average structure of Holmes 2010 MD simulation.

5.2 Molecular dynamics simulation of filament models

A comparison of the three recent filament models in the ADP state was performed in which they were subjected to MD simulation. Structural and dynamic properties from MD simulations of the ATP-bound Holmes 2010 F-actin model were also calculated and were found to be very similar to those with ADP bound and thus are not further discussed here.

In Fig. 5.3 A is shown the backbone root mean-square deviation (RMSD) from the starting structure averaged over the 13 actin molecules in the simulation primary box. The RMSDs of Oda 2009 and Holmes 2010 are similar to that obtained from MD of G-actin, stabilizing around 2.5-3 Å, while the Holmes 2004 protomers reach significantly higher values of ~4.5 Å, indicating structural instability.

Fig. 5.3 B shows the average number of hydrogen bonds within the actin monomers. After an initial equilibration phase, the number of internal hydrogen bonds remains stable for all models. Over the last 5 ns of simulation time numbers for the Holmes 2010 model and G-actin stabilize at ~300 and ~295, respectively, significantly higher than Oda 2009, which converges to ~290. Holmes 2004 is the lowest of the three models at ~280-~285 hydrogen bonds. In

contrast, the Oda 2009 model contains the largest number of hydrogen bonds between the protomers in the filament (Fig. 5.3 C).

The propeller angle formed by the centers of mass of the four subdomains of the actin monomer (see Fig. 5.5) is significantly higher in G-actin (~22°) than in the protomers of F-actin models (~2-3°). As shown in Fig. 5.3 D the low propeller angles, in the range of 2-3°, of the protomers of all three filament models increase significantly on MD simulation to averages ranging from ~7° (Oda) to ~9° (Holmes 2010).

The structural deviation among the 13 actin molecules in the simulation repeating unit over time is a further indication of stability of a model (Fig. 5.3 E). A certain degree of conformational variation among the protomers is to be expected as a result of thermal fluctuations of the filament around the native state. However, excessive structural variation, especially when accompanied by unfolding of secondary structure elements is likely to arise from the relatively poor quality of the modeled structure that was used to initiate the MD simulation. Here again, the Holmes 2004 model exhibits the highest variation among the protomers and the Holmes 2010 model the lowest.
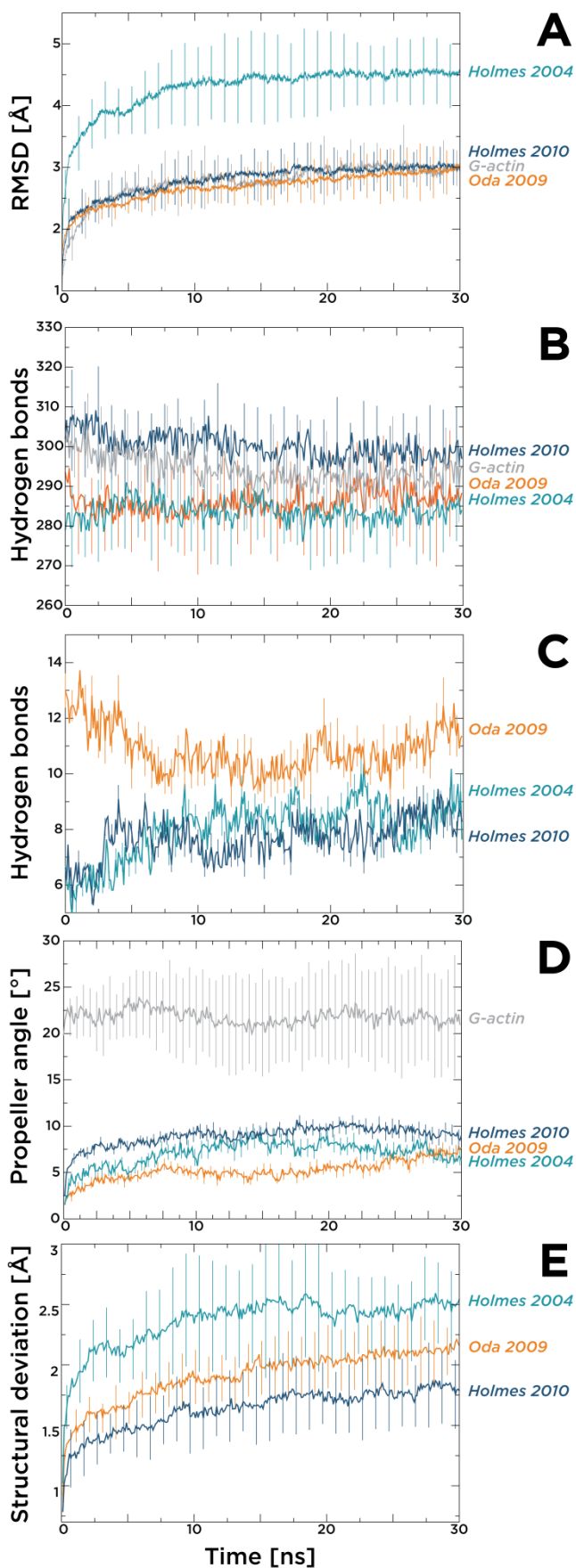
Fig. 5.3. MD time series of structural properties of actin. Each plot represents the average over the 13 actin molecules in the ADP-state.

A - Backbone RMSD from starting structure.

B - Number of protein hydrogen bonds within an actin molecule.

C - Number of hydrogen bonds between a protomer and its two unique interfaces with neighboring protomers (same strand and opposite strand) towards the barbed end of the filament.

D - Propeller angle of the centers of mass of the four subdomains of the actin molecule.

E - Structural deviation of 13 actin protomers from each other.

Figure 5.4 visualizes the different degrees of conformational deviation among the 13 protomers of each model at the end of the simulation. Some parts of the protomer structure, such as the DNase I binding loop and the variable stretch of residues 227-237 (hereafter referred to as V-stretch), exhibit a high degree of variation in all three models, consistent with the high B-factors of these residues in crystallographic G-actin structures. However, although those parts of the structure with low crystallographic B-factors also exhibit medium and low fluctuations in the Oda 2009 and Holmes 2010 models, respectively, they exhibit high fluctuations in Holmes 2004.
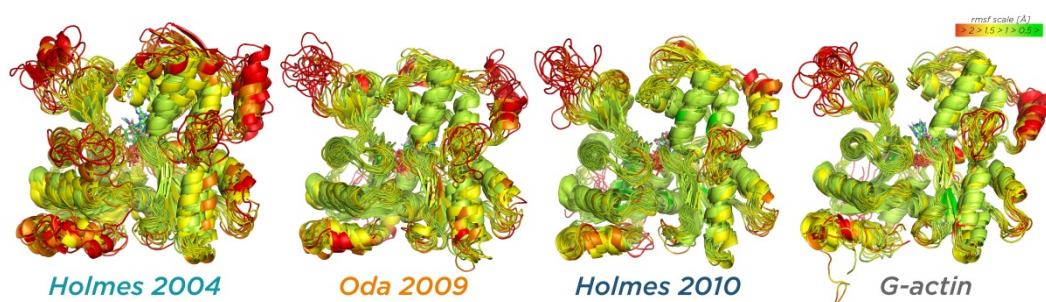
Fig. 5.4. Superposition of the 13 protomer structures after 30 ns of MD simulation by a mass-weighted RMSD fit of the protein backbone. The structures are color-coded by RMS fluctuation per residue over the entire simulation time, where very flexible residues are shown in red and residues with little fluctuation of their position in green.

Figure 5.5 A compares the backbone per-residue RMS fluctuations of the MD simulations of G-actin and the three models. The DNase I binding loop (residues 39-50) and residues 220-250 are highly mobile parts of the protein. On average, the fluctuations of the Holmes 2004 simulations are the highest and those of Holmes 2010 the lowest, the latter again being similar to G-actin.
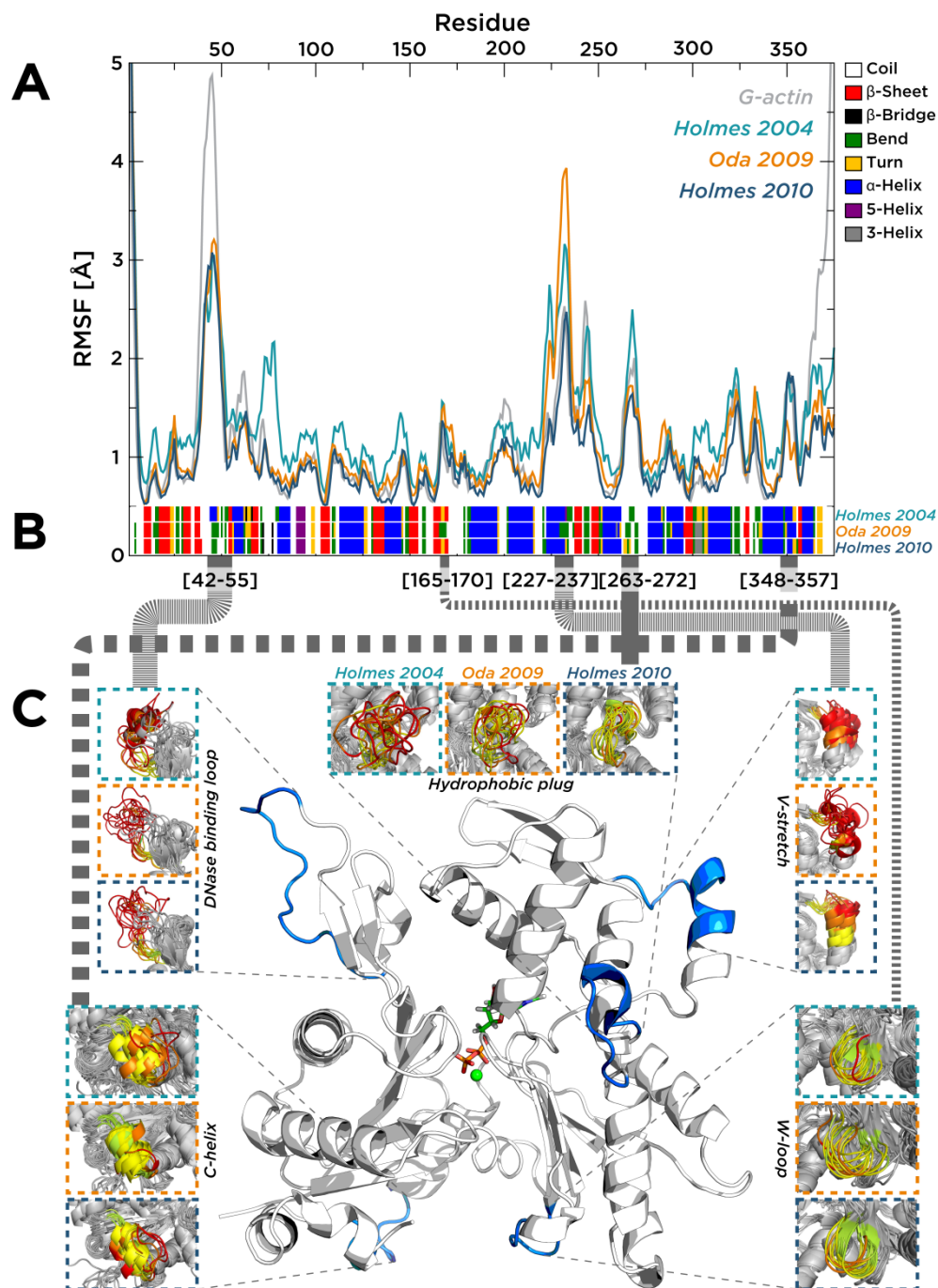
Fig. 5.5. Comparison of Root mean-square fluctuation, secondary structure and local conformational details between the MD simulations of Holmes 2004 & 2010 model, Oda model and G-actin.

A - Root mean-square fluctuation per residue, averaged over 13 actin molecules.

B - Secondary structure profiles of the three filament models, averaged over protomers and over the last 5 ns. For each residue, the most highly occupied state of the 13 profiles is shown.

C - Highlighted are five regions of the protomer in which the secondary structure significantly varies among the simulations of the three models: DNase I binding loop (residues 42-55); W-loop (residues 165-170); residues 227-237; hydrophobic plug (residues 263-272); residues 348-357.

Five segments in which the secondary structures (Fig. 5.5 B) in the simulations of the models are significantly different are highlighted in Fig. 5.5 C. The conformation of the DNase I binding loop has been hypothesized to be coupled to the nucleotide state of actin [21]. This loop is disordered in all of the over 40 G-actin crystal structures resolved, with the exception of a tetramethylrhodamine-labeled ADP-bound G-actin structure in which it is an α-helix [21]. It has been suggested that a change of conformation of the loop might explain the different association rates of the ATP- and ADP-bound G-actin to the filament [21], and also that the α-helix may contribute to the higher flexibility of ADP-F-actin relative to the ATP-bound form [108]. A recent simulation study suggested that the α-helix conformation may be favored only in F-actin [39]. However, these hypotheses have been contested and it has been suggested that the helix is an artifact of crystallization [36]. Several subsequent studies found no relation between the nucleotide state and the conformation of the DNase I binding loop in G-actin [45, 109]. Among the three models considered here, only Holmes 2004 has a DNase I binding loop in α-helical conformation, and this was found to unfold entirely in 6 of the 13 protomers (and, as shown in Fig. 5.4, in all but one simulation of monomeric G-actin). In the other two models the loop explores disordered conformations throughout the simulations.

The W-loop (residues 165-170), to which WH2-domain containing proteins bind, forms a β-hairpin in the simulations of both Holmes 2004 and Holmes 2010 but a bend in the Oda 2009 MD. The solvent-exposed V-stretch (residues 227-237) includes part of an α-helix and exhibits high RMS fluctuations in the simulations. In most of the Oda-simulation protomers the helix partially unfolds. In the Holmes 2004 simulation the helix remains mostly intact but its position varies among the 13 protomers.

The conformation of the 'hydrophobic plug' (GLN263-SER271) in the Holmes 2004 model differs from that in the two newer filament models. In 1990 Holmes *et al.* suggested that this loop may alter its position upon integration of the G-actin monomer into the filament by detaching from the surface of the actin molecule and extending into a hydrophobic pocket in the opposing strand, thus stabilizing the filament. However, later research suggested that the radius of gyration of the earlier actin filament models (such as Holmes 2004; ~24.8 Å), and thus the distance between the two strands of the long-pitched helix, had been overestimated. The radii of gyration of Oda 2009 and Holmes 2010 are 23.7 and 24 Å, respectively, and in the MD both increase slightly, by 0.3 and 0.2 Å, respectively. Due to the closer proximity of the two strands, an

extended hydrophobic plug is not required for the stability of the actin filament [51]. In the present MD simulations, the hydrophobic plug showed a high degree of structural variation in Holmes 2004 and some variation in the Oda simulation but was highly conserved among the Holmes 2010 protomers. Residues 348-357 form an α-helix (C-helix) that is located near the C-terminus and remains stable in the Oda simulations but unfolds in some protomers of the two Holmes simulations.
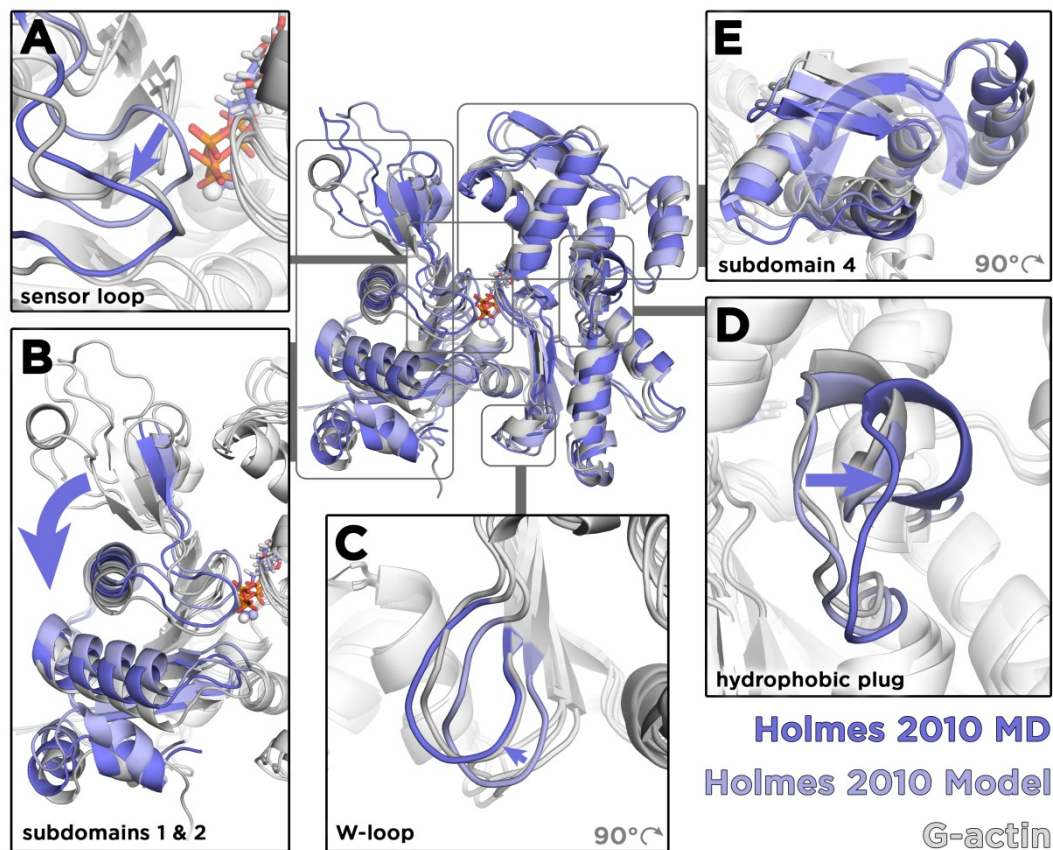
Fig. 5.6. Localized conformational differences between the structures of G-actin (PDB 1J6Z), the Holmes 2010 model and the average Holmes 2010 MD structure. The two Holmes structures were aligned to the crystallographic structure of G-actin by means of a RMSD fit of the entire actin molecule.

Figure 5.6 superimposes the average protomer from the Holmes 2010 MD simulation, the initial Holmes 2010 model and the G-actin structure from which the model was derived. For this, an average protomer structure was calculated from selected time-averaged protomer structures (see Chapter 2.3)

from the Holmes 2010 simulation and superimposed on the G-actin structure. Five structural differences between the three conformations are apparent. The positions of the sensor loop containing the methylated HIS73 (residues 70-78; Fig. 5.6 A) and the loop formed by residues 165-170 (Fig. 5.6 C) in the Holmes 2010 model differ from those in the G-actin crystal structure. During the simulation however, these two loops revert back to the G-actin crystal structure positions again. Fig. 5.6 B shows that the twisting of the two lobes of the G-actin structure, that is responsible for the flattening of the protomers in the filament model, is lessened during the simulation. In contrast, the slight rotation of subdomain 4 (Fig. 5.6 D) in the Holmes 2010 model is amplified in the MD. The hydrophobic plug slightly changes its position during MD simulation (Fig. 5.6 E) but does not adopt the extended conformation of previous Holmes filament models.

5.3 Implications of the nucleotide state

The nucleotide-induced conformational changes of actin and the activation of the ATPase activity on transition from G- to F-actin make the nucleotide binding site critical to understanding the functional cycle of the protein. Hence, the hydrogen-bonding networks between the nucleotide and actin molecule were characterized for each individual protomer. In one of the protomers of the Holmes 2004 model, the ADP molecule left the binding pocket entirely, and in many of the other protomers the position of the ADP changed significantly by translation or rotation during the simulation. Because of this instability, the nucleotide binding site of the Holmes 2004 simulation was not investigated further. The occupancies of individual hydrogen bonds in the nucleotide binding site of each protomer of the Oda 2009 and Holmes 2010 (ATP & ADP) simulations are shown in Tables 5.1-5.3.

ADP		Oda 2009													average A1-A13	average selected
		A1	A2	A3	A4	A5	A6	A7	A8	A9	A10	A11	A12	A13		
ADP O*B - LYS 18 HZ*		92	100	100	93	100	100	100	100	100	100	100	100	100	98	98
ADP O*B - SER 14 HN		96	14	0	94	100	81	100	100	6	100	99	99	97	75	99
ADP H2' - GLU 214 OE*		100	99	65	60	0	99	65	39	0	31	60	7	100	55	53
ADP H3T - ASP 157 OD*		99	100	2	81	0	99	2	98	0	56	0	56	91	52	43
ADP O*B - GLY 15 HN		100	0	0	63	0	0	86	97	0	28	81	66	0	40	72
ADP O2A - LEU 16 HN		31	0	44	0	0	0	99	0	0	99	95	99	0	35	85
ADP O1A - LYS 18 HZ*		0	3	55	6	1	23	89	0	0	96	83	65	0	32	67
ADP O2' - LYS 213 HZ*		92	78	0	24	13	100	0	32	0	0	0	1	72	31	19
ADP O2A - ASP 157 HN		0	32	43	0	99	0	0	0	96	0	0	0	0	20	0
ADP O2A - GLY 15 HN		0	0	56	0	38	96	8	0	0	35	4	14	0	19	12
ADP O*B - GLY 13 HN		0	0	0	0	0	0	31	99	0	98	0	0	0	17	26
ADP O1A - LEU 16 HN		0	0	45	0	85	90	0	0	0	0	0	0	0	16	0
ADP O1A - GLY 302 HN		96	0	0	0	0	0	0	0	0	0	0	0	91	14	19
ADP O3' - LYS 213 HZ*		5	34	10	0	80	0	0	0	0	0	0	0	44	13	1
ADP H3T - THR 303 OG*		0	0	0	0	68	0	35	0	0	0	0	0	0	7	7
ADP O2A - LYS 18 HZ*		87	1	0	6	0	0	0	0	0	0	0	0	0	7	17
ADP O3A - SER 14 HG1		0	0	0	0	0	0	0	0	0	0	0	0	72	5	0
ADP H3T - GLU 214 OE*		0	0	0	0	0	0	0	0	0	0	69	0	0	5	14
ADP O*B - ASN 12 HD22		17	0	0	0	0	0	0	39	0	2	0	0	0	4	4
ADP H61 - ARG 335 O		0	0	0	0	0	0	0	0	0	40	12	0	0	4	10
ADP H62 - MET 305 O		0	0	0	0	0	0	47	1	0	0	0	0	3	3	9
ADP O*B - GLN 137 HE2*		0	0	0	0	0	0	11	0	0	0	1	20	0	2	6
ADP O*B - LEU 16 HN		2	0	0	0	0	0	0	25	0	0	0	0	0	2	0
ADP O1A - GLY 15 HN		0	0	13	0	12	0	0	0	0	0	0	0	0	1	0
ADP H3T - SER 155 O		0	0	0	0	0	0	0	0	22	0	0	0	0	1	0
ADP H3T - GLY 156 O		0	0	0	0	0	0	0	0	0	0	0	14	0	1	3
sum of h-bonds within >30%-cutoff		610	394	266	421	214	502	541	466	106	510	518	493	460		

Table 5.1. Occupancy (%) of hydrogen bonds between ADP and protein of 13 Oda 2009 protomers during last 5 ns of MD. Each column A1-A13 represents the occupancies of a protomer. The table is sorted by average occupancy. Because some nucleotides had a very low number of typical hydrogen bonds in the simulations, only protomers with a high number of typical nucleotide contacts were used to calculate a meaningful average hydrogen-bond pattern and protomer structure (as described in Chapter 2.3). Thus, hydrogen bonds that are formed >30% of the time are considered representative for this simulation. This 30% cutoff is represented by the horizontal line. The bottom line of the table sums the percentages of these representative hydrogen bonds for each protomer. Only those protomers with a high occupancy of representative hydrogen bonds (shown in blue) were considered for further analysis. The average hydrogen-bond occupancy of only those selected protomers is given in the last column.

ADP — Holmes 2010

ADP		A1	A2	A3	A4	A5	A6	A7	A8	A9	A10	A11	A12	A13	average A1-A13	average selected
ADP H3T - ASP 157 OD*		99	99	0	0	41	23	88	41	98	74	16	99	100	59	64
ADP O2A - GLY 15 HN		0	100	100	100	0	0	99	0	0	98	0	100	99	53	100
ADP O*B - SER 14 HN		0	0	100	100	100	40	100	6	0	0	97	0	91	48	65
ADP O2A - LEU 16 HN		0	99	98	100	11	0	100	0	0	0	0	100	100	46	100
ADP H2' - GLU 214 OE*		100	100	0	0	2	0	39	19	100	26	0	100	100	45	57
ADP O1A - LYS 18 HZ*		0	100	92	100	0	0	100	0	0	1	0	87	100	44	97
ADP O*B - SER 14 HG1		0	2	100	100	0	92	100	0	0	0	79	0	99	44	67
ADP O2' - LYS 213 HZ*		96	64	0	0	0	0	30	8	98	17	0	99	89	38	47
ADP O*B - LYS 18 HZ*		0	0	43	0	0	0	0	97	0	100	97	0	0	25	7
ADP O2A - LYS 18 HZ*		0	0	0	0	100	88	0	0	98	0	0	0	0	22	0
ADP O*B - ASP 157 HN		0	92	0	0	0	0	0	0	0	0	0	56	90	18	40
ADP O*B - GLN 137 HE2*		10	0	99	23	0	0	0	2	0	99	1	0	0	18	20
ADP H2' - ASP 157 OD*		0	0	62	91	4	0	3	17	0	0	4	0	0	13	26
ADP O3A - ASP 157 HN		1	0	1	64	0	0	90	0	0	0	0	0	0	12	26
ADP O2A - SER 14 HN		54	53	0	0	0	0	0	0	0	40	0	1	0	11	9
ADP O1A - LEU 16 HN		0	0	0	0	0	0	0	0	0	92	0	0	0	7	0
ADP O2A - GLY 302 HN		0	0	0	0	0	0	0	87	0	0	0	0	0	6	0
ADP O2A - SER 14 HG1		42	0	0	0	0	0	0	0	0	13	0	0	0	4	0
ADP O2A - GLN 137 HE2*		0	0	0	0	0	48	0	0	0	0	0	0	0	3	0
ADP O3A - SER 14 HG1		0	0	0	0	0	1	0	0	0	0	42	0	0	3	0
ADP O3A - SER 14 HN		0	0	0	0	0	28	0	0	0	0	0	0	0	2	0
ADP O3' - LYS 213 HZ*		1	0	0	0	0	0	2	0	2	13	0	0	0	1	0
sum of h-bonds within >30%-cutoff		295	564	490	500	154	155	656	74	296	216	192	585	778		

Table 5.2. ADP-hydrogen-bond occupancy in per cent of 13 Holmes 2010 protomers during last 5 ns of MD. The table is sorted by average occupancy.

ATP — Holmes 2010

ATP		A1	A2	A3	A4	A5	A6	A7	A8	A9	A10	A11	A12	A13	average A1-A13	average selected
ATP H3T - ASP 157 OD*		69	92	100	95	50	87	74	100	97	5	65	94	46	74	88
ATP O*B - GLN 137 HE2*		1	86	90	57	82	99	98	0	0	92	92	0	42	56	93
ATP O*B - LYS 18 HZ*		93	100	83	0	0	100	99	0	15	0	53	13	65	47	96
ATP O2A - LYS 18 HZ*		30	0	73	73	0	5	5	97	0	0	71	94	56	38	21
ATP H2' - GLU 214 OE*		100	0	19	2	90	42	13	100	84	22	9	1	2	37	19
ATP O*B - SER 14 HN		9	100	99	0	0	99	86	10	49	0	0	0	0	34	96
ATP O1A - GLY 302 HN		23	96	24	69	1	0	1	75	70	1	1	86	0	34	30
ATP O2A - LEU 16 HN		0	57	1	0	0	100	100	0	0	0	53	33	95	33	65
ATP O*B - SER 14 HG1		0	99	0	98	0	100	100	0	0	0	13	19	0	33	75
ATP O*G - GLY 158 HN		89	0	0	0	41	0	0	89	91	77	0	0	0	29	0
ATP O*G - SER 14 HG1		100	0	0	0	0	0	0	100	100	0	0	0	0	23	0
ATP O2' - LYS 213 HZ*		0	0	12	24	66	0	0	77	62	0	0	0	0	18	3
ATP O3A - ASP 157 HN		1	0	56	37	4	0	1	39	21	0	2	18	0	13	14
ATP N3 - LYS 213 HZ*		0	97	0	0	8	0	5	0	0	0	0	0	0	8	26
ATP O*B - ASP 157 HN		1	0	0	4	47	0	0	30	0	19	0	0	0	7	0
ATP O*B - LEU 16 HN		0	0	0	0	0	0	0	100	0	0	0	0	0	7	0
ATP O*B - GLY 15 HN		0	0	0	0	0	0	0	92	1	0	0	0	0	7	0
ATP O3' - LYS 213 HZ*		0	0	0	1	3	0	0	35	53	0	0	0	0	7	0
ATP O*G - SER 14 HN		13	0	0	0	0	0	0	70	0	0	0	0	0	6	0
ATP H2' - ASP 157 OD*		0	0	0	0	0	0	0	0	0	0	4	15	43	4	0
ATP O2' - ARG 210 HH1*		0	24	0	0	16	0	0	0	0	11	0	0	0	3	6
ATP O*G - ASP 157 HN		41	0	0	0	0	0	0	0	3	0	0	0	0	3	0
ATP O*B - GLY 13 HA1		3	4	2	0	0	23	5	0	2	0	0	0	0	3	9
sum of h-bonds within >30%-cutoff		325	630	489	394	223	632	576	382	315	120	357	340	306		

Table 5.3. ATP-hydrogen-bond occupancy in per cent of 13 Holmes 2010 protomers during last 5 ns of MD. The table is sorted by average occupancy.

A schematic representation of the resulting average hydrogen-bond network of the ATP- and ADP-forms of the Holmes 2010 filament is given in Fig. 5.7. In agreement with the crystal structures of G-actin, SER14 forms two hydrogen bonds with the γ-phosphate group in the ATP simulation but these shift to the β-phosphate group in the MD of ADP-bound actin. Likewise, the interaction of LYS18 also shifts, from the β-phosphate group in the ATP simulation to the α-phosphate group with ADP. In both simulations (ATP and ADP) of the Holmes 2010 model, LEU16 forms a hydrogen bond with the α-phosphate group and ASP157 interacts with H3T of the adenosine group. Other significant differences include the complete absence of an interaction of GLY15 with the α-phosphate oxygen in the ATP simulation. In G-actin, the HN atoms of GLY15 and ASP157 interact with the oxygen of the β-phosphate group. These two contacts do not occur in the ATP-bound simulation of the Holmes 2010 model.
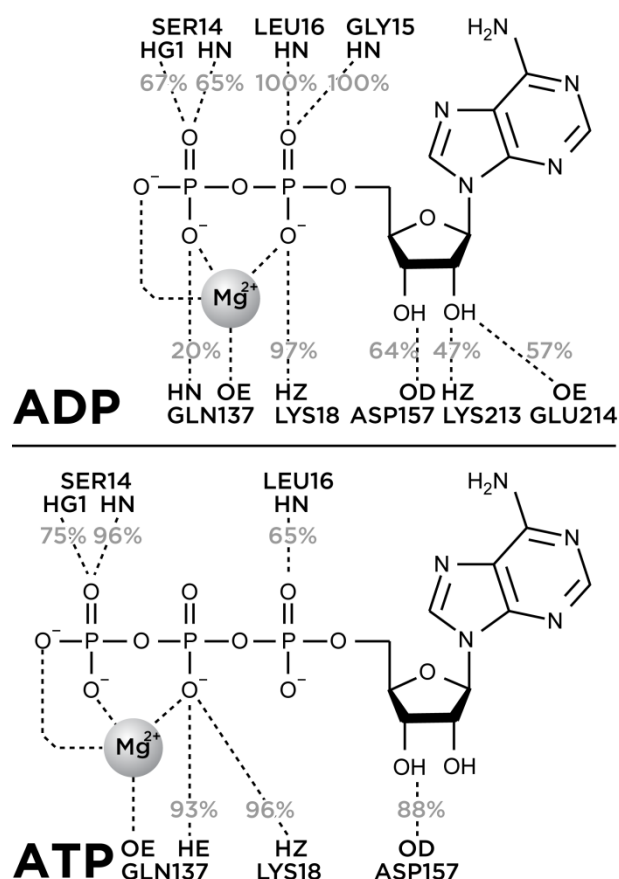

Fig. 5.7. Differences in average nucleotide binding patterns of actin protomers from the Holmes 2010 ATP- and ADP-filament simulations. Percentages correspond to the fraction of the last 5 ns simulation time the hydrogen bond was formed. Water molecules surrounding the magnesium ion and nucleotide are not shown.

The most significant difference in the hydrogen bonding patterns between the ATP-bound and ADP-bound systems may concern the hydrogen bond between GLN137 and the oxygen of the β-phosphate, which forms 93% of the time in the ATP-bound case but only 20% of the time for the ADP-bound actin simulation. This interaction was not observed in crystallographic structures of G-actin: in PDB entry 1NWK [25] of ATP-bound G-actin, for example, the distance between GLN137 and the oxygen of the β-phosphate group is 6.7 Å. GLN137 is located at the bottom of the nucleotide binding cleft, at the hinge between the two large domains of the actin molecule. As illustrated in Fig. 5.8, the flattening of the G-actin structure during filament formation is responsible for bringing GLN137 closer to the nucleotide, permitting the formation of a stable hydrogen bond during MD simulation of the model. These findings suggest that the repositioning of GLN137 during the G- to F-actin transition may play a key role in invoking the ATPase activity in F-actin.
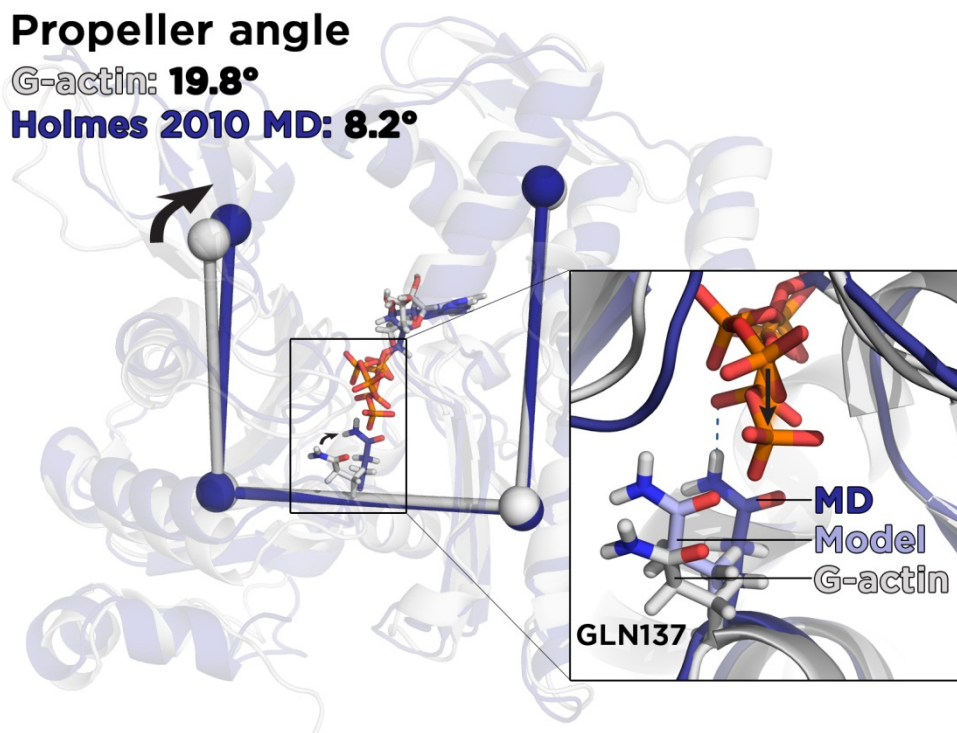

Fig. 5.8. Possible activation mechanism of ATPase activity in F-actin. The propeller angle is the dihedral angle formed by the centers of mass of the four subdomains. It is significantly lower in F-actin than G-actin (PDB entry 1NWK; grey). The inset shows how the twisting of the actin molecule in the filament (Holmes 2010, light blue) brings GLN137 in close proximity to the ATP. During MD simulation of the ATP-bound Holmes 2010 model (dark blue), this distance decreases further and a stable hydrogen bond between GLN137 and ATP is formed.

5.4 Discussion

5.4.1 Comparison of models

The resolution of fiber diffraction and EM data used to construct pre-2009 F-actin models was not sufficient to reveal the global conformational change taking place during the G- to F-actin transition. However, the higher resolution X-ray data obtained by Oda *et al.* [51] clearly indicate that a twist of the two domains of the U-shaped actin monomer leading to a flattening of the monomer structure is the main global conformational change upon assembly of G-actin to the filament. This global change is incorporated in both the present Holmes 2010 model and that of Oda 2009. Although the two models exhibit similar low-resolution structures they differ significantly in their details. In Oda 2009 adjustments of the local structure were made so as to reduce the *R*-factor. However, in the present model, these adjustments have been avoided thus preserving the stereochemistry and keeping the local structure as close as possible to that of the crystallographic G-actin.

The progression in quality of the three structural models examined is apparent upon subjecting them to MD simulation. Among the three tested models, the structural stability of Holmes 2004 is the lowest: the average RMSD of the protomers and the structural variation among the 13 protomers are both significantly higher than for the other two models. Both in the initial model and during the MD simulation the distance between the filament strands is the highest. Further, all protomers in the simulation of the Holmes 2004 model show unfolding of some of the secondary structural elements. In the majority of protomers, the ADP is unstable within the nucleotide binding site and even leaves the binding pocket entirely in one of the protomers.

The relative structural instability of the Holmes 2004 model may be partly due to the quality of the experimental diffraction data and partly due to the way the structure had to be generated: the experimental data were not sufficiently detailed to permit structural change within the four subdomains, and so the model was built by treating the G-actin subdomains as independent rigid bodies, adjusting their positions during the fitting. No side-chain optimization at the interface between protomers within the filament was performed.

In comparison to Holmes 2004, the simulations of the Oda 2009 and Holmes 2010 filaments exhibit higher structural stability and their observed properties are closer to the expected values. The higher structural stability of the Oda

2009 model in comparison to another older model was also found in a recent MD study [110]. The average RMSD of the Oda 2009 and Holmes 2010 model protomers is very close to that of the simulation of the G-actin crystal structure. In contrast, the propeller angle formed by the four subunits of the actin molecule is much higher in the G-actin simulation than in the simulations of the F-actin models. This is to be expected, as the major conformational transition that occurs upon incorporation of G-actin into the filament is believed to be a twist of the actin molecule that flattens the structure and significantly reduces the size of the cleft between the two domains [51, 109]. However, in all three simulations of F-actin models, the initially very small propeller angle of 2-3° increases significantly to about 7-9°, while still remaining well below the 22° of the G-actin simulation. The fact that all three models show this same trend may indicate that the flattening twist of the actin molecule imposed during model building is slightly too high. In the simulation of Oda 2009 the increase of the propeller angle during MD is steady but slower than that of the other two models. This may arise from the fact that the inter-protomer interface was optimized in the Oda model but not in the two Holmes models, resulting in a higher number of non-bonded interactions between protomers within the filament (Fig. 5.3 C) and thus stabilizing the inter-protomer interface and delaying the propeller angle increase over the simulation time.

In contrast to the interactions between protomers, the number of hydrogen bonds within the actin molecules is significantly lower throughout the simulation of the Oda 2009 model than in G-actin or Holmes 2010. An explanation for this difference may again be in the different approach that was taken to build the two models. As part of the model refinement process, Oda *et al.* used a simulated annealing procedure to minimize the R-factor. As a result, hydrogen bonds within the actin molecule were disrupted. In contrast, the Holmes 2010 model is essentially the crystallographic structure of G-actin with a twist into a more planar form, carried out with as little impact on the native intra-protomer interactions as possible. Indeed, the average hydrogen-bond count in the simulation of the Holmes 2010 model is even slightly higher than that of the crystallographic G-actin structure, consistent with the more open structure of the G-actin monomer.

The present Holmes 2010 F-actin model possesses both a global conformation in agreement with the recent Oda 2009 model and a consistent intra-protomer stereochemistry. As such it should form a useful basis for atomic-detail investigations into F-actin structure-dynamics-function relationships.

5.4.2 ATP *vs* ADP state

Experimental studies suggest that the conformation of ATP- and ADP-F-actin must differ, as global properties such as the persistence length or the binding affinity of some actin-binding proteins depend on the nucleotide state of the filament. The structural differences between simulations of the ATP- and ADP-bound Holmes 2010 model observed here are relatively small. Longer simulation times than are currently possible are likely to be necessary to fully observe the conformational changes between the two states of the filament. Hence, we focus here on the local differences in the nucleotide binding pocket, from which potential global conformational differences of the protomer will originate. Although the initial protein structures were identical, we found that in MD simulation the nucleotide-binding pocket of the ATP- and ADP-bound Holmes 2010 filaments differ significantly from each other. Furthermore, differences also exist between the ATP-binding patterns of the G-actin X-ray structure and the average ATP-bound F-actin protomer, as would be expected as, in contrast to G-actin, F-actin does exhibit significant ATPase activity.

Exploration of the ATP-hydrolysis mechanism of F-actin is very challenging for several reasons. Actin exhibits a particularly slow ATPase activity which is related to the relative sparseness of functional groups that interact with the polyphosphate tail. A high-resolution crystallographic structure of actin is only available only of the monomeric form, which effectively does not exhibit hydrolytic activity. For this reason, only limited conclusions can be drawn from analyzing the structure of the nucleotide binding site in G-actin X-ray structures or performing quantum mechanical calculations on them. Several studies have investigated possible mechanisms of hydrolysis of ATP in actin [48, 49, 50]. A study of actin mutants Oda *et al.* revealed the significance of GLN137 for filament polymerization and cleavage of the γ-phosphate group: replacing this glutamine with an alanine caused a 4-fold slowdown of ATP-hydrolysis [50]. Further, Oda *et al.* suggested that the twist of the ATP-bound actin monomer upon integration into the filament leads to relocation of GLN137 bringing it in close proximity to ATP [51]. In agreement with another recent MD study of the actin filament [110], the present simulations support this hypothesis. Unlike in the crystal structures of G-actin or the simulation of the ADP-bound Holmes 2010 model, GLN137 is close to the ATP in the MD of the Holmes 2010 model, forming a stable hydrogen bond with the oxygen atom of the β-phosphate group, and may therefore play a direct role in hydrolysis.

5.5 Summary

Here, we present a new model of the actin filament (F-actin) that incorporates the global structure of the recently published model by Oda *et al.* but also conserves internal stereochemistry. The improved quality of the model is apparent in a comparison made of the model with other recent F-actin models using molecular dynamics simulation, monitoring a number of structural determinants, in particular RMSD, RMSF, hydrogen bonding patterns and propeller angle. We find that the Holmes 2010 model retains its structural integrity the best. The hydrogen bonding network between protomers is best maintained in the Oda 2009 model but the number of hydrogen bonds within the protomer is significantly reduced during the simulation in comparison to Holmes 2010 and G-actin. The Holmes 2004 model shows the least structural integrity among the three models. In addition, simulations of the Holmes 2010 model are carried out in states with both ATP or ADP bound and local hydrogen-bonding differences characterized. In agreement with previous studies, we predict the importance of GLN137 for activation of ATPase activity after the G- to F-actin transition. However, in contrast to other suggested mechanisms for ATP hydrolysis in actin, our results indicate a direct interaction of GLN137 with ATP. MD simulations now give us a deeper insight in the structure of F-actin and its implications to its function but further studies are required to fully understand the effects of the nucleotide on the structure of the filament.

CHAPTER 6

CONCLUDING REMARKS

Several aspects of the G- and F-actin structure in relation to their nucleotide-driven functional cycle have been studied in this thesis. The first aspect we studied is the structural differences between ATP- and ADP-G-actin. We used molecular dynamics simulations to study the 'open' and 'closed' conformational states of G-actin in aqueous solution, with either ATP or ADP in the nucleotide binding pocket. We show that with both ATP and ADP bound the open state closes in the absence of actin-bound profilin. Thus, the open state is not a stable form of monomeric actin in solution. We suggest that the open state is a short lived intermediate in the nucleotide-exchange pathway. The results are consistent with the overwhelming excess of closed state structures reported in comparison to the single crystallographically resolved G-actin structure in the open state structure that points towards a negligible population of the open state. The open state structure of profilin-bound G-actin was only obtained under high salt conditions, while profilin-bound G-actin under physiological salt concentrations adopted the closed conformation [20]. Furthermore, the nucleotide in the open state is significantly more exposed to solvent, suggesting that it is indeed not the position of the nucleotide in the native state of G-actin. In agreement with numerous other studies, we are thus convinced that the open-*vs*-closed-state hypothesis to discriminate between ATP- and ADP state of G-actin can be dismissed while an ensemble of G-actin structures with slightly varying nucleotide cleft might exist *in vivo*.

An alternative model proposes the nucleotide-induced structural change in G-actin to be a conformational transition in the DNase I binding loop. According to this model, the DNase I binding loop adopts an α-helical fold in the ADP state but unfolds when ATP is bound. The MD simulations of G-actin carried out in this study do not support the model. A few instances of the α-helical fold were indeed observed, but were extremely short-lived and present in both ATP-

and ADP-bound states. Thus, no correlation could be established between the conformation of the DNase I binding loop and the nucleotide state.

Using molecular dynamics simulations we found a new state of ATP-bound G-actin which has not (yet) been experimentally determined. We term this novel conformation 'superclosed state' due to its smaller nucleotide binding cleft in comparison to the closed state. The state was structurally well defined and observed in several independent simulations starting from different closed state crystal structures. The superclosed state exhibits striking resemblance with the conformation of the protomer structure of F-actin models. Therefore, we speculate that the biological role of this state may be the polymerization-competent form of ATP-bound G-actin. This speculation is reinforced by the fact that the superclosed state was only seen in the ATP-bound form that is known to have a higher affinity to bind F-actin compared to ADP-G-actin. Moreover, the difference in binding rates of ATP- and ADP-bound G-actin to the filament dictate the existence of structural differences between the two states. The presence of the superclosed state as the polymerization-competent form of ATP-G-actin is a model that plausibly explains the dilemma of the structural similarities of the experimentally-determined G-actin structures in the ATP- and ADP state. Our model is convincing since, unlike the open-*vs*-closed state and DNase I binding loop hypotheses, it does not contradict existing biochemical studies.

Limitations of the X-ray technique may be one of the reasons why the superclosed state has not been observed experimentally to date. In X-ray crystallography only unique, stable crystallizable states of the protein may be observed. Thus, it is possible that crystal packing interactions favor a closed state of G-actin even though in solution an ensemble of structural states with varying population exits. A specific limitation in the case of G-actin is that its native state can't be crystallized due to its propensity to form filaments. Thus, all crystallographically reported G-actin structures have been either co-crystallized with another protein or modified by various methods.

No crystallographically determined structure of the actin filament exists but models of the F-actin structure based on fiber diffraction, electron microscopy studies or a combination of both have been proposed. Fiber diffraction studies reaching resolutions up to 3.3-5.6 Ångstrom point towards the existence of a highly-populated, single conformation of the filament [51]. In contrast, some electron microscopy studies suggest the structure of the actin filament to be polymorphic and allosteric [111]. Thus, research in the structural properties of

F-actin remains controversial. MD simulations allow us to probe the dynamics of F-actin and the structural integrity of the different models.

In this thesis we present a new model of the actin filament, the Holmes 2010 model, based on the global protomer structure of the model by Oda *et al.* and additionally conserves internal stereochemistry. A comparison of our model with other recent F-actin models using molecular dynamics simulation, shows the improved quality of the model in terms of conservation of structural integrity. Arguably, the Oda model has an improved actin-actin interface with respect to the Holmes 2010 model, since it was refined to maximize inter-protomer contacts. Combining the strengths of the Holmes 2010 model with the Oda 2009 model could improve the F-actin mode further. We would like to note that the F-actin model did not exhibit an unnaturally high dynamics or structural fluctuations disputing the high variability within the filament proposed by some EM studies.

In addition, simulations of the 2010 Holmes model were carried out in both states with ATP and ADP bound to characterize local hydrogen-bonding differences. Mutation studies introducing point mutations within the nucleotide binding site suggested an important role for the residue GLN137 in the activation of the ATPase activity in F-actin. Quantum chemical (DFT) calculations on G-actin, suggested an indirect role with the GLN137 residue interacting with the nucleotide via a crystallographic water molecule. Since the calculations were carried out in G-actin due to the absence of an F-actin crystal structure, the significance of the results in explaining the ATP hydrolysis mechanism in F-actin are limited. The results point to the existence of a direct interaction of GLN137 with ATP for activation of ATPase activity after the G- to F-actin transition. In the F-actin model, the flattening of the actin molecule during the transition from G- to F-actin, brings GLN137 in close proximity to the ATP molecule and a hydrogen bond between the two is established in the MD simulations. The hydrogen bond is present in 90% of the simulation time pointing to its possible role in the hydrolysis cycle. However, the studies of the activation of ATPase activity in F-actin, both experimentally and computational - including this work, are still inconclusive and further work is necessary to explore this mechanism.

The present thesis illustrates the complex relationship of structure and function in the actin system the study of which is particularly challenging due to the incomplete and inconsistent data provided by various experimental methods. We believe that we could show how computational studies such as MD simulation may help to fill some of the gaps left by experimental studies to

get the full picture of the actin system. It is our hope that our findings such as the proposed model of the superclosed state as a polymerization-competent form for G-actin assembly to the filament will be pursued in further studies.

CHAPTER 7

FUTURE PERSPECTIVES

The work presented in this thesis is neither the beginning nor the end of necessary and interesting research of actin. Interesting, because after more than 60 years of study [112] fundamental questions about actin structure and dynamics and how these determine function remain unanswered. The questions addressed and the answers given here might, however, encourage further work on the topics presented in this thesis.

As one of the achievements of this work is the suggestion of an alternative interpretation of the different binding rates of ATP-bound and ADP-bound G-actin molecules to the filament, namely through a novel state of ATP-G-actin: the superclosed state, it is my natural wish that further work is initiated to test and hopefully verify the existence of this state. One experimental technique that may help to validate my hypothesis by determining the distances between two domains (such as subdomains 2 and 4) is electron paramagnetic resonance (EPR). An advantage of this method would be to measure populations of distances and thus indirectly testing the presence of the superclosed state - as opposed to measuring a single state as in X-ray crystallography. Furthermore, this method could verify the absence of G-actin in the open state.

The Holmes 2010 model has been published in collaboration with Kenneth C. Holmes as part of this thesis. Although the model shows a higher structural integrity than previous models, it lacks structural refinement at the inter-protomer interface. A promising approach towards an improved actin filament model would be to combine the strengths of the Oda 2009 and Holmes 2010 models.

Another focus of this thesis is the structure of F-actin. An experimentally-determined structure of the actin filament would answer many of the present questions involving the filament but no such structure at atomic detail exists to date. X-ray crystallography has been the most suitable technique to determine

the atomic structure of protein complexes. Crystallization of F-actin is challenging because of different reasons, such as the heterogeneous length of individual actin filaments. Several attempts have been made to grow crystals of F-actin and derivatives. A crystal structure of actin dimers that were cross-linked in F-actin was solved, but the two actin molecules were not arranged in a helical manner [113]. Further, preparation of a mini-thin filament with a well-defined length has been reported but their crystallization has not yet been possible [114]. Advances in novel techniques may allow obtaining a high resolution structure of the actin filament in the future. One such method is coherent X-ray diffractive imaging (CXDI), which allows 3D reconstruction of the image of single molecule nanoscale structures such as proteins and thus without the requirement of a protein crystal [115].

In this thesis, for the first time, MD simulations were used as a tool to identify problems with modeled atomic structures of F-actin. Due to the success of this method it should become a complementary tool to assess the quality of models in the future. In fact the method could be used to analyze structural integrity of modeled structures of other large protein complexes. This approach seems especially promising for studies on systems that proved to be challenging for conventional experimental methods such as membrane proteins.

With further investigations combining experimental analysis with computer simulation of actin at different length scales some of the important questions of structure-function relationships in both monomeric and filamentous actin may be answered.

REFERENCES

1. Lodish, H. et al. Molecular Cell Biology (W. H. Freeman and Company, 1999).

2. Golyshina, O.V. et al. Ferroplasma acidiphilum gen. nov., sp. nov., an acidophilic, autotrophic, ferrous-iron-oxidizing, cell-wall-lacking, mesophilic member of the Ferroplasmaceae fam. nov., comprising a distinct lineage of the Archaea. *Int J Syst Evol Microbiol* **50 Pt 3**, 997-1006 (2000).

3. Allen, P.G. et al. Phalloidin binding and rheological differences among actin isoforms. *Biochemistry* **35**, 14062-9 (1996).

4. Segura, M. & Lindberg, U. Separation of non-muscle isoactins in the free form or as profilactin complexes. *J Biol Chem* **259**, 3949-54 (1984).

5. Chaponnier, C. et al. The specific NH2-terminal sequence Ac-EEED of alpha-smooth muscle actin plays a role in polymerization in vitro and in vivo. *J Cell Biol* **130**, 887-95 (1995).

6. van den Ent, F., Amos, L.A. & Lowe, J. Prokaryotic origin of the actin cytoskeleton. *Nature* **413**, 39-44 (2001).

7. van den Ent, F., Moller-Jensen, J., Amos, L.A., Gerdes, K. & Lowe, J. F-actin-like filaments formed by plasmid segregation protein ParM. *EMBO J* **21**, 6935-43 (2002).

8. Roeben, A. et al. Crystal structure of an archaeal actin homolog. *J Mol Biol* **358**, 145-56 (2006).

9. Hara, F. et al. An actin homolog of the archaeon Thermoplasma acidophilum that retains the ancient characteristics of eukaryotic actin. *J Bacteriol* **189**, 2039-45 (2007).

10. Sheterline, P., Clayton, J., Sparrow, J. C. Actin (Oxford University Press, 1998).

11. Laing, N.G. et al. Mutations and polymorphisms of the skeletal muscle alpha-actin gene (ACTA1). *Hum Mutat* **30**, 1267-77 (2009).

12. Leavitt, J. et al. Variations in expression of mutant [beta] actin accompanying incremental increases in human fibroblast tumorigenicity. *Cell* **28**, 259-268 (1982).

13. Noegel, A.A. & Schleicher, M. Phenotypes of cells with cytoskeletal mutations. *Curr Opin Cell Biol* **3**, 18-26 (1991).

14. Chik, J.K., Lindberg, U. & Schutt, C.E. The structure of an open state of beta-actin at 2.65 A resolution. *J Mol Biol* **263**, 607-23 (1996).

15. Dominguez, R. & Graceffa, P. Solution properties of TMR-actin: when biochemical and crystal data agree. *Biophys J* **85**, 2073-4 (2003).

16. Minehardt, T.J., Kollman, P.A., Cooke, R. & Pate, E. The open nucleotide pocket of the profilin/actin x-ray structure is unstable and closes in the absence of profilin. *Biophys J* **90**, 2445-9 (2006).

17. Estes, J.E., Selden, L.A., Kinosian, H.J. & Gershman, L.C. Tightly-bound divalent cation of actin. *J Mus Res & Cell Mot* **13**, 272-284 (1992).

18. Carlier, M.-F., Pantaloni, D. & Korn, E.D. Fluorescence measurements of the binding of cations to high-affinity and low-affinity sites on ATP-G-actin. *J Biol Chem* **261**, 10778-10784 (1986).

19. Kabsch, W., Mannherz, H.G., Suck, D., Pai, E.F. & Holmes, K.C. Atomic structure of the actin:DNase I complex. *Nature* **347**, 37-44 (1990).

20. Schutt, C.E., Myslik, J.C., Rozycki, M.D., Goonesekere, N.C. & Lindberg, U. The structure of crystalline profilin-beta-actin. *Nature* **365**, 810-6 (1993).

21. Otterbein, L.R., Graceffa, P. & Dominguez, R. The crystal structure of uncomplexed actin in the ADP state. *Science* **293**, 708-11 (2001).

22. Rould, M.A., Wan, Q., Joel, P.B., Lowey, S. & Trybus, K.M. Crystal structures of expressed non-polymerizable monomeric actin in the ADP and ATP states. *J Biol Chem* **281**, 31909-19 (2006).

23. Klenchin, V.A., Khaitlina, S.Y. & Rayment, I. Crystal structure of polymerization-competent actin. *J Mol Biol* **362**, 140-50 (2006).

24. Isambert, H. et al. Flexibility of actin filaments derived from thermal fluctuations. Effect of bound nucleotide, phalloidin, and muscle regulatory proteins. *J Biol Chem* **270**, 11437-44 (1995).

25. Graceffa, P. & Dominguez, R. Crystal structure of monomeric actin in the ATP state. Structural basis of nucleotide-dependent actin dynamics. *J Biol Chem* **278**, 34172-80 (2003).

26. Belmont, L.D., Orlova, A., Drubin, D.G. & Egelman, E.H. A change in actin conformation associated with filament instability after P_i release. *Proc Nat Acad Sci U.S.A.* **96**, 29-34 (1999).

27. Page, R., Lindberg, U. & Schutt, C. Domain motions in actin. *Journal of molecular biology* **280**, 463-474 (1998).

28. Steitz, T., Shoham, M. & Bennett Jr, W. Structural dynamics of yeast hexokinase during catalysis. *Philosophical Transactions of the Royal Society of London. Series B, Biological Sciences* **293**, 43-52 (1981).

29. Zhang, Y. & Zuiderweg, E. The 70-kDa heat shock protein chaperone nucleotide-binding domain in solution unveiled as a molecular machine that can reorient its functional subdomains. *Proceedings of the National Academy of Sciences* **101**, 10272 (2004).

30. Kinosian, H.J., Selden, L.A., Gershman, L.C. & Estes, J.E. Interdependence of profilin, cation, and nucleotide binding to vertebrate non-muscle actin. *Biochemistry* **39**, 13176-88 (2000).

31. Kudryashov, D. & Reisler, E. Solution properties of tetramethylrhodamine-modified G-actin. *Biophysical journal* **85**, 2466-2475 (2003).

32. Strzelecka-Golaszewska, H., Moraczewska, J., Khaitlina, S.Y. & Mossakowska, M. Localization of the tightly bound divalent-cation-dependent and nucleotide-dependent conformation changes in G-actin using limited proteolytic digestion. *Eur J Biochem* **211**, 731-42 (1993).

33. Yao, X., Nguyen, V., Wriggers, W. & Rubenstein, P. Regulation of yeast actin behavior by interaction of charged residues across the interdomain cleft. *Journal of Biological Chemistry* **277**, 22875 (2002).

34. Guan, J., Almo, S., Reisler, E. & Chance, M. Structural Reorganization of Proteins Revealed by Radiolysis and Mass Spectrometry: G-Actin Solution Structure Is Divalent Cation Dependent†. *Biochemistry* **42**, 11992-12000 (2003).

35. Berman, H.M. et al. The Protein Data Bank. *Nucleic Acids Res* **28**, 235-42 (2000).

36. Sablin, E.P. et al. How does ATP hydrolysis control actin's associations? *Proc Nat Acad Sci U.S.A.* **99**, 10945-7 (2002).

37. Schüler, H. ATPase activity and conformational changes in the regulation of actin. *Biochim Biophys Acta* **1549**, 137-47 (2001).

38. Zheng, X., Diraviyam, K. & Sept, D. Nucleotide effects on the structure and dynamics of actin. *Biophys J* **93**, 1277-83 (2007).

39. Pfaendtner, J., Branduardi, D., Parrinello, M., Pollard, T.D. & Voth, G.A. Nucleotide-dependent conformational states of actin. *Proc Natl Acad Sci U S A* **106**, 12723-8 (2009).

40. Holmes, K.C., Popp, D., Gebhard, W. & Kabsch, W. Atomic model of the actin filament. *Nature* **347**, 44-9 (1990).

41. Egelman, E.H. Actin allostery again? *Nat Struct Biol* **8**, 735-6 (2001).

42. Kuznetsova, I., Antropova, O., Turoverov, K. & Khaitlina, S. Conformational changes in subdomain I of actin induced by proteolytic cleavage within the DNase I-binding loop: energy transfer from tryptophan to AEDANS. *FEBS letters* **383**, 105-108 (1996).

43. DalleDonne, I., Milzani, A. & Colombo, R. The tert-butyl hydroperoxide-induced oxidation of actin Cys-374 is coupled with structural changes in distant regions of the protein. *Biochemistry* **38**, 12471-80 (1999).

44. Kim, E. & Reisler, E. Intermolecular dynamics and function in actin filaments. *Biophysical Chemistry* **86**, 191-201 (2000).

45. Dalhaimer, P., Pollard, T.D. & Nolen, B.J. Nucleotide-mediated conformational changes of monomeric actin and Arp3 studied by molecular dynamics simulations. *J Mol Biol* **376**, 166-83 (2008).

46. Blanchoin, L. & Pollard, T.D. Hydrolysis of ATP by polymerized actin depends on the bound divalent cation but not profilin. *Biochemistry* **41**, 597-602 (2002).

47. Reisler, E. & Egelman, E.H. Actin structure and function: what we still do not understand. *J Biol Chem* **282**, 36133-7 (2007).

48. Vorobiev, S. et al. The structure of nonvertebrate actin: implications for the ATP hydrolytic mechanism. *Proc Nat Acad Sci U.S.A.* **100**, 5760-5 (2003).

49. Akola, J. & Jones, R.O. Density functional calculations of ATP systems. 2. ATP hydrolysis at the active site of actin. *J Phys Chem B* **110**, 8121-9 (2006).

50. Iwasa, M., Maeda, K., Narita, A., Maeda, Y. & Oda, T. Dual roles of Gln137 of actin revealed by recombinant human cardiac muscle alpha-actin mutants. *J Biol Chem* **283**, 21045-53 (2008).

51. Oda, T., Iwasa, M., Aihara, T., Maeda, Y. & Narita, A. The nature of the globular- to fibrous-actin transition. *Nature* **457**, 441-5 (2009).

52. Korn, E., Carlier, M. & Pantaloni, D. Actin polymerization and ATP hydrolysis. *Science* **238**, 638 (1987).

53. Selby, C.C. & Bear, R.S. The structure of actin-rich filaments of muscles according to x-ray diffraction. *J Biophys Biochem Cytol* **2**, 71-85 (1956).

54. Oosawa, F. & Kasai, M. A theory of linear and helical aggregations of macromolecules. *J Mol Biol* **4**, 10-21 (1962).

55. Egelman, E.H., Francis, N. & DeRosier, D.J. F-actin is a helix with a random variable twist. *Nature* **298**, 131-5 (1982).

56. W. T. Astbury, S.V.P., R. Reed, L. C. Spark. An electron microscopy and X-ray study of actin. *Biochim Biophys Acta* **1**, 379-392 (1947).

57. C. Cohen, J.H. An X-ray diffraction study of F-actin. *Biochim Biophys Acta* **21**, 177-178 (1956).

58. J. Hanson, J.L. The structure of F-actin of actin filaments isolated from muscle. *J Mol Biol* **6**, 46-60 (1963).

59. Trinick, J., Cooper, J., Seymour, J. & H., E.E. Cryo-electron microscopy and three-dimensional reconstruction of actin filament. *J Microsc* **141**, 349-360 (1986).

60. Lorenz, M., Popp, D. & Holmes, K.C. Refinement of the F-actin model against X-ray fiber diffraction data by the use of a directed mutation algorithm. *J Mol Biol* **234**, 826-36 (1993).

61. Tirion, M.M., ben-Avraham, D., Lorenz, M. & Holmes, K.C. Normal modes as refinement parameters for the f-actin model. *Biophys J* **68**, 5-12 (1995).

62. Holmes, K.C., Angert, I., Kull, F.J., Jahn, W. & Schroder, R.R. Electron cryo-microscopy shows how strong binding of myosin to actin releases nucleotide. *Nature* **425**, 423-7 (2003).

63. Holmes, K. Actin In A Twist. *Nature* **457**, 389-390 (2009).

64. Galkin, V., VanLoock, M., Orlova, A. & Egelman, E. A new internal mode in F-actin helps explain the remarkable evolutionary conservation of actin's sequence and structure. *Current Biology* **12**, 570-575 (2002).

65. Bennett, W. & Steitz, T. Glucose-induced conformational change in yeast hexokinase. *Proceedings of the National Academy of Sciences of the United States of America* **75**, 4848 (1978).

66. McDonald, R., Steitz, T. & Engelman, D. Yeast hexokinase in solution exhibits a large conformational change upon binding glucose or glucose 6-phosphate. *Biochemistry* **18**, 338-342 (1979).

67. Wilbanks, S., Chen, L., Tsuruta, H., Hodgson, K. & McKay, D. Solution small-angle X-ray scattering study of the molecular chaperone Hsc70 and its subfragments. *Biochemistry* **34**, 12095-12106 (1995).

68. Robinson, R. et al. Crystal structure of Arp2/3 complex. *Science* **294**, 1679 (2001).

69. Flaherty, K.M., McKay, D.B., Kabsch, W. & Holmes, K.C. Similarity of the three-dimensional structures of actin and the ATPase fragment of a 70-kDa heat shock cognate protein. *Proc Nat Acad Sci U.S.A.* **88**, 5041-5 (1991).

70. Bork, P., Sander, C. & Valencia, A. An ATPase domain common to prokaryotic cell cycle proteins, sugar kinases, actin, and hsp70 heat shock proteins. *Proceedings of the National Academy of Sciences* **89**, 7290 (1992).

71. Oda, T., Stegmann, H., Schröder, R.R., Namba, K. & Maéda, Y. Modeling of the F-actin structure. *Adv Exp Med Biol* **592**, 385-401 (2007).

72. Chen, X., Cook, R.K. & Rubenstein, P.A. Yeast actin with a mutation in the "hydrophobic plug" between subdomains 3 and 4 (L266D) displays a cold-sensitive polymerization defect. *J Cell Biol* **123**, 1185-95 (1993).

73. Musib, R., Wang, G., Geng, L. & Rubenstein, P. Effect of polymerization on the subdomain 3/4 loop of yeast actin. *Journal of Biological Chemistry* **277**, 22699 (2002).

74. Shvetsov, A., Musib, R., Phillips, M., Rubenstein, P. & Reisler, E. Locking the Hydrophobic Loop 262- 274 to G-Actin Surface by a Disulfide Bridge Prevents Filament Formation†. *Biochemistry* **41**, 10787-10793 (2002).

75. Scoville, D. et al. Hydrophobic Loop Dynamics and Actin Filament Stability. *Biochemistry* **45**, 13576-13584 (2006).

76. Gordon, J.C. et al. H++: a server for estimating pKas and adding missing hydrogens to macromolecules. *Nucleic Acids Res* **33**, W368-71 (2005).

77. Yao, X., Grade, S., Wriggers, W. & Rubenstein, P.A. His(73), often methylated, is an important structural determinant for actin. A mutagenic analysis of HIS(73) of yeast actin. *J Biol Chem* **274**, 37443-9 (1999).

78. Leach, A. Molecular modelling: principles and applications (Addison-Wesley Longman Ltd, 2001).

79. Pearlman, D. et al. AMBER, a package of computer programs for applying molecular mechanics, normal mode analysis, molecular dynamics and free energy calculations to simulate the structural and energetic properties of molecules. *Computer Physics Communications* **91**, 1-41 (1995).

80. MacKerell, A.D., Bashford, D., Bellott, M., Dunbrack, R.L., Evanseck, J.D., Field, M.J., Fischer, S., Gao, J., Guo, H., Ha, S., Joseph-McCarthy, D., Kuchnir, L., Kuczera, K., Lau, F.T.K., Mattos, C., Michnick, S., Ngo, T., Nguyen, D.T., Prodhom, B., Reiher, W.E., Roux, B., Schlenkrich, M., Smith, J.C., Stote, R., Straub, J., Watanabe, M., Wiorkiewicz-Kuczera, J., Yin, D., & Karplus, M. All-atom empirical potential for molecular modeling and dynamics studies of proteins. *J Phys Chem B* **102**, 3586-3616 (1998).

81. Jorgensen, W. & Tirado-Rives, J. The OPLS potential functions for proteins. Energy minimizations for crystals of cyclic peptides and crambin. *Journal of the American Chemical Society* **110**, 1657-1666 (1988).

82. van Gunsteren, W. & Berendsen, H. Computer simulation of molecular dynamics: Methodology, applications, and perspectives in chemistry. *Angewandte Chemie International Edition in English* **29**, 992-1023 (1990).

83. McCammon, J., Gelin, B. & Karplus, M. Dynamics of folded proteins. *Nature* **267**, 585-590 (1977).

84. Phillips, J.C. et al. Scalable molecular dynamics with NAMD. *J Comput Chem* **26**, 1781-802 (2005).

85. Darden, T., York, D. & Pedersen, L. Particle mesh Ewald: an Nlog(N) method for Ewald sums in large systems. *J Chem Phys* **98**, 10089-10092 (1993).

86. Ryckaert, J.-P. & Ciccotti G, B.H. Numerical integration of the cartesian equations of motion of a system with constraints: Molecular dynamics of n-alkanes. *J Comput Phys* **23**, 327-341 (1977).

87.   Jorgensen W L, C.J., Madura J D, Impey R W, Klein M L. Comparison of simple potential functions for simulating liquid water. *J Chem Phys* **79 (2)**, 926-935 (1983).

88.   Evans, D.J. & Holian, B.L. The Nose-Hoover thermostat. *J Chem Phys* **83**, 4069-4074 (1985).

89.   Hayward, S. & Lee, R.A. Improvements in the analysis of domain motions in proteins from conformational change: DynDom version 1.50. *J Mol Graph* **21(3)**, 181-183 (2002).

90.   Aguda, A.H., Burtnick, L.D. & Robinson, R.C. The state of the filament. *EMBO Rep* **6**, 220-6 (2005).

91.   Burtnick, L., Urosev, D., Irobi, E., Narayan, K. & Robinson, R. Structure of the N-terminal half of gelsolin bound to actin: roles in severing, apoptosis and FAF. *The EMBO Journal* **23**, 2713-2722 (2004).

92.   McLaughlin, P., Gooch, J., Mannherz, H. & Weeds, A. Structure of gelsolin segment 1-actin complex and the mechanism of filament severing. (1993).

93.   Robinson, R. et al. Domain movement in gelsolin: a calcium-activated switch. *Science* **286**, 1939 (1999).

94.   Otterbein, L., Cosio, C., Graceffa, P. & Dominguez, R. Crystal structures of the vitamin D-binding protein and its complex with actin: structural basis of the actin-scavenger system. *Proceedings of the National Academy of Sciences of the United States of America* **99**, 8003 (2002).

95.   Irobi, E. et al. Structural basis of actin sequestration by thymosin- 4: implications for WH2 proteins. *The EMBO Journal* **23**, 3599 (2004).

96.   Klenchin, V. et al. Trisoxazole macrolide toxins mimic the binding of actin-capping proteins to actin. *Nature Structural & Molecular Biology* **10**, 1058-1063 (2003).

97.   Bubb, M. et al. Polylysine induces an antiparallel actin dimer that nucleates filament assembly: crystal structure at 3.5-A resolution. *Journal of Biological Chemistry*, 201371200 (2002).

98.   Hertzog, M. et al. The [beta]-Thymosin/WH2 Domain:: Structural Basis for the Switch from Inhibition to Promotion of Actin Assembly. *Cell* **117**, 611-623 (2004).

99. Otomo, T. et al. Structural basis of actin filament nucleation and processive capping by a formin homology 2 domain. *Nature* **433**, 488-494 (2005).

100. Wriggers, W. & Schulten, K. Stability and dynamics of G-actin: Back-door water diffusion and behavior of a subdomain 3/4 Loop. *Biophys J* **73**, 624-639 (1997).

101. Kabsch, W. & Sander, C. Dictionary of protein secondary structure: pattern recognition of hydrogen-bonded and geometrical features. *Biopolymers* **22**, 2577-637 (1983).

102. De La Cruz, E.M. et al. Polymerization and structure of nucleotide-free actin filaments. *J Mol Biol* **295**, 517-26 (2000).

103. Rich, S.A. & Estes, J.E. Detection of conformational changes in actin by proteolytic digestion: evidence for a new monomeric species. *J Mol Biol* **104**, 777-92 (1976).

104. Rouayrenc, J.F. & Travers, F. The first step in the polymerisation of actin. *Eur J Biochem* **116**, 73-7 (1981).

105. Holmes, K.C., Schröder, R.R., Sweeney, H.L. & Houdusse, A. The structure of the rigor complex and its implications for the power stroke. *Philos Trans R Soc Lond B Biol Sci.* **359**, 1819-28 (2004).

106. Oda, T., Makino, K., Yamashita, I., Namba, K. & Maeda, Y. The helical parameters of F-actin precisely determined from X-ray fiber diffraction of well-oriented sols. *Results Probl Cell Differ* **32**, 43-58 (2001).

107. Pollard, T.D. & Borisy, G.G. Cellular motility driven by assembly and disassembly of actin filaments. *Cell* **112**, 453-465 (2003).

108. Chu, J.-W. & Voth, G.A. Allostery of actin filaments: molecular dynamics simulations and coarse-grained analysis. *Proc Nat Acad Sci U.S.A.* **102**, 13111-6 (2005).

109. Splettstoesser, T., Noe, F., Oda, T. & Smith, J.C. Nucleotide-dependence of G-actin conformation from multiple molecular dynamics simulations and observation of a putatively polymerization-competent superclosed state. *Proteins* **76**, 353-64 (2009).

110. Pfaendtner, J., Lyman, E., Pollard, T.D. & Voth, G.A. Structure and Dynamics of the Actin Filament. *Journal of molecular biology* **396**, 252-263 (2009).

111. Egelman, E.H. A tale of two polymers: new insights into helical filaments. *Nat Rev Mol Cell Biol* **4**, 621-30 (2003).

112. Feuer, G., Molnar, F. & et al. Studies on the composition and polymerization of actin. *Hung Acta Physiol* **1**, 150-63 (1948).

113. Kudryashov, D.S. et al. The crystal structure of a cross-linked actin dimer suggests a detailed molecular interface in F-actin. *Proc Nat Acad Sci U.S.A.* **102**, 13105-10 (2005).

114. Gong, H. et al. Mini-thin filaments regulated by troponin–tropomyosin. *Proceedings of the National Academy of Sciences of the United States of America* **102**, 656 (2005).

115. Marchesini, S. et al. Coherent X-ray diffractive imaging: applications and limitations. *Opt Express* **11**, 2344-53 (2003).